2000

# Urban influences on summertime convective thunderstorms in Atlanta

Qinglu Lin
*San Jose State University*

# INFORMATION TO USERS

This manuscript has been reproduced from the microfilm master. UMI films the text directly from the original or copy submitted. Thus, some thesis and dissertation copies are in typewriter face, while others may be from any type of computer printer.

**The quality of this reproduction is dependent upon the quality of the copy submitted.** Broken or indistinct print, colored or poor quality illustrations and photographs, print bleedthrough, substandard margins, and improper alignment can adversely affect reproduction.

In the unlikely event that the author did not send UMI a complete manuscript and there are missing pages, these will be noted. Also, if unauthorized copyright material had to be removed, a note will indicate the deletion.

Oversize materials (e.g., maps, drawings, charts) are reproduced by sectioning the original, beginning at the upper left-hand corner and continuing from left to right in equal sections with small overlaps.

Photographs included in the original manuscript have been reproduced xerographically in this copy. Higher quality 6" x 9" black and white photographic prints are available for any photographs or illustrations appearing in this copy for an additional charge. Contact UMI directly to order.

Bell & Howell Information and Learning
300 North Zeeb Road, Ann Arbor, MI 48106-1346 USA
800-521-0600

# Urban Influences on Summertime Convective Thunderstorms in Atlanta

A thesis Presented to
The Faculty of the Department of Meteorology
San Jose State University

In Partial Fulfillment
Of the Requirements for the Degree
Master of Science

By

Qinglu Lin

May 2000

Approved for the Department of Meteorology

R. Bornstein

Professor Robert Bornstein

S.-T C. R. Rafkin

Professor Scot Rafkin

Stanley Changnon

Dr. Stanley Changnon

Approved for San Jose State University

William Fisher

**Abstract**

Urban Influences on

Summertime Convective Thunderstorms in Atlanta

By Qinglu Lin

Six summer convective precipitation events over Atlanta during a nine-day period in July-August 1996 were studied. Data from 40 mesonet and NWS surface sites were analyzed, and divergence values calculated. Results showed general agreement between the locations of maximum urban heat island, confluence, convergence, cloud, and precipitation values for three storms found to be probably urban induced.

The urban building barrier effect divided two of the three non-urban initiated (and thus moving synoptic-scale) storms, with cloud areas moving north and south of the city, respectively. The final moving synoptic storm was so complex that urban effects could not be discerned.

The storm division identified in this study is different from storm splitting. The former implies that a group of storms move in two directions from a specific location. The latter implies that a single initial storm splits into two separated cells, given appropriate vertical wind shear conditions.

## Acknowledgments

I would like to thank to Prof. Bob Bornstein for support from his ATLANTA project. I would also like to state my appreciation to Prof. Bornstein for his insight and guidance in all stages of the research and this publication.

During the research, as a member of the ATLANTA project, a great deal of help was also received from other members of the ATLANTA research team. Thanks to Drs. Gerrit Hoogenboom and Haider Taha for Mesonet data, Dr. Douglas Miller for NWS data, and Drs. Jan Hafner and Stanley Kidder for IR and water vapor satellite image data. Special thanks to Jan Hafner for help in image processing, and to Mike Voss for computer support. This work was supported by NASA grant No. NAS8-97106.

Finally, my appreciation would go to all members of my family and my wife Jiangyan Wu. Without their help, I could not be a graduate student and I could not finish my studies at San Jose State University.

# Table of Contents

Page

List of Tables ..... vii

List of Figures ..... viii

1. Introduction ..... 1

2. Data Analysis ..... 17

3. Results ..... 23

a. Synoptic Background ..... 23

b. Case Studies ..... 26

*26 July* ..... 27

*27 July* ..... 30

*30 July* ..... 32

*31 July* ..... 33

*1 August* ..... 36

*3 August* ..... 39

4. Conclusion ..... 41

References ..... 47

Appendix: List of symbols ..... 57

# List of Tables

1 Urban Cloud and Precipitation Studies

2 Urban Influenced Storms

# List of Figures


1 Topographic height values (100 m interval) for Atlanta area. Also shown are mesonet sites (red Os), NWS sites (green Xs), and Atlanta boundary (red line).

2 Time-height velocity cross section (see Fig. 14 for mesoscale speed code) for Peachtree City (elevation 264 m MSL) rawinsonde for 0000 UTC on 27 July to 1200 UTC on 3 August.

3 Same as Fig. 3, but for temperature (K); dashed vertical lines marks time of missing sounding.

4 NWS 500 HPa analysis for 0000 UTC on 26 July.

5 NWS 850 HPa analysis for 0000 UTC on 26 July.

6 NWS 850 HPa analysis for 1200 UTC on 27 July.

7 NWS 850 HPa analysis for 0000 UTC on 28 July.

8 NWS 850 HPa analysis for 1200 UTC on 3 August.

9 NWS surface analysis for 1800 UTC on 26 July.

10 NWS surface analysis for 1200 UTC on 28 July.

11 NWS surface analysis for 1800 UTC on 28 July.

12 NWS surface analysis for 1200 UTC on 29 July.

13 NWS surface analysis for 1800 UTC on 1 August.

## List of Figures (continued)


14 Surface wind velocity and temperature (solid lines, 0.5 K interval) observations for Atlanta area for 1400 EDT on 26 July. Urban outline (heavy solid line) and key topographic height contours (dashed lines) also used in subsequent figures.

15 Surface wind velocity and potential temperature (solid lines, 0.5 K interval) observations for Atlanta area for 1400 EDT on 26 July.

16 Surface divergence (positive values) and convergence (negative values) analysis ($2x10^{-5}$ $s^{-1}$ interval) for Atlanta area for 1500 EDT on 26 July.

17 IR thermal image (GOES 8 Channel 5) for 1545 EDT on 26 July, in which cloud top temperatures indicated as follows: green from 245 to 235 K, red 235 to 210 K, and white < 210 K. Also shown are boundaries of: states, Atlanta, and International Airport.

18 Accumulated precipitation (1 mm interval) for Atlanta area for 1615-2000 EDT on 26 July.

19 Water vapor image (GOES 8 Channel 3) for 1515 EDT on 26 July, in which water vapor amounts decrease with color-change from white, red, green to gray.

20 Surface wind field and relative humidity (solid lines, 5% interval) for Atlanta area for 1400 EDT on 26 July.

## List of Figures (continued)


21 Water vapor image, as in Fig. 19, but for 1600 EDT on 26 July.

22 Surface wind velocity and potential temperature, as in Fig. 15 but for 0600 EDT on 27 July.

23 Surface divergence, as in Fig. 16 but for 0700 EDT on 27 July and with increment of $10^{-5}$ $s^{-1}$.

24 IR thermal image, as in Fig. 17 but for 0815 EDT on 27 July.

25 IR thermal image, as in Fig. 17, but for 0945 EDT on 27 July.

26 Accumulated precipitation (0.5 mm interval) for Atlanta area but for 0915-1115 EDT on 27 July.

27 Surface wind field and relative humidity, as in Fig. 20 but for 1100 EDT on 27 July.

28 Surface wind velocity and potential temperature, as in Fig. 15 but for 0600 EDT on 30 July.

29 Surface divergence, as in Fig. 23 but for 0615 EDT on 30 July.

30 IR thermal image, as in Fig. 17 but for 0645 EDT on 30 July.

31 Accumulated precipitation, as in Fig. 18 but for 0630-0645 EDT on 30 July.

32 Water vapor image, as in Fig. 19 but for 0645 EDT on 30 July.

33 Surface wind field and relative humidity, as in Fig. 20 but for 0715 EDT on 30 July.

## List of Figures (continued)


33 Surface wind velocity and potential temperature, as in Fig. 15 but for 0300 EDT on 31 July.

34 Surface divergence, as in Fig. 23 but for 0330 EDT on 31 July.

35 IR thermal image, as in Fig. 17 but for 0315 EDT on 31 July.

36 Accumulated precipitation, as in Fig. 18 but for 0100-0445 EDT on 31 July.

37 Surface wind field and relative humidity, as in Fig. 20 but for 0400 EDT on 31 July.

38 Surface wind velocity and potential temperature, as in Fig. 15 but for 0000 EDT on 1 August.

40a-c IR thermal image, as in Fig. 17 but for 0115, 0315, and 1145 EDT, respectively, on 1 August.

41 Surface divergence, as Fig. 23 but for 0400 EDT on 1 August.

42 Accumulated precipitation, as in Fig. 18 but for 0000-1030 EDT on 1 August.

43 Surface wind velocity and potential temperature, as in Fig. 15 but for 1100 EDT on 1 August.

44 Surface divergence, as in Fig. 16 but for 1045 EDT on 1 August.

45 Accumulated precipitation (2 mm interval) for Atlanta area but for 1045-1200 EDT on 1 August.

## List of Figures (continued)


46 Surface wind field and relative humidity, as in Fig. 20 but for 1100 EDT on 1 August.

47 Surface wind velocity and potential temperature, as in Fig. 15 but for 0800 EDT on 3 August.

48 Surface divergence, as in Fig. 23 but for 0815 EDT on 3 August.

49 IR thermal image, as in Fig. 17 but for 1045 EDT on 3 August.

50 IR thermal image, as in Fig. 17 but for 1145 EDT on 3 August.

51 IR thermal image, as in Fig. 17 but for 1245 EDT on 3 August.

52 IR thermal image, as in Fig. 17 but for 1415 EDT on 3 August.

53 Accumulated precipitation, as in Fig. 45 but for 0945-1245 EDT on 3 August.

54 Water vapor image, as in Fig. 19 but for 0945 EDT on 3 August.

55 Water vapor image, as in Fig. 19 but for 1045 EDT on 3 August.

56 Surface wind field and relative humidity, as in Fig. 20 but for 1300 EDT on 3 August.

## 1.Introduction

Urban climate characteristics have been summarized, for example, in the textbook by Landsberg (1981) and in the literature review articles Bornstein and Oke (1981), Bornstein (1987), and Imamura and Bornstein (1992). In addition, specialized urban climate conferences have been held, for example, in: Brussels (WMO 1968), Philadelphia (AMS 1972), Mexico City (WMO 1986), Boston (AMS 1987), Berkeley (Garbesi et al. 1989), Kyoto (Bitan 1989), Guadalajara (WMO 1990), Dhaka (WMO 1994), Waldbronn (Cermak et al. 1995), San Francisco (Dowling and Knox 1996), Tohwa (Tsutsumi and Bornstein 1996), Albuquerque (AMS 1998), and Essen (Kuttler et al. 1999). These reviews and conference volumes show a consensus on the causes and nature of a variety of urban climate impacts, e.g., the urban heat island (UHI), urban moisture island, and urban wind flow fields. No such consensus can be found, however, on the causes and nature of urban effects on precipitation.

Case studies and/or climatological studies have documented differences in precipitation distributions in and around urban areas in various topographic and climatological settings. While such differences have been attributed to a variety of urban surface, aerosol, thermodynamic, and fluid dynamic causes, in most cases precise cause and effect documentation was not possible. Such attributions, therefore, were generally based only on urban climate theory and investigator experience. A sim-

ilar quandary exists with documentation of successful artificial precipitation enhancement research, as control cases are not possible.

In sections of the following literature review that deal with urban effects on precipitation, causal factors put forth by individual investigators are thus repeated, even when stated contentions are not the result of scientific investigation. This is done to demonstrate the range of proposed causal mechanisms.

Urban climate research initially focused on 1.5 m air temperature UHIs, i.e., the relative warmth of a city compared to that in its surrounding environs. The UHI should be defined as the difference between the actual temperature now (at the urbanized site) and the hypothetical one that would now exist if the site had not be urbanized. Since this determination cannot be made for most cities, UHI magnitude is thus estimated by the horizontal temperature difference between the urban center and the surrounding non-urban region. Cities generally show nighttime 1.5 m UHIs that: form after sunset, reach a maximum near midnight, remain fairly constant throughout the night, decrease after sunrise, and can become urban "cold islands" around midday (Bornstein and Oke 1981).

Nocturnal UHIs result from the following urban alterations to the surface energy balance (Bornstein 1987):

- daytime solar energy storage in building and ground surfaces and its subsequent slow release during nighttime periods, a process important in summer and in warm-climate cities
- anthropogenic heat production by fossil fuel combustion to provide nighttime heating in cold climates and daytime cooling in warm climates
- nighttime reduction of outgoing longwave radiation due to absorption by both elevated pollutant layers and urban structures.

These factors reduce the rate of nocturnal urban cooling, thus maintaining temperatures at values higher than those of nearby rural areas. Local weather conditions determine particular daily UHI magnitude, as clear skies favor rapid rural nocturnal cooling and high wind speeds advect away excess urban heat.

Nighttime UHI intensity generally decreases in magnitude from the 1.5 m level up to heights of several hundred meters (Bornstein 1968). Above this layer, a weak shallow "crossover layer" frequently exists, in which temperatures are lower than rural values at the same elevation. Such layers arise from radiative emissions from the top of the polluted urban planetary boundary layer (PBL) according to Bornstein (1987).

During nocturnal UHI periods, the urban PBL is near-neutral (and hence better mixed than nearby rural regions), due to mechanical and

thermal processes. The nocturnal urban PBL is dome-shaped during near-calm conditions and plume-shaped during higher speed periods, when it is advected over the downwind surface-based stable rural boundary layer.

The near-neutral nighttime urban PBL is capped by a weak thin elevated inversion layer (Bornstein 1968). Such layers are remnants of rural surface based inversions destroyed from below by thermal and/or mechanical surface-convection as they advect over the city. The latter is associated with rough urban surfaces, while the former relates to anthropogenic heat release.

Daytime 1.5 m urban "cool islands" can result from:

- absorption/reflection of atmospheric solar insolation by atmospheric aerosols
- building absorption of surface solar radiation
- latent heat effects produced by urban trees and green spaces in cities located in dry climates.

Storage and release of solar energy is controlled by the thermal inertia (TI) of a surface, defined as the square root of the product of its density, specific heat , and thermal conductivity. For a given solar flux, surfaces with high TI values (e.g., wet soil) experience smaller temperature changes than those with low TI values (e.g., dry soils). Urban TI values

are intermediate, as they result from all features of the three-dimensional urban canopy-layer (Imamura 1991).

Surface radiative (and not 1.5 m) UHIs thus partially depend on precipitation patterns, i.e., maximum daytime surface UHIs occur in cities surrounded by wet rural soils, while maximum nighttime surface UHIs occur in cities surrounded by dry rural soils. Maximum daytime surface UHIs detected from either satellite or aircraft thermal-band radiometric observations are larger than maximum nocturnal surface and 1.5 m UHI values (Roth et al. 1989). They are also larger than daytime 1.5 m UHI values, due to rapid daytime convective mixing.

Daytime rural and urban surface boundary layers (SBLs) are both generally unstable, while the upper portions of both PBLs are close to neutral. Mechanical and thermal convection can, however, elevate regional inversion bases located within 2 km of urban surfaces.

Air traversing an urban area encounters changes in surface and atmospheric characteristics that alter existing mean and turbulent wind velocity fields (Bornstein and Johnson 1977). In particular, UHIs cause pressure field deformations, buildings produce barrier effects, and large urban surface roughness length values ($z_0$) increase surface frictional drag .

Urban wind speed values decrease (relative to those in surrounding rural areas) during periods with fast regional flows, as $z_0$ values increase

over cities, from 1 cm for open countryside to 1 m for woodlands, suburbs, and small towns to 3 m for large cities. Urban areas also increase both thermal (due to UHI effects) and mechanical (due to surface roughness effects) turbulence. This latter increase occurs, even with reduced urban speeds (Roth 1998).

During UHI periods (with near calm synoptic flows), inward directed "country breezes" that develop due to the urban thermal low produces speed maxima near urban centers. With non-zero synoptic flows, UHI induced flows are superimposed onto prevailing winds, advecting the maximum speed region to the downwind urban edge.

A critical synoptic scale wind speed thus divides low synoptic speed (and hence UHI induced pressure gradient force accelerated) flow cases from the synoptic speed (and hence urban friction decelerated) flow cases (Bornstein and Johnson 1977). Urban-rural horizontal wind speed differences extend several hundred meters into the urban boundary layer during daytime and nighttime periods, and are frequently capped by return flow layers of equal depth (Bornstein 1987).

Urban areas also perturb background synoptic horizontal flow directions, e.g., UHIs produce confluence into urban centers in otherwise calm conditions. During periods with prevailing background flows, the confluence is superimposed onto the existing flow and is advected downwind from the urban center.

During non-UHI periods, a building barrier (separate from a pure surface roughness effect) induced difluence divides regional flows as they approach a city (Bornstein and LeRoy 1990). The effect results as the following sequentially occurs upwind of the city: barrier effect reduces speeds, an aerodynamic surface high-pressure zone forms, and the flow divides around the city. Such effects are more common during stable nighttime conditions (when flow around cities is maximum) than during unstable daytime conditions (when flow over cities is maximum). Evidence of barrier division comes from observed effects of New York City (NYC) on regional flow patterns, moving synoptic fronts (Loose and Bornstein 1977, Gaffen and Bornstein 1984), moving sea breeze fronts (Bornstein and Thompson 1981), and moving thunderstorms (Bornstein and LeRoy 1990).

The barrier effect produces difluence at the upwind urban edge, with downstream cyclonic turning to the left (looking downstream) of the flow and downstream anticyclonic turning to the right (Panayiotou 1995). It also produces confluence at both lateral urban edges (where air deflected around the city converges with the undisturbed prevailing flow) and downwind of the city (where the flow re-unites).

The above convergence/divergence effects produce urban vertical velocity patterns consistent with three-dimensional, mass-consistent,

non-divergent flows. Urban induced vertical motions are larger during unstable daytime hours than during stable nighttime hours.

The altered urban thermodynamic and dynamic fields, in conjunction with cloud condensation nuclei (CCN) effects, thus could affect urban cloud and precipitation fields. Such mechanisms were suggested by the climatological (annual and/or seasonal) and case studies listed in Table 1. Suggested mechanisms for each study are listed in the following sections to demonstrate the range of proposed mechanisms.

The first such in-depth climatological study (Changnon 1961) used 1950-59 data from three NWS stations and 13 recording rain gauges in and around Champaign-Urbana. Results showed an annual precipitation maximum at the downwind urban edge (urban average 864 versus 762 mm in surrounding rural areas). The four seasons showed the same pattern, with winter showing both the maximum urban precipitation excess (16%) and the furthest downwind influence. Summer showed the minimum excess (7%) and had its maximum over the city.

Changnon noted that these results agreed with ideas expressed by Landsberg (1981), who had suggested that urban precipitation influences would be greatest in winter, if the following were the important urban impacts: increased nuclei, urban water vapor flux, and winter mechanical turbulence. Thermal turbulence would be important in summer.

Changnon (1968) then studied the area in and around Chicago using 1951-65 climatological data from 10 NWS stations. Results again show-ed an urban annual precipitation maximum, but it occurred in summer and was located 48 km downwind of southeast edge of Chicago, i.e., in the city of La Porte.

In comparison to average values at nine surrounding sites, La Porte had the following excesses: 31% more annual precipitation, 28% more warm season (convective) precipitation, 34% more days with more than 6.5 mm precipitation, and 38% more thunderstorm days. Note that these values imply that each thunderstorm produced less La Porte precipitation. Analysis indicated that most convective increases consisted of 'solo storms' only over La Porte in early morning hours. He related these excesses to concurrent UHIs.

The La Porte anomaly was first challenged by Holtzman and Thom (1970), who identified observational error as its source; this idea was refuted by Changnon (1970). When Holzman (1971) again challenged this analysis using runoff data, Hidore (1971) concluded that the data supported Changnon. A third challenge to the anomaly was mounted by Machta et al. (1977) who argued that the anomaly existed during only the 1928-63 period, when a single cooperative observer was active. Before and after this period, the local precipitation maximum existed at Valpariso, 30 km southwest of La Porte. Changnon and Huff (1977)

countered that the observer was in fact active until 1969, and that the La Porte site had been moved in both 1967 and 1970. In fact, if an urban induced precipitation maximum exists, whether it is over La Porte or nearby Valparaiso should not matter.

A hydrologic analysis by Clark (1979) concluded that the La Porte anomaly was localized, and that its 1964 apparent dissipation was most likely due to gage and/or observational error. Changnon (1980) listed three other possible causes for its demise: reduction in CCN, broadened areal extent to encompass adjacent sites (like Valperiso), or movement to an ungaged location (like Lake Michigan) due to changing synoptic weather patterns, the one he believed most likely. Time may tell who is correct.

A seasonal climatological study of 1951-60 thunderstorm rain data from 608 gauges around London was carried out by Atkinson (1968). Results showed an urban maximum thunder rainfall total directly over London annually (urban average 102 versus 61 mm immediately around city) and for summer (81 versus 51-61 mm), the season with about 80 % of the total annual thunder precipitation. The summer increase over the city center, in agreement with the Champaign-Urbana results, was attributed to increased urban thermal convective activity.

A climatological precipitation study for eight U.S. cities by Huff and Changnon (1973) showed that the six largest ones experienced warm

season rainfall increases of 9-17% during the 1955-70 period. Of the six, Midwest cities showed increases with cold frontal systems, while coastal cities showed increases during air mass conditions. Midwest increases were due to enhancement, and not initiation, of moderate to heavy storms. The six cities also showed increases in summer thunder- (13-41%) and hail- (90-450%) day frequencies, mostly during morning per-iods.

Finally, the Midwest cities showed thunder maxima over and just downwind of the city, with rainfall and hail maxima located 25-55 km downwind. Maximum values of all events were, however, in or near the coastal cities. The authors suggested that enhancement was related to city size, industrial nuclei, and urban thermal effects.

A nine-year (1961-69) climatological UHI and precipitation study of the Detroit-Windsor area by Sanderson et al. (1973) showed small positive or negative urban impacts in every season but summer, when a large 20 % urban enhancement was found over the urban area, as had been found in Champaign-Urbana and London. Since maximum UHIs occurred in fall, they were unable to separate urban from lake influences.

A more detailed seasonal climatological study of Detroit-Windsor precipitation by Sanderson and Gorski (1978) used six years (1970-75) of data. Seasonal precipitation totals were related to prevailing seasonal wind directions. Results agreed with those of the previous study, except

that the urban summer maximum precipitation amount (and not rain days) extended somewhat downwind of the city

Goldreich and Manes (1979) studied urban effects on precipitation at many sites in Tel Aviv with 70 years of data, and demonstrated a 6% per decade maximum increase in annual rainfall due to unspecified urbanization factors. They also demonstrated that peak rainfall occurrence moved several days during the rainy winter season towards fall.

Annual or seasonal climatological studies can only indicate average urban precipitation effects on groups of storms, each of which can have a maximum impact at a different location. Averaging also reduces the maximum (positive or negative) urban signature in any group of storms, while case studies of individual storms can delineate the location and magnitude of maximum (positive or negative) urban impacts.

One early case study of a single summer afternoon thunderstorm was by Parry (1956), who found that a storm over Reading, England was triggered by the city and was localized over the city center. The probable cause was identified as the UHI. These summer convective results were thus in agreement with those from the later climatological results from Champaign-Urbana and London discussed above.

Atkinson (1971, 1975, and 1977) studied three warm season convective precipitation events in London, England, and generally found the same results as Parry. The first event showed precipitation enhancement

over the city for a moving thunderstorm due to the high urban temperature. The second event showed that clouds crossing the city experienceed conditions favorable for growth and increased precipitation rate, due to urban frictionally induced convergence. The final event showed UHI induced precipitation enhancement for a severe thunderstorm over the city center and downwind. Studies over Washington, D. C. by Harnack and Landsberg (1975) showed that UHI induced cloud formation over the city created maximum summer shower precipitation over and just down-wind of the city, as in Champaign-Urbana and London.

The first comprehensive urban precipitation study that involved urban PBL measurements was the 1971-75 METROMEX study in St. Louis. Many papers have described its urban effects on warm season temperature, wind flow, moisture, cloud, and precipitation values. A comprehensive summary by Changnon et al. (1981) showed thunderstorm, rainfall, lightning, and hail increases over St. Louis in a wide fan-shaped area extending up to 65 km downwind of the city.

In particular, as compared to surrounding areas, Braham (1981) showed that first summer echoes over St. Louis were twice as frequent, and had lower bases and tops. Resulting convective clouds also reached greater heights, lasted longer, and were more likely to merge. Changnon (1992) listed the following as the major urban causal factors: CCN; moisture fluxes; sensible and latent heat fluxes; and convergence induced

updrafts due to mechanical, thermal, and urban building barrier flow effects.

He concluded that the summer rainfall maximum over the downwind urban edge (like at Champaign-Urbana) during late afternoon hours resulted from modification of PBL dynamics due to surface thermal and frictional forcings. Achtemeier (1983) found that widespread mid-west convective rainfall seldom occurs without larger scale convergence, but that convergence centers needed to form only at most 15 minutes prior to precipitation initiation.

Analysis of the METROMEX and 1941-80 NWS climatological data for the remaining three seasons by Huff and Changnon (1986) showed maximum precipitation enhancements northeast of St. Louis in both data sets, with increases of 14% in spring, 5% in winter, and 7% in fall. Of the 10-15% altered rain events, however, most were well organized precipitating convective storms.

Further analysis of the non-summer METROMEX data set by Changnon et al. (1991) identified the downwind quadrant for each precipitation event. Fall results showed a 13% downwind urban event increase and a 17% precipitation enhancement, with peak rainfall downwind of the city; however, little winter and spring period effects were found. Fall season results thus agreed with the earlier summer results,

as they showed a 25% enhancement in isolated air-mass showers with well-organized convective systems.

Analysis of climatological summer convective radar echoes by Bornstein and LeRoy (1990) showed NYC effects on both summer daytime thunderstorm formation and movement. During conditions with nearly calm regional flows, an UHI effect was said to initiate convective activity, and thus to produce a radar echo maximum over the city. Thunderstorms moving with stronger regional flows, however, divided and moved around the city, apparently due to a building-barrier divergence effect. Radar echo maxima were thus found on both lateral edges and downwind of the city, while a minimum was located over the city. The barrier effect to moving storms had not been postulated in previous studies, but Spar and Romberg (1968) had noted a then unexplained downward trend in precipitation values at Central Park in NYC that would be consistent with thunderstorm division.

Summer cloud-to-ground lightning activity was studied in 16 midwest cities by Westcott (1995). Results also showed a 40-80% enhancement of lightning frequency, again over and downwind of many of the cities. Spatial distributions of the first 50 lightning flashes of each storm suggested that the urban area did not initiate new storms, but only affected existing thunderstorms.

The climatological convective precipitation study of Selover (1997) showed that urbanization of Phoenix, Arizona over a 65-year period from 1930 produced a precipitation pattern (from moving summer convective storms) with an urban minimum surrounded by lateral and downwind maximum values. These maxima are thus consistent with the NYC results for moving thunderstorms.

In summary, previous (seasonal and annual) climatological and case studies have indicated that urban areas may influence the formation and/or movement of precipitation events, resulting in a variety of altered rainfall characteristics, such as timing, amount, frequency, and location of maximum relative to the city center (i. e., over, just downwind, or far downwind). These effects have been attributed (in most cases without analysis) to a variety of urban causes, such as UHI convergence/convection, CCN excesses, urban roughness effects, and/or building-barrier induced divergences.

The current study thus seeks to develop a consistent hypothesis concerning urban effects on summer convective storms that could explain as many as possible of these previous studies. The hypothesis will be developed by the analysis of 1996 summer meteorological data collected over Atlanta, Georgia.

## 2. Data Analysis

While no previous study of Atlanta urbanization has investigated its effects on precipitation, some have focused on its air quality and/or urban climate. The city was the site of a Southern Oxidant Study (SOS) urban intensive field study (Chameides and Cowling 1995). As biogenic isoprene emissions are known to increase with temperature, SOS results indicated that deforestation associated with Atlanta urbanization increased its UHI, thus producing a net increase in Atlanta isoprene emissions. Predicted ozone patterns in Atlanta were found dependent on the:

- method of mixing height estimation (Marsik et al. 1995)
- temporal and spatial availability of PBL wind measurements (Al-Wali and Samson 1996)
- vertical diffusion parameterization used in the UAM-IV photochemical model (Nowacki et al. 1996).

As these parameter (mixing depth, wind velocity, and mixing coefficients) formulations did not properly include urban impacts, the model results imply that Atlanta-induced effects on regional transport and mixing patterns were not properly simulated.

The SAI Meteorological Model (SAIMM) was used on a 4 x 4 km grid to provide input to the UAM-IV and-V photochemical air quality models for three 1992 Atlanta summer ozone episodes by Douglas et al. (1994),

one of which was a SOS test period. Flow field predictions and observations were analyzed for accuracy, but not for urban effects.

The overall goal of Project ATLANTA (ATlanta Land use Analysis: Temperature and Air quality) is investigation of regional climate and air quality impacts from past, current, and future urbanization of Atlanta, Georgia (Quattrochi et al. 1998). The groups involved in the project have the following goals:

- analysis of 20 years of satellite-derived land-use data to determine changing urbanization patterns and resulting changes in surface characteristics (e.g., albedo and vegetative index)
- analysis of meteorological data (e.g., UHI, wind, and clouds) to determine regional impacts from urbanization
- analysis of changing air pollutant emission patterns
- analysis of changing in regional air quality patterns
- mesoscale meteorological modeling of observed and future meteorological patterns
- regional air quality modeling of observed and future air quality patterns.

Results to date include those from a modeling study of the Atlanta UHI by the nonhydrostatic RAMS meso-meteorological model, in conjunction with satellite-derived surface/soil parameters (Hafner and Kidder 1999). Results from both a dry soil day and a wet soil day in February

showed that 2 m and surface UHI values were positive during the night and negative during the day, and that surface UHI values were almost always greater than 2 m values. While differences between the results at both levels for the two cases were within 0.2 K, at 2 m the larger nighttime UHI value existed on the dry soil day, while the larger daytime urban cool island value existed on the moist soil day. Note that these results (except the last one) are consistent with the theory of Imamura (1991) discussed above.

Another Project ATLANTA UHI modeling study was carried out by Taha (1999) using the hydrostatic CSUMM mesoscale model, whose surface-energy storage-term was urbanized by use of the objective hysteresis model (OHM) of Grimmond et al. (1991). Results showed that the maximum 1.5 m UHI value for a summer daytime period increased from 1.4 K to 2.9 K with inclusion of the OHM scheme.

Effects from possible moderation of summertime daytime Atlanta UHIs (via specified increases in both its surface albedo and green areas) were also modeled with CSUMM (Taha 1998); predicted meteorological fields were then used in UAM-IV simulations. Results showed a reduction in maximum predicted Atlanta ozone concentrations of up to 12 ppb.

Project ATLANTA data were obtained for 42 sites in the Atlanta mesonet surface meteorological network (Hoogenboom 1996) for the period from 26 July to 3 August 1996. Only 27 sites, however, were within

the analysis domain of Fig. 1, selected to correspond to the photochemical modeling domain of Project ATLANTA. Of the remaining 15 sites, five were, however, close enough to domain boundaries to be included in subsequent analyses.

Mesonet sites provided data at 15-minute intervals, starting on the hour; the end-time of each interval was used as the period identifier. Data from eight NWS surface sites in the domain were also used; these data are collected hourly, on the hour. The term "surface" applied to the above data refers to the standard WMO observational height of 1.5 m, except for the 10 m observational height of wind velocity measurements. Surface observations were augmented by data from a single regular NWS rawinsonde site located at Peachtree City (site FFC in Fig. 1). Time-height velocity (Fig. 2) and temperature (Fig. 3) cross sections were constructed from its data.

The inverse distance-square weighting objective-analysis scheme of Daley (1991) was used to interpolate the combined mesonet and NWS surface temperature, horizontal wind speed, relative humidity, and precipitation data onto a grid. Grid spacing was selected as 5 x 5 km, a value slightly smaller than the average distance between observational sites in the densest part of the network, i.e., in and around Atlanta.

Thus, if $s_o(r_k)$, with $1 \le k \le K$, defines the K "nearby" observations of parameter $s$ (at locations $r_k$,) that influence $s_a(r_i)$ (objective-analysis value of parameter $s$ at the $i$-*th* analysis grid point $r_i$,), then $s_a(r_i)$, is given by

$$s_a(r_i) = \sum_{k=1}^{K} w_{ik} s_o(r_k) \Big/ \sum_{k=1}^{K} w_{ik} \qquad (1)$$

and

$$w_{ik} = 1/\Delta r_{ik}, \qquad (2)$$

where all symbols are defined in the Appendix. Weights $w_{ik}$, are thus independent of observed values $s_o(r_k)$, but dependent only on $\Delta r_{ik}$, the distance between analysis point $r_i$ and observation point $r_k$

Trial and error showed that objective analysis fields are strongly dependent on selected $K$-values, e.g., a large $K$ smoothed out too many details in potential temperature fields. The following $K$ values were thus selected for the different parameters by trial and error: 2 for temperature and relative humidity; and unity for wind speed and precipitation. Gridded horizontal wind speed component values were then used to calculate Eulerian horizontal divergence fields from

$$D = \frac{\partial u}{\partial x} + \frac{\partial v}{\partial y} . \qquad (3)$$

As the final step before use of the contour analysis routines in the MATLAB software package, a five-point smoothing operator was used 10 times sequentially (value determined by trial and error) for all gridded objective-analysis parameters (except 20 times for divergence). Smoothing produced non-jagged contour patterns, but did not alter distribution patterns (shown by comparisons between observed and interpolated values), except for extreme values. Given the sparsity of observational sites (Fig. 1) in outer some domain areas (helped by the five external sites mentioned above), the analyses in these areas will not be considered in the following discussions. The best analyses are thus those in the data-rich areas in and around Atlanta.

In the following smoothing equation, each $s_a(m,n)$ value was previously denoted as $s_a(r_i)$ in (1):

$$\tilde{s}(i,j) = a \cdot s_a(i,j) + b \cdot [s_a(i+1,j) + s_a(i-1,j) + s_a(i,j+1) + s_a(i,j-1)], \qquad (4)$$

where smoothing coefficients a and b are restricted by

$$a + 4 * b = 1. \qquad (5)$$

In the current application, the commonly used values of 0.5 and 0.125 were adopted for a and b, respectively.

While the topography of the urban Atlanta region (Fig. 1) shows generally flat terrain (elevations between 200 and 300 m), a hill (up to about 700 m in elevation) exists north of the city. Potential temperature values were thus calculated from gridded temperatures (without subsequent smoothing) by use of the following PBL approximation (to remove elevation effects associated with topographic features):

$$\theta = T + \Gamma_D z_t. \qquad (6)$$

GOES 8 thermal IR (Channel 5) and vertically integrated (200-500 HPa) water vapor (Channel 3) images were also available at 30 min intervals. Geographic (state, city, and airport) boundaries were added to each image. The most significant (deepest and hence coldest) cloud area temperatures in each IR image are shown as follows: below 235 K in red; and between 235 and 245 K in green.

## 3. Results

### a. Synoptic background

On 26 July at 0000 and 1200 UTC, a 500 mb long wave trough extended from Quebec to Mississippi (Fig. 4). At the southern end of the trough, over Atlanta, the prevailing flow was westerly at 15 kts (8 m $s^{-1}$). The 500 mb reflection of the subtropical high was positioned east of Flor-

ida, with its axis oriented east to west. During the next seven days, the 500 mb pattern over Georgia remained fairly similar (i.e., westerly or south-westerly flow at 15-25 kts), with a slight eastward movement of the trough and either a slight strengthening or weakening of the high.

At the 850 mb level on 26 July at 0000 UTC, both the trough and high were visible (Fig.5). Northwest flow at 10 kts prevailed over Atlanta, while westerly or west-southwesterly flow (15-30 kts) prevailed to the south. A frontal wind shear line thus existed south of Atlanta along the 156 dam contour. By 1200 UTC on the 27th, the 159 dam contour associated with the 850 mb subtropical high crossed Atlanta (i.e., the front passed), producing west-southwesterly flow at 10 kts over the city (Fig.6).

By 0000 UTC on the 28th, a small closed low had formed north of Georgia in the area previously occupied by the now weaker subtropical high (Fig.7); however, the low was gone 12 hours later. The high then alternated between periods when it enlarged/strengthened or receded/weakened until 1200 UTC on 1 August. During this period, winds over Atlanta were generally southwesterly or westerly at about 10-30 kts.

From 1200 on the 2nd until 0000 UTC on the 3rd, the 850 mb trough had a northeast to southwest orientation, and its southern edge (west of Georgia) formed a (break-off) closed low; winds over Atlanta thus remained westerly. The closed low appeared on only one 850 mb chart (i.e., 0000 UTC on the 3rd), and the weak pressure gradient that replaced

the closed low at 1200 UTC produced the first southerly flow of the period over Atlanta at 10 kts (Fig. 7)

At 0000 UTC on 26 July, a southwest to northeast oriented surface cold front was moving toward to Atlanta. When the front overtook (and merged) with a weaker cold front at 1800 UTC (Fig.9), they transformed into an east to west oriented stationery front located just south of Atlanta. From 0000 on the 27th to 1800 UTC on the 28th, the front oscillated south to north of Atlanta, producing southwesterly flow over the city at 5-10 kts.

On some surface maps during this period, the western section of the front was drawn through Atlanta, though this sometimes required either a local perturbation to accommodate Atlanta data (Fig. 10) or positioning the front in a local high over the city (Fig. 11). This section of the front was eliminated from the analysis of 0000 UTC on the 29th. Interactions between larger scale patterns and urban Atlanta influences will be discussed in the following section.

During the next 18 hours, the Atlanta area was dominated by a weak high, and by a slow moving wave cyclone and its quasi-stationary front (eastern extension of leading warm front). The front was first located north of the Georgia border during this 18-hour period (Fig. 12), then slowly moved north (as its associated low moved slowly eastward), reaching New England by 0060 UTC on 1 August. By this time, the slow

moving trailing cold front of this system approached the NE corner of Georgia. It became quasi-stationary just south of the city from 1800 UTC on the 1st (Fig. 13) until the end of the test period on the 3rd.

The above generally westerly flow conditions above the PBL are also seen in the Peachtree city rawinsonde data (Fig. 2), which likewise shows short periods with southerly or easterly PBL flow conditions. In addition, corresponding temperatures (Fig. 3) do not show a significant elevated subsidence inversion, because the generally weak 850 mb General Circulation high pressure area was located too far south of Atlanta throughout most of the period. Finally, no significant trend is seen in PBL temperatures.

**b. Case studies**

A summary of the six precipitation events found during the study period are shown in Table 2, in which: Eastern Daylight Savings time (EDT) is UTC minus five hours. UHI values represent differences between urban center potential temperatures and those in its coldest nearby environ. Convergence values are domain-wide (grid-point) maxima, while maximum and total precipitation values are single station (not necessarily urban) values.

At the start of some precipitation events, rain occurred at only one site (or at two sites, but for only one 15 min period). Such events were

not included in the following discussion and in the rain periods listed in Table 1.

***26 July***

In this case, a generally weak 1.5 m daytime UHI center existed slightly NE of Atlanta, due to advection of heat from the city by a generally SW (about 2.5 m/s) regional flow located south of the city. The UHI is visible in both the temperature (Fig. 14) and potential temperature (Fig. 15) fields at 1400 EDT, with the latter parameter showing weaker gradients over the hills north of the city. The maximum UHI value at this time increased from about 1.0 K to about 1.75 K when these topographic influences were eliminated via use of potential temperature. Maximum potential temperature UHI values during this case ranged from 2.0-2.5 K from 1200 to 1415 EDT, after which clouds were initiated (discussed below). Solar blockage due to cloud formation (seen in satellite images) was probably responsible for the gradually weakened UHI over the subsequent two-hour period.

While confluence over Atlanta can be seen in Fig. 15, the divergence field of Fig. 16 was calculated using (3) on wind speed component values observed one hour after those of Fig. 15. The synoptic component of the confluence can be seen in the predominantly northwesterly flow at

all sites in the northwest quadrant of the figure versus the southwesterly flow at all sites south of Atlanta. The resulting east-west synoptic confluence zone coincides in time and space with the synoptic front described above, and is centered over Atlanta.

The local maximum convergence of $-10 \times 10^{-5}$ $s^{-1}$ (strongest of the six cases) is found advected somewhat towards the downwind urban edge of Atlanta (Fig. 16), with a somewhat weaker lobe extending southward. This entire area is part of the synoptic-scale frontal convergence zone that extends from west of the city, through the city, and up to the northeast domain corner. The magnitudes at the western and northeastern ends of this convergence line are unknown, due to the relative data scarcity in those areas. It however appears that UHI-induced convergence has been superimposed on the synoptic-scale convergence.

Evidence for this superposition is also found in the ring of local divergence maxima around the city. These divergence centers could have formed when air flowed out (drawn by the Atlanta UHI) from areas with the northwesterly and southwesterly synoptic flows.

GOES-8 IR thermal-images at 30 min intervals showed clouds moving into the Atlanta areas along the cold front. The first significant (red area, defined above) localized convective cloud formation occurred over the southern-extension of the convergence area in Fig. 16 around at 1415 EDT, reached peak intensity at 1745 EDT (Fig. 17), and dissipated

by 2000 EDT. Note that while other (subsequently formed) significant cloud areas exist in Fig. 17, this case shows an independent urban induced cloud/precipitation area. As the afternoon SBL became more unstable, convective cloud formation somewhere along the front became likely, but UHI-induced convergence favored the formation observed in the section over Atlanta.

Precipitation was thus initiated at 1445 EDT in the convergence lobe 25 km south (i.e., almost directly locally upwind) of the center of Atlanta (Fig. 16). The precipitation lasted until 2000 EDT, but its center moved slowly 40 km further upwind (i.e., to the SW) as it was apparently advected with the moving front. The accumulation over the most intense precipitation period (1615-2000 EDT) shows a maximum value of 14 mm centered about 60 km south (i.e., generally upwind) of the center of Atlanta (Fig. 18).

Goes-8 images of integrated water vapor provide additional information concerning cloud formation over the southern edge of the city. The 1515 EDT image (Fig. 19) shows the image-wide maximum water vapor located within the Atlanta urban-induced convergence/precipitation area, as such convective cloud tops can easily reach up to 500 HPa. Surface relative humidity (RH) values before precipitation onset (Fig. 20) show minimum values in the convergence/precipitation area, while those after onset (Fig. 21) show the area having maximum values, as expected.

In summary, this afternoon precipitation event seems to have been initiated, as urban UHI-induced convergence apparently enhanced that associated with a weak slow-moving synoptic cold front.

***27 July***

In this case, a clearly defined nighttime UHI was centered directly over Atlanta (Fig. 22) in association with a generally weak disorganized regional flow, upon which an also weak (about 1 m/s) UHI-induced confluent flow formed. The UHI ranged in value from 2.0-3.0 K, existed from 0000 to 0900 EDT, and showed local maxima at 0100 and 0600 EDT. The UHI was relatively weak on this morning (even with the low wind speeds), because of the regional cloud cover (see below).

Confluence is again found over Atlanta (Fig. 22), while calculated convergence values (Fig. 23) yielded a maximum over Atlanta of only $2.0 \times 10^{-5}$ $s^{-1}$ at 0700 EDT. This nighttime convergence is weaker than that of the previous daytime case because of the weak nighttime regional winds and the weak UHI. Note that large local maximum values near data-sparse domain boundaries are suspect. It is hard to locate the weak stationary front shown on the concurrent NWS surface charts, given the generally low wind speeds. It is most likely located, however, within the line of weak convergence (oriented southwest to northeast) that passes through the city.

GOES-8 IR thermal-images showed a localized group of synoptic-scale frontal convective cloud cells (cloud area too large to represent a single convective cell) moving towards Atlanta from the southwest at 0815 EDT (Fig. 24). The location of this cloud area appears to verify the frontal location discussed above. By 0945 EDT, the group of cells apparently divided into two groups, which moved north and south of the city (Fig. 25). A similar division effect on moving summer daytime convective thunderstorms over NYC was postulated by Bornstein and LeRoy (1990) to result from an urban barrier effect, as discussed above.

Precipitation started at 0630 EDT at a location 90 km upwind (i.e., southwest) of the city, moved towards the city along the front, and then reached the city at 0845 EDT. Rainfall accumulation during the intense precipitation period of 0915-1115 EDT (Fig. 26) shows a divided upwind urban maximum, the two parts of which could be interpreted as associated with the two intense cloud area of Fig. 25.

Goes-8 water vapor images are not shown, given the regional synoptic moisture of this case. As with the previous case, after the start of rainfall, RH values are high in areas with high precipitation values, and vise versa (Fig. 27).

In summary, in this case the urban barrier effect apparently dominated the UHI/convergence effect, as synoptic frontal cloud cover did not allow for the rural cooling required for nocturnal UHI formation. The

area of maximum precipitation is thus not over the UHI area, as in the previous UHI-dominated case in which the city apparently initiated the convective activity. In this case, however, precipitation resulted from a group of existing moving frontal cells that divided (apparently by an urban induced barrier effect) into two upwind lateral groups (one on either side of the city).

***30 July***

In this case, a clearly defined nighttime UHI was again centered directly over Atlanta at 0600 EDT (Fig. 28) in association with a weak disorganized regional flow, upon which was imposed a moderate (up to 3.5 m/s) UHI-induced confluent flow. Moderate UHI values (2.5-4.0 K) existed from 0000 to 0800 EDT, with a local maximum at 0600 EDT. Regional cloud cover was again present, but not as extensively as in the previous case, due to the now more northward location of the subtropical high and to the subsequent synoptic frontal absence (as discussed above). Rural nocturnal cooling rates were thus only partially reduced, and thus only a somewhat larger UHI formed, as compared to the previous case.

Confluence at 0615 EDT was centered somewhat downwind of the Atlanta urban center (Fig. 29), as a southwesterly background flow developed upwind of the city. Calculated convergence values thus show a downwind maximum over northeastern Atlanta of $5.5 \times 10^{-5}$ $s^{-1}$ at 0615

EDT. This value is stronger than that of the previous nighttime case, be-cause of the now faster maximum urban winds associated with the now stronger UHI. Note that while the convergence areas west and northeast of Atlanta look similar to those of 26 July, it is hard to discern a front in this figure, and NWS surface charts did not show a front in the area.

GOES-8 IR thermal-images showed a significant localized area of synoptic-scale clouds north of Atlanta, at the northern edge of the 850 HPa subtropical high. By 0645 EDT (Fig. 30) a significant (apparently urban-induced) localized cloud area developed in the above mentioned convergence zone at the downwind urban edge (i.e., NE urban corner) and nowhere else in the immediate vicinity of the city. Weak precipitation occurred twice (at 0430 and 0545 EDT), but for only 15 min periods at single sites outside the city. Strong precipitation, however, occurred at 0630 EDT at one site at the center of the urban convergence zone, as on the 26th. The rain lasted for only 30 min, but 7.5 mm accumulated (Fig. 31). This local cloud/precipitation area was again associated with concurrent local GOES water vapor (Fig. 32) and surface RH maxima (Fig. 33).

In summary, this morning precipitation event seems to have been initiated within a moderate urban UHI-induced convergence zone, in the

absence of a regional frontal convergence (in contract to the event of the 26th), according to both the NWS and mesoscale analyses.

***31 July***

In this case, a clearly defined strong nighttime UHI was again centered directly over Atlanta in association with a generally weak (1 m/s) southwesterly regional flow, upon which a 2 m/s UHI-induced confluent-flow formed (Fig. 34). Strong UHI values (2.0-5.0 K) existed from 0000 to 0700 EDT, with a maximum over the city center at 0300 EDT. Rain then moved in from the southwest, perhaps as a squall line ahead of the approaching trailing cold front discussed above. It reached the city at 0330 EDT, and the UHI thus weakened.

Confluence is yet again found over Atlanta (Fig. 34), while calculated convergence values (Fig. 35) thus again show a strong maximum slightly downwind of the center of Atlanta of $8.5 \times 10^{-5}$ $s^{-1}$ at 0330 EDT. The convergence should be urban induced, as the synoptic front was not close to the city at this time. This nighttime convergence is strong because of fast urban induced winds that formed in the previous cloud-free (subtropical high pressure dominated) nocturnal cooling period.

GOES-8 IR thermal-images again show a significant localized area of synoptic-scale convective cloud cells moving towards Atlanta (as on 27 July), but now from the west. Cells in the part of the cloud area that passed over the city at 0245 EDT weakened (Fig. 36), while the remaining

cells continued to move eastward. This case thus may be only a weak example of the urban barrier effect.

Strong precipitation moved to the urban edge at about 0215 EDT from the west, and lasted about 2.5 hours over the city. Accumulations from 0100 to 0445 EDT show maximum values of 13 and 8 mm under the significant cloud areas just north and southwest, respectively, of Atlanta (Fig. 37).

Rain then began 130 km north of Atlanta in association with the advancing cold front discussed above; and sporadically fell until 1315 EDT. At that time, weak precipitation again started up over Atlanta, lasted for about an hour, never went beyond its southern urban boundary, and then again retreated northward. Sporadic rain fell over the urban area (never at more than one urban site at a time) for the remainder of the day and into the early morning of 1 August. This latter pattern occurred in conjunction with weak regional winds (from the south), but with no significant urban impacts (according to the GOES thermal images).

Goes-8 water vapor images are not shown, again given the synoptic precipitation for this case, as for the case of the 27th. As with all previous cases after the start of rainfall, RH values (Fig. 38) are high in areas with high precipitation values (i.e., north of city), and vise versa south of the city.

In summary, in this case the barrier effect may have again dominated the UHI/convergence effect (as on 27 July). The difference between the strength of the two effects was reduced, however, given the stronger UHI on this day. The area of maximum precipitation was thus again not over the UHI area, but was somewhat localized in the two upwind lateral areas.

***1 August***

In this case, a weak nighttime UHI was centered directly over Atlanta at 0000 EDT in association with a generally moderate (2 m/s) southwesterly regional flow, upon which an UHI-induced slightly confluent flow formed (Fig. 39). UHI values only ranged from 1.5-2.5 K (because of regional cloudiness associated with the now present trailing cold front discussed above) existed from 0000 to 0300 EDT and showed a maximum at 0000 EDT. GOES-8 IR thermal-images showed a significant localized area of synoptic-scale convective clouds moving towards Atlanta (as on 27 and 31 July), but now they came from WSW (Fig. 40a). Regional precipitation (unaffected by the city) thus existed 100 km upwind of the city center from midnight until 0315 EDT. By 0330 EDT, the rain approached the city, and thus the UHI weakened. As this early precipitation was without urban influence, the rest of the discussion of this case focuses on the period from 0330 to 1200 EDT.

By 0400 EDT, only a slight (non-UHI-induced) confluence was found over Atlanta, and thus calculated convergence values (Fig. 41) yielded a weak local maximum over Atlanta of $2.5.0x10^{-5}$ $s^{-1}$. While various equivalent (in magnitude) convergence areas are found north and south of the city, it is not possible to locate the trailing cold front that entered northern Georgia about this time (as discussed above).

The apparent division of the synoptic-scale convective cloud cells moving towards Atlanta, for which a slight beginning could be seen in the GOES-8 IR thermal-image of Fig. 40a, is clearer at 0315 EDT (Fig. 40b). The two groups of cells, like on the two other similar days, have apparently moved north and south of the city. This pattern of cloud movement towards Atlanta, followed by an apparent general (in most cases) tendency for cloud/rain elements to move around (most to the north) the city continued until 1030 EDT (Fig. 42). Note, however, that the western precipitation maximum in the figure is due to storms between 0000 and 0315 EDT, while the eastern maximum is due to those between 0330 to 1030 EDT. Note the lack of urban influence in the precipitation gradient over the city.

At 1100 EDT, the area south of Atlanta was slightly warmer than surrounding areas (Fig. 43), not due to an UHI effect but to cooling associated with the precipitation north of the city. This warm area allowed for the formation a convergence maximum of $5.0x10^{-5}$ $s^{-1}$ at 1045 EDT

(Fig. 44). A convective cloud then formed in that warm convergence area at 1115 EDT, remained there for about two hours (Fig. 40c), and produced local precipitation (Fig. 45); sporadic rain at one or two sites occurred until 1515 EDT.

Goes-8 water vapor images (again not shown) show the outflow tops of the precipitating clouds of this case, as for the 27th and 30th cases. As with all previous cases after the start of rainfall, RH values at 1100 EDT (Fig. 46) are again high in areas with high precipitation values (i.e., north of city).

In summary, in this complex (long lasting, with numerous cloud groups) case the barrier flow/cloud division effect again apparently dominated the UHI/convergence effect (as on 27 July) in the early morning hours, even though an UHI did exist before the first of many synoptic rainstorms reached the city. While GOES thermal images seem to show cloud division, no accompanying surface flow or precipitation division could be seen, as precipitation values over the city until 1030 EDT showed no urban effects.

Exclusion of the precipitation from the one cloud that moved over the city (and then rapidly developed) from Fig. 42 might have shown diverging precipitation effect on this day. A convective storm formed at 1115 EDT in a convergence zone located in a warm area south of the city that resulted from non-urban effects. Urban effects were thus minimized

on this day due to the strength and duration of the precipitation from the prevailing synoptic system. It was thus not possible to clarify any pos-sible urban precipitation effects on this storm, and it is thus not listed as an urban influenced storm in Table 2.

***3 August***

In this case, a strong nighttime UHI (maximum value of 5.0 K at 0000 EDT) again existed over Atlanta and to the northeast (Fig. 47). This extension could be due to early morning slope heating, as this is the only case during this time period. It extended into the morning hours, with a secondary maximum of 3.0 K at 0900 EDT. A weak (2.5 m/s) northeasterly regional flow existed east-northeast of Atlanta, with a confluent flow again over the city (at about 0.5 m/s).

Regional surface frontal confluence can be seen just south of Atlanta at 0800 EDT in Fig. 47 in association with the quasi-stationary cold front described above, although the front position is less apparent in the wind field 15 min latter (Fig. 48). Moderate surface convergence ($2.5 \times 10^{-5}$ $s^{-1}$ at 0815 EDT) is seen 40 km upwind (northeast) of Atlanta in the UHI extension of the previous figure. The apparent UHI-induced (northeasterly) inflow northeast of Atlanta is seen to extend to a depth of 100 m AGL in Fig. 2.

GOES-8 IR thermal-images again showed a small area of convective cloud formation on the downwind (relative to the above-PBL

southwesterly flow of Fig. 2) lateral (i.e., east) edge of Atlanta at about 0945 LST; one hour later (Fig. 49) the area is enlarged. It then advected slightly downwind during the next hour (Fig. 50), at which time a new cloud mass formed in its wake. By 1245 EDT, a similar cloud mass had formed downwind on the northern lateral edge (Fig. 51). Two hours later, the cloud on the northern edge had advected somewhat to the northeast and strengthened, while the newer of the southeastern clouds had intensified in its original location (Fig. 52). These cloud elements were apparently urban convergence induced, based on an assumed continuation of the earlier flows of Fig. 48.

Precipitation was initiated at the downwind eastern urban edge in the first small cloud element (mentioned above) at 0945 EDT, concentrated over the city for about one hour, and then was advected downwind at 1045 EDT. Accumulation over the entire period (0945-1245 EDT) shows a maximum value of 22 mm centered on the eastern edge of Atlanta (Fig. 53).

The 0945 EDT Goes-8 water-vapor image (Fig. 54), in conjunction with those before and after (both not shown), shows cloud-top vapor over the northern half of the city. After one hour (Fig. 55), the maximum water vapor has advected to an area above the downwind urban edge, i.e., over the area of the apparently urban-induced surface convergence/cloud/precipitation area. Surface RH values after precipitation onset

(Fig. 56), as expected, show maximum values in the convergence/precipitation area.

In summary, this morning precipitation event seems to have been initiated by urban UHI-induced convergence, not associated with a quasi-stationary front located by the NWS south of the city.

**4. Conclusion**

Six summer convective precipitation events over Atlanta during a nine day period in July-August 1996 were studied. Data were analyzed from one rawinsonde site, 40 mesonet and NWS sites, and satellite thermal IR and water vapor images. Observed temperature, relative humidity, and wind speed values were interpolated into gridded values, and then smoothed. Eulerian divergence values were calculated from the smoothed wind speeds, while potential temperature values were calculated from the smoothed temperature values to eliminate topographic effects on UHI values.

Results showed a general agreement in time and space between the locations of maximum UHI, confluence, convergence, cloud, relative humidity, and precipitation values for three storms that are probably urban induced (Table 2). In particular, results showed the three storms (two just after sunrise and one a few hours after noon) were probably initiated in UHI-induced convergence zones. The afternoon event occurred

during what is normally the most convective time of the day. Note that while the 1.5 m UHI for this case was centered somewhat downwind (northeast) of the city center, satellite observations by Roth et al. (1989) have shown that daytime UHI values are maximum at the ground (and not at 1.5 m) in urban centers. The convergence zone on this day was hence located directly over the city center (and to the south), and the horizontal convergence was driven by unstable SBL vertical convective motions.

The other two initiated cases occurred before establishment of unstable thermally convective SBL lapse rate conditions, and hence their convergence zones resulted from horizontal pressure gradient forces, which then forced (by mass conservation) the upward motions that produced the precipitation events. Since the maximum UHI in these two cases is displaced towards the eastern urban edge, the convergence center (and hence the precipitation center) is also likewise displaced.

The urban building barrier effect divided two of the three non-urban initiated (synoptic-scale) storms, with split-off areas moving north and south of the city, respectively. Thus by definition, the building barrier divergence effect in these cases should be more important than the UHI-induced convergence effect. The final moving synoptic storm was so complex (it started at midnight, lasted 12 hours, and consisted of many individual convective elements) that urban effects could not be discerned.

Bornstein and LeRoy (1990) have previously shown that New York City (NYC) effects either summer daytime thunderstorm formation or movement. They found convective activity initiated over the UHI convergence zone in the NYC urban center during conditions with nearly calm regional flows. Thunderstorms moving with regional flows, however, tended to divide and move around the city due to its building barrier effect.

The current Atlanta results thus apparently agree with the NYC results with respect to thunderstorm initiation and division. Note that the NYC moving storms generally occurred during late afternoon periods, only one of the current Atlanta storms occurred during this period.

The current Atlanta results, however, also show examples of an intermediate case, not specifically resolved in the NYC study, but found in other studies. This case apparently involves formation of convective cells at the downwind urban edge during periods with intermediate regional flow speeds (when the 1.5 m UHI is advected to the downwind urban edge).

Note that the storm division identified in this study is different from storm splitting. The former implies that a group of storms move in two directions from a specific location (such as upwind of city). The latter implies that a single initial storm splits into two separated supercells, given appropriate vertical wind shear conditions.

For example, modeling experiments by Weisman and Klemp (1986) have shown that strong clockwise (i.e., veering) of wind vectors below 1 km, in conjunction with a strong unidirectional shear between 1 and 7 km, favors development of a right flank storm. Although the bifurcating storms of July 27 showed stronger convective activity on the downwind right side, counterclockwise (i.e., backing) of wind vector occurred below 1 km at 1200 UTC (Fig. 2).

A factor that, however, complicates the current results, i.e., the convergence over the southeast U.S. implied by the persistent quasi-stationary/cold front shown on the daily NWS surface weather maps. This regional convergence could have created regional low speed conditions, which then allowed for formation of both the mesoscale Atlanta UHI and its urban induced convergence zone. Urban enhancement of regional convergence zones was found by McNider et al. (1998) as responsible for high ozone concentrations in southern U.S. cities.

It is, however, possible that the regional convergence implied by the daily NWS surface weather maps was only an artifact of the few urban synoptic sites in the analyses, i.e., that the indicated synoptic front was only a line (sometimes contorted) through a series of independent local urban convergence zones. Mesoscale analyses of the regional synoptic data might decide this question.

Future efforts should also involve analyses of climatological temperature and precipitation records from Atlanta to determine possible correlations between its changing UHI and precipitation fields. Such a study should follow the lead of METROMEX, and separately consider only a single storm type moving in one direction.

Re-analyses of the NWS surface weather maps for this period should be carried out for the mesoscale study area. Additionally, re-analyses should also be carried out of real-time three-dimensional LAPS meteorological diagnostic fields produced by FSL every 20 minutes during the period of the current study. Such analyses could provide additional details concerning the six events documented in the current study, as could analysis of existing NEXRAD radar data sets.

The current mesoscale UHI, surface wind velocity, convergence, and precipitation analyses should be used to validate MM5 simulations of convective thunderstorms over the Atlanta region, both those previously carried out by FSL and new ones specially designed to identify possible urban effects. Given the difficulty in producing a convective thunderstorm at a time and place that matches an observed storm, one or more of the following strategies (in order of preference) could produce a base case for such a modeling exercise:

- carry out simulations until one produces a thunderstorm at the observed time and place

> perturb RAMS at the appropriate (determined by trial and error) time and place to reproduce an observed thunderstorm

> simulate an idealized (but perturbed) thunderstorm case.

Urban and topographic influences on regional Atlanta temperature, transport, convergence, and precipitation patterns should then be evaluated by comparison of base case results with those from additional simulations in which topographic and/or urban influences are sequentially eliminated. FSL-LAPS meteorological fields could be used as initial conditions for these simulations.

Finally, the current results, as well as the proposed MM5 results, could be used to design a detailed field study to gather the data necessary to answer some of the (general and site-specific) questions related to urban effects on precipitation raised by the current study. Such a study should include a strong component of vertical measurement platforms (e.g., radar, sodar, Lidar, profiler, tetroon, tracer, and aircraft), such as with the SCOS'97 study over the Los Angles basin. Such a study should also include both summertime and wintertime storms.

## References


Achtemeier, P., 1983: The relationship between the surface wind field and convective precipitation over the St. Louis area. *J. Appl. Meteor.*, **22**, 982-99.

Al-Wali K. I., and P. J. Samson, 1996: Preliminary sensitivity analysis of urban airshed model simulations to temporal and spatial availability of boundary layer wind measurements. *Atmos. Environ.*, **30**, 2027-2042.

AMS, 1972: Conference on Urban Environment and Second Conference. on Biometeorology. AMS Preprint Volume, 31 Oct.-2 Nov., Philadelphia, PA, 443 pp.

AMS, 1987: *Modeling the Urban Boundary Layer.* Amer. Meteor. Soc., Boston, MA, 542 pp.

AMS, 1998: Second Urban Environment and 13th Conference on Biometeorology and Aerobiology. AMS Preprint Volume, 2-6 Nov., Albuquerque, NM, 369 pp.

Atkinson, B. W., 1968: A preliminary examination of the possible effect of London's urban area on the distribution of thunder rainfall 1951-60. *Trans. Pap. Inst. Brit. Geogr. Publ.*, **48,** 118 pp.

Atkinson, B. W., 1971: The effect of an urban area on precipitation from a moving thunderstorm. *J. Appl. Meteor.*, **10,** 47-55.

Atkinson, B. W., 1975: The mechanical effect of an urban area on convective precipitation. Occasional Paper 3, Dept. of Geography, Queen Mary College, University of London, 27 pp.

Atkinson, B. W., 1977: Urban effect on precipitation: an investigation of London's influence on the severe storm in August 1975. Occasional Paper 8, Dept. of Geography, Queen Mary College, University of London, 31 pp.

Bitan, A., 1989: Fourth international Conference on Urban Climate, Planning and Building. Proceedings, 2 Vols., 6-11 November, Kyoto, Japan, Elsevier Sequoia, Lousanne, Switzerland, 1114 pp.

Bornstein, R., 1968: Observations of the urban heat island effect in New York City. *J. Appl. Meteor.*, **7**, 575-582.

Bornstein, R., 1987: Mean diurnal circulation and thermodynamic evolution of urban boundary layers. In Modeling the Urban Boundary Layer, A. Blackadar, Ed., AMS, Boston, MA, 53-93.

Bornstein, R., and A. D. Johnson, 1977: Urban-rural wind velocity differences. *Atmos. Environ.*, **11**, 597-604.

Bornstein R., and G. M. Leroy, 1990: Urban barrier effects on convective and frontal thunderstorms. Preprint volume, 4th Conference on Mesoscale Processes, AMS, 25-29 June, Boulder, CO, 188-192.

Bornstein, R., and T. R. Oke, 1981: Influence of pollution on urban climatology. *Adv. Environ. Soc. and Engin.*, **2**, 171-202.

Bornstein, R., and W. T. Thompson, 1981: Effects of frictionally retarded sea breeze and synoptic frontal passes on sulfur dioxide concentrations in NYC. *J. Appl. Meteor.*, **20**, 843-858.

Braham, R. R., Jr., 1981: Urban precipitation process. METROMEX: A Review and Summary. *Meteor. Monogr.*, **18,** 75-115.

Cermak, J., A. Davenport, E. Plate, and D. Viegas, 1995: Wind Climate in Cities. Kluwer Academic Publishers, Dordrecht, Germany, 772 pp.

Chameides. W. L., and E. B. Cowling, 1995: The state of the southern oxidants study: policy-relevant findings in ozone pollution re-search, North Carolina State Univ. Report, Raleigh, NC, 89 pp.

Changnon, S. A., 1961: A climatological evaluation of precipitation patterns over an urban area. Preprint Volume, Air Over Cities Conference, U.S. PHS, SEC Tech. Report A62-5, 37-67.

Changnon, S. A., 1968: The La Porte weather anomaly - fact or fiction? *Bull. Amer. Meteor. Soc.*, **49,** 4-11.

Changnon, S., A., 1970: The La Porte precipitation anomaly. Reply. *Bull. Amer. Meteor. Soc.*, **51,** 337-342.

Changnon, S., A., 1977: La Porte again: a new anomaly. *Bull. Amer. Meteor. Soc.*, **58,** 1069-72.

Changnon, S. A., 1980: Evidence of urban and lake influences on precipitation in the Chicago area. *J. Appl. Meteor.*, **19,** 1137-1159.

Changnon, S. A., 1992: Inadvertent weather modification in urban areas: lessons for global climate change. *Bull. Amer. Meteor. Soc.*, **73,** 619-27.

Changnon, S. A., and F. A. Huff, 1977: La Porte again: A new anomaly. *Bull. Amer. Meteor. Soc.*, **58,** 1069-1072.

Changnon, S. A., R. G. Semonin, A. H. Auer, R. R. Braham, Jr., and J. M. Hales, 1981: *METROMEX: A review and summary. Meteor. Monogr.*, **18,** 181 pp.

Changnon, S. A., R. Shealy, and R. Scott, 1991: Precipitation changes in fall, winter, and spring caused by St. Louis. *J. Appl. Meteor.*, **30,** 126-34.

Clark, R., 1979: A hydrologic reanalysis of the La Porte anomaly. *Bull. Amer. Meteor. Soc.*, **60,** 415-421.

Daley, R., 1991: *Atmospheric data analysis.* Cambridge Univ., Atmospheric and Space Science Series, No. 2., 457 pp.

Douglas, S., C. Steiner, S. Shepard, A. Hudischewskyj, L. Gardner, N. K. Lolk, J. Morgan, and J. Haney, 1994: Final report: comparison of the UAM-IV and UAM-V photochemical models for three Atlanta-area ozone episodes. Systems Applications International San Rafael, CA, Report No. SYSAPP-94/106, 320 pp.

Gaffen, D., and R. D. Bornstein, 1988: Case study of urban interactions with a synoptic scale cold front. Landsberg Memorial Volume, *Meteor. and Atmos. Phys*, **38,** 185-194.

Dowling, N., and J. Knox, 1996: Supercities: Environmental Quality and Sustainable Development. Special Issue, *Atmos. Environ.* **30,** 675-818.

Fitzgerald, J. W., and P. A. Spyers-Duran, 1973: Changes in cloud nucleus concentration and cloud droplet size distribution associated with pollution from St. Louis. *J. Appl. Meteor.,* **12,** 511-516.

Gaffen, D., and R. D. Bornstein, 1988: Case study of urban interactions with a synoptic scale cold front. Landsberg Memorial Volume, *Meteor. and Atmos. Phys*, **38,** 185-194.

Garbesi, K., H. Akbari, and P. Martien, 1989: Proceedings of The Heat Island Workshop, 23-24 Feb., LBNL Report, Berkeley, CA, 250 pp.

Goldreich Y., and A. Manes, 1979: Urban effects on precipitation patterns in the Greater Tel-Aviv area. *Arch. Met. Geoph. Biokl.*, Ser. B, **27**, 213-224.

Grimmond, S., H. Cleugh, and T. Oke, 1991: An objective urban heat storage model and its comparison with other schemes. *Atmos. Environ.*, **25B,** 311-26.

Hafner, J., and S. Q. Kidder, 1999: Urban heat island modeling in conjunction with satellite-derived surface/soil parameters. *J. Appl. Meteor.*, **38,** 448-465.

Harnack, R. P., and H. E. Landsberg, 1975: Selected cases of convective precipitation caused by the metropolitan area of Washington, D. C. *J. Appl. Meteor.*, **14,** 1050-1060.

Hidore, J., 1971: More on the La Porte fallacy. *Bull. Amer. Meteor. Soc.*, **52**, 573-4.

Holzman, B. G., 1971: More on the La Porte fallacy. *Bull. Amer. Meteor. Soc.*, **52,** 572-573.

Holzman, B. G., and H. C. S. Thom, 1970: The La Porte precipitation anomaly. *Bull. Amer. Meteor. Soc.*, **51,** 335-337.

Hoogenoom, G., 1996: The Georgia Automated Environmental Monitoring Network. Proceedings, 22nd conference on Agriculture and Forest Meteorology, Atlanta, CA, AMS, 343-6.

Huff, F. A., and S. A. Changnon, 1973: Precipitation modification by major urban areas. *Bull. Amer. Meteor. Soc.*, **54,** 1220-1232.

Huff, F. A., and S. A. Changnon, 1986: Potential urban effect on precipitation in winter and transition seasons at St. Louis, Missouri. *J. Climate Appl. Meteor.*, **25,** 1887-1906.

Imamura, I., 1991: Observational studies of urban heat island character-istics in different climate zones. Ph.D. dissertation, Institute of Geoscience, University of Tsukuba, Japan,156 pp.

Imamura, I., and R. Bornstein, 1992: Review of urban climate and dispersion. Final report to U. S. Army, Atmospheric Sciences Laboratory, Contract No. DAA103-86-D-0001, 259 pp.

Kuttler, W., T. Oke, and R. Bornstein, 1999: International Conference on Urban Climatology (ICUC'96). Atmos. Environ., **33,** 3877-4222.

Landsberg, H. E., 1981: *The Urban Climate.* International Geophys. Series 28, Academic Press, New York, 275 pp.

Loose, T., and R. Bornstein, 1977: Observations of mesoscale effects on frontal movement through an urban area. *Mon. Wea. Rev.,* **105,** 567-571.

Machta, L., J. Angell, and J. Korshover, 1977: Demise of the La Porte precipitation anomaly. *Bull. Amer. Meteor. Soc.,* **58,** 1068-1069.

Marsik, F. J., K. W. Ficher, T. D. McNonald, and P. J. Samson, 1995: Comparison of methods for estimating mixing height used during the 1992 Atlanta Field Intensive. *J. Appl. Meteor.,* **34,** 1802-1814.

McNider, R., W. Norris, A. Song, S. Mueller, and R. Bornstein, 1998: The role of convergence zones in producing extreme concentration events. Preprint Vol., 10TH Joint AMS/AWMA Conference on the Applications of Air Pollution Meteorology, Phoenix, AZ, 68-72.

Nowacki, P., P. J. Samson, and S. Sillman, 1996: Sensitivity of urban airshed model (UAM-IV) calculated air pollutant concentrations to the vertical diffusion parameterization during convective meteorological situations. *J. Appl. Meteor.*, **35,** 1790-1803.

Panayioyou, C., 1995: Application of the prognostic URBMET/TVM meso-β meteorological model to Phoenix, Arizona. M.S. Thesis, San Jose State University, 85 pp.

Parry, M. 1956: An 'urban rainstorm' in the Reading area. *Weather,* **11,** 41-48.

Quattrochi, D., J. Luvall, M. Estes, C. Lo, S. Kidder, J. Hafner, H. Taha, R. Bornstein, R. Gillies, and K. Gallo, 1998: Project Atlanta: A study of how the urban landscape affects meteorology and air quality through time. Preprint Vol., Second AMS Urban Environment Conference, Albuquerque, NM, 104-7.

Roth, M., 1998: Vertical structure of turbulence over cities. Preprint Vol., Second AMS Urban Environment Conference, Albuquerque, NM, 121-124.

Roth, M., Oke, T. R., and Emery, W. J., 1989: Satellite-derived urban heat island from three coastal cities and the utilization of such data in urban climatology. *Int. J. Rem. Sens.* **19**, 105-115

Sanderson, M., and R. Gorski, 1978: The effect of metropolitan Detroit-Windsor on precipitation. *J. Appl. Meteor.*, **17,** 423-427.

Sanderson, M., I. Kumanan, T. Tanguay, and W. Schertzer, 1973: Three aspects of the urban climate of Detroit-Windsor. *J. Appl. Meteor.*, **12,** 629-638.

Selover, N., 1997: Convective precipitation patterns in an urban desert – topographic or urban influences? AAG Conf., Fort Worth, TX, 78-82.

Spar, J., and P. Romberg, 1968: Note on an apparent trend in annual precipitation at New York City. *Mon. Wea. Rev.*, **96,** 169.

Taha, H., 1998: Impacts of cool cities on air quality: A preliminary modeling assessment for Nashville, Dallas, and Atlanta. Lawrence Berkeley National Lab., Report No. 42256, Berkeley, CA, 21 pp.

Taha, H., 1999: Modifying a mesoscale meteorological model to better incorporate urban heat storage: a bulk-parameterization approach. *J. Appl. Meteor.*, **38**, 466-473.

Tsutsumi, J., and R. Bornstein, 1996: Conference on the Urban Thermal Environment Studies in Tohwa (CUTEST). Special Issue, *Atmos. Environ.*, **30,** 359-544.

Weisman, M., and J. Klemp, 1986: Characteristics of isolated convective storms. In *Mesoscale Meteorology and Forecasting*, Ed. By P. Ray, AMS, Boston, MA, 331-358.

Westcott N. E., 1995: Summertime cloud-to-ground lightning activity around major Mid-west urban areas. *J. Appl. Meteor.*, **34,** 1633-42.

WMO, 1968: Urban climates. Technical Note 108. Proceedings of the Symposium on Urban Climates and Building Climatology, Brussels, WMO/WHO, 361 pp.

WMO, 1986: Urban Climatology and its Applications with Special Regard to Tropical Areas. WMO Report No. 652, 534 pp.

WMO, 1990: Proceedings of the International Symposium on Urban Climate, Air Pollution and Planning in large Tropical Cities, Guadalajara, Mexico, 25-29 Nov. 1990, 149 pp.

WMO, 1994: Report of the Technical Conference on Tropical Urban Climates, 28 March-2 April 1993, Dhaka, Bangladesh, 588 pp.

## Appendix: List of Symbols

| | |
|---|---|
| a, b | smoothing coefficients |
| C | convergence (D < 0) |
| D | divergence |
| K | number of nearby sites used in interpolation scheme |
| k | summation index |
| $r_i$ | vector to i-th analysis point |
| $r_k$ | vector to k-th observation point |
| s | any parameter |
| $s_a$ | objective-analysis value of s |
| $s_o$ | observed value of s |
| $\tilde{s}$ | smoothed value of s |
| T | temperature |
| t | time |
| u, v | eastward and northward wind speed component, respectively |
| $w_{ik}$ | weight of observation point $r_k$ on analysis point $r_i$ |
| x, y | east-west and south-north coordinate, respectively |
| $z_0$ | roughness length |
| $z_t$ | topographic height |

## Appendix: List of Symbols (continued)

| | |
|---|---|
| (m, n) | general grid index |
| (i, j) | specific grid index |
| $\Delta r_{ik}$ | distance from $r_i$ to $r_k$ |
| $\Gamma_D$ | dry adiabatic lapse rate |
| $\theta$ | potential temperature |

Table 1. Urban Cloud and Precipitation Studies

| Reference | City | Data type / Period | Precipitation types or indicators | Urban precipitation alterations | Urban storm alterations |
|---|---|---|---|---|---|
| Parry (1956) | Reading, England | Case study 06/22/51 | Convective | Enhancement over city | Not investigated |
| Changnon (1961) | Champaign-Urbana | Seasonal climatological 1950-59 | All types | Seasonal enhancement over downwind urban edge, except for summer max over city center | Not investigated |
| Changnon (1968) | Chicago-La Porte | Warm season and annual climatological 1951-65 | All types, with thunderstorm focus | Annual and warm season enhancement 48 km downwind | Thunderstorm frequency enhancement 48 km downwind |
| Atkinson (1968) | London | Seasonal climatological 1951-60 | All types, with thunderstorm focus | Enhancement over city center in summer | Increased thunderstorm frequency |
| Atkinson (1971) | London | Case study 09/09/55 | Moving thunderstorm | Max over city | Cloud growth over city |

Table 1. Urban Cloud and Precipitation Studies (continued)

| Reference | City | Data type / Period | Precipitation types or indicators | Urban precipitation alterations | Urban storm alterations |
|---|---|---|---|---|---|
| Huff and Changnon (1973) | Eight US cities | Summer climatelogical | Thunderstorm | Urban enhancement: 16-50 km downwind of 3 and over urban of 3. Indeterminate or none at 2 | Thunder frequency enhancement at six cities; no apparent enhancement at two |
| Sanderson et al. (1973) | Detroit-Windsor | Seasonal Climatelogical 1961-69 | All types | Only large summer enhancement over urban area | Not investigated |
| Atkinson (1975) | London | Case study 09/01/60 | Convective | Max over city | Cloud growth over city |
| Harnack and Landsberg (1975) | Washington, D.C. | Case studies 1972 & 1973 | Three summer shower cases | Max over city or just downwind | Cloud formation over city |
| Atkinson (1977) | London | Case study 08/14/75 | Severe thunderstorm | Max over downwind part of city | Cloud growth over city |

Table 1. Urban Cloud and Precipitation Studies (continued)

| Reference | City | Data type / Period | Precipitation types or indicators | Urban precipitation alterations | Urban storm alterations |
|---|---|---|---|---|---|
| Sanderson and Gorski (1978) | Detroit-Windsor | Seasonal Climatological 1970-75 | All types | Max over upwind, downwind, or city center | Increase number of precip days |
| Goldreich and Manes (1979) | Tel-Aviv | Climatological 1870-1939 | All types | Enhancement over city and downwind | Shift in peak precip towards fall |
| Changnon (1981) | Chicago | Seasonal climatological and summer case studies 1931-78 | All types | Increased in all seasons over 40 years; except summer decreased at some sites over last 15 years. Summer max at downwind urban edge | Summer thunderstorms more frequent over city |
| Changnon et al. (1981) | St. Louis | Summer climatological 1971-75 | Convective | Downwind max | Not investigated |

Table 1. Urban Cloud and Precipitation Studies (continued)

| Reference | City | Data type / Period | Precipitation types or indicators | Urban precipitation alterations | Urban storm alterations |
|---|---|---|---|---|---|
| Bornstein and Leroy (1990) | New York City | Climatelogical (daytime) 08/77 and 07/78 | Convective (radar echo activity) | Not investigated | Urban max for stationary echoes, Moving echoes bifurcate around city |
| Changnon et al. (1991) | St. Louis | Seasonal Climatological (except summer) 1971-75 | All types | Enhancement downwind for fall and spring. Little change for winter | Not investigated |
| Westcott (1995) | 16 Midwest cities | Summer climatelogical 1989-92 | Lightning activity | Not investigated | Frequency enhancement over and downwind of many cities |
| Selover (1997) | Phoenix | Summer climatelogical 1930-94 | Convective | City center rain days reduced between 1965 and 1994 | Moving storms avoided city center |

Table 1. Urban Cloud and Precipitation Studies

| Reference | City | Data type / Period | Precipitation types or indicators | Urban precipitation alterations | Urban storm alterations |
|---|---|---|---|---|---|
| Parry (1956) | Reading, England | Case study 06/22/51 | Convective | Enhancement over city | Not investigated |
| Changnon (1961) | Champaign-Urbana | Seasonal climatological 1950-59 | All types | Seasonal enhancement over downwind urban edge, except for summer max over city center | Not investigated |
| Changnon (1968) | Chicago-La Porte | Warm season and annual climatological 1951-65 | All types, with thunderstorm focus | Annual and warm season enhancement 48 km downwind | Thunderstorm frequency enhancement 48 km downwind |
| Atkinson (1968) | London | Seasonal climatological 1951-60 | All types, with thunderstorm focus | Enhancement over city center in summer | Increased thunderstorm frequency |
| Atkinson (1971) | London | Case study 09/09/55 | Moving thunderstorm | Max over city | Cloud growth over city |

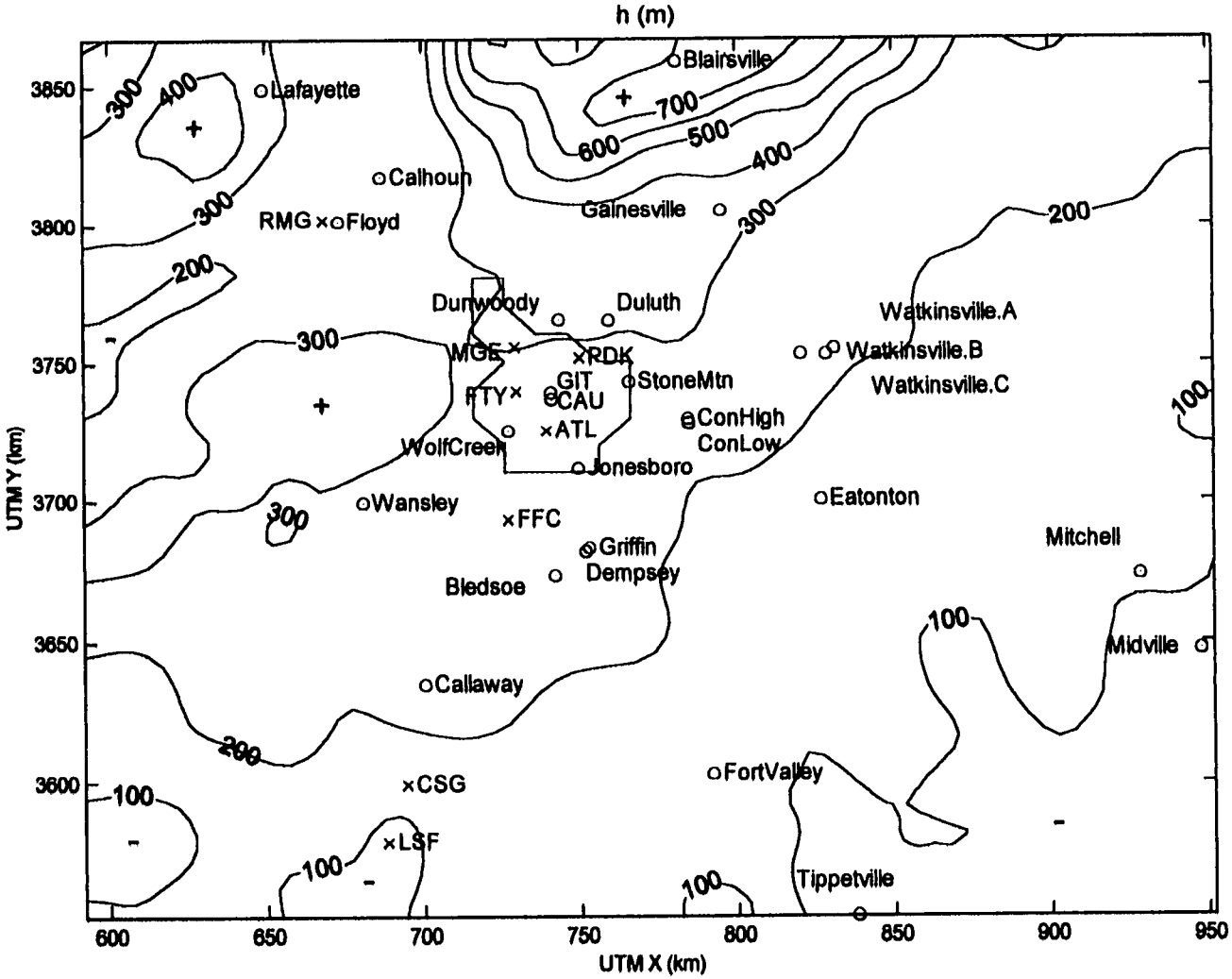
h (m)
Blairsville
Lafayette
Calhoun
Gainesville
RMG
Floyd
Dunwoody
Duluth
Watkinsville.A
Watkinsville.B
Watkinsville.C
MGE
RDK
GIT
StoneMtn
FTY
CAU
ATL
ConHigh
ConLow
WolfCreek
Jonesboro
Wansley
FFC
Eatonton
Griffin
Dempsey
Bledsoe
Mitchell
Midville
Callaway
CSG
FortValley
LSF
Tippetville
UTM Y (km)
UTM X (km)

Figure 1

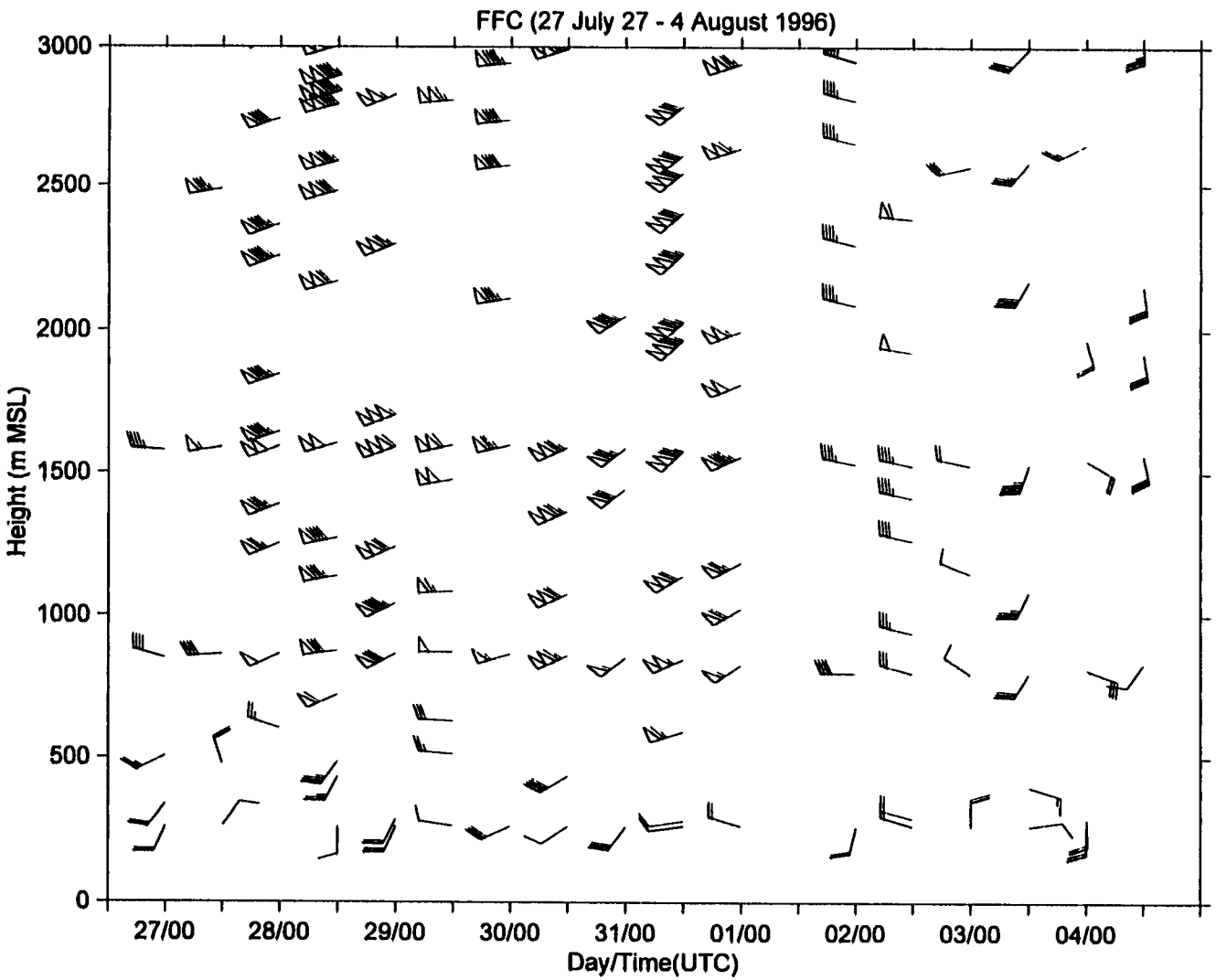
FFC (27 July 27 - 4 August 1996)
Height (m MSL)
3000
2500
2000
1500
1000
500
0
27/00
28/00
29/00
30/00
31/00
01/00
02/00
03/00
04/00
Day/Time(UTC)

Figure 2

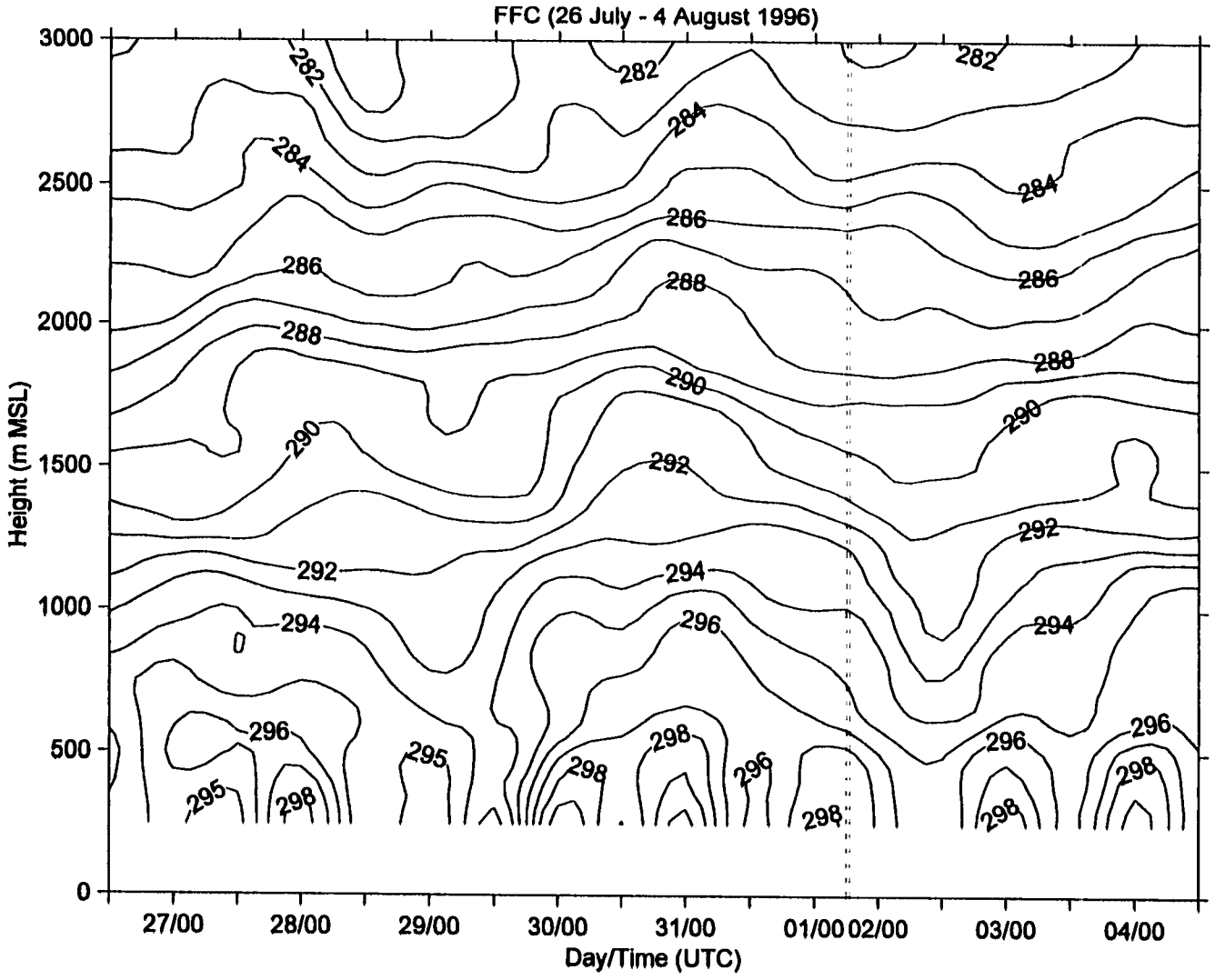
FFC (26 July - 4 August 1996)
Height (m MSL)
3000
2500
2000
1500
1000
500
0
27/00
28/00
29/00
30/00
31/00
01/00
02/00
03/00
04/00
Day/Time (UTC)
282
284
286
288
290
292
294
296
295
298

Figure 3

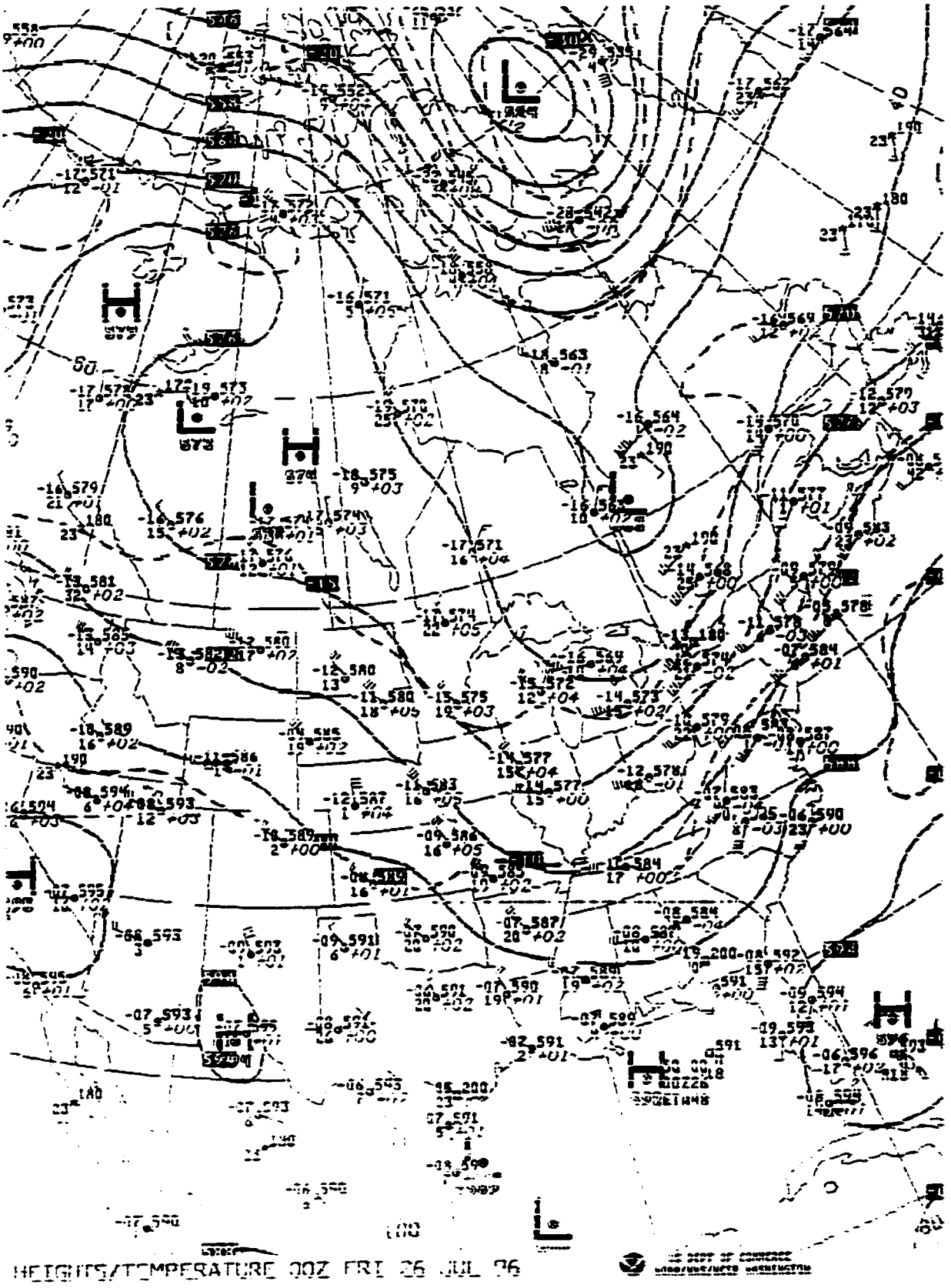


Figure 4

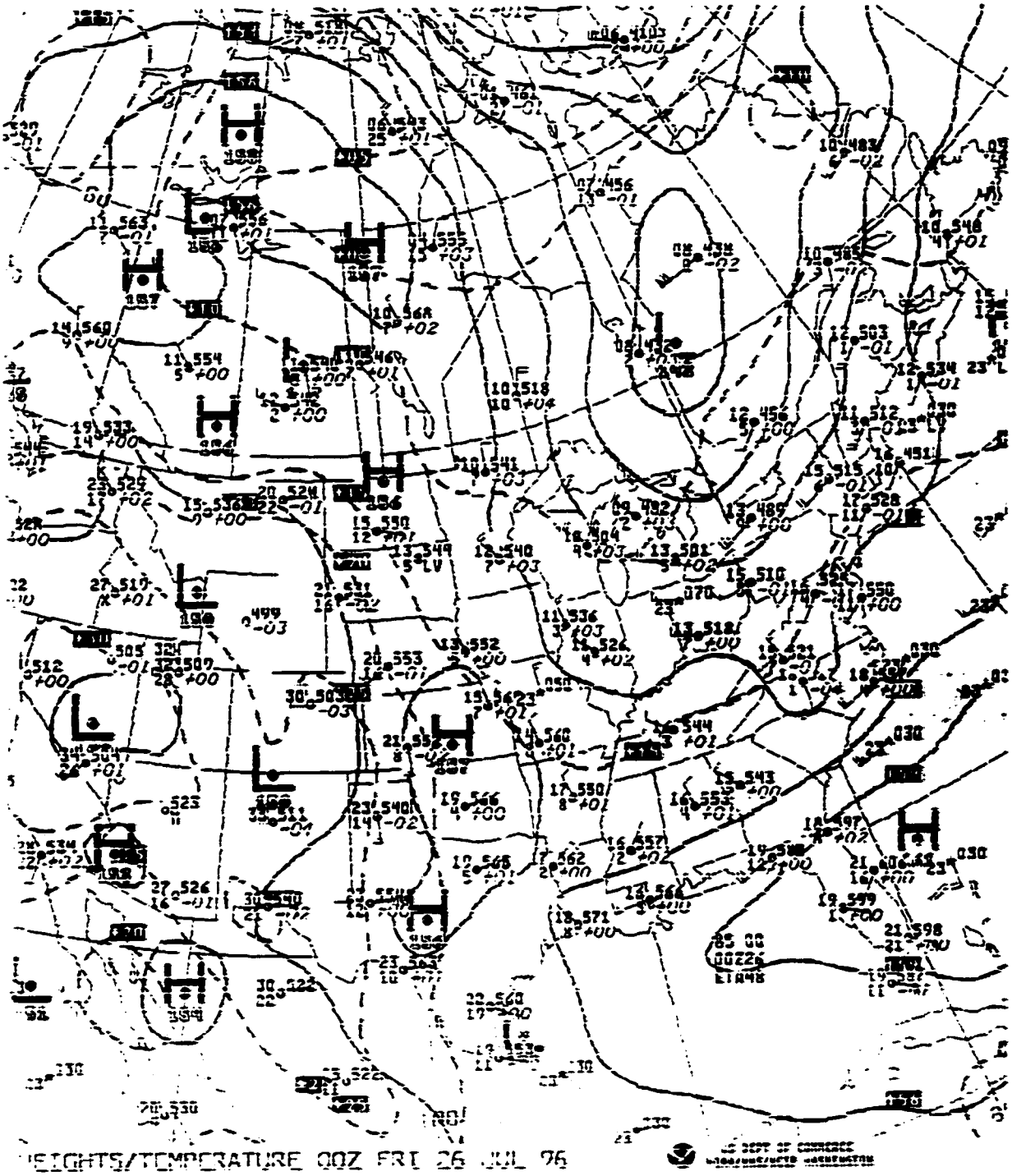


Figure 5

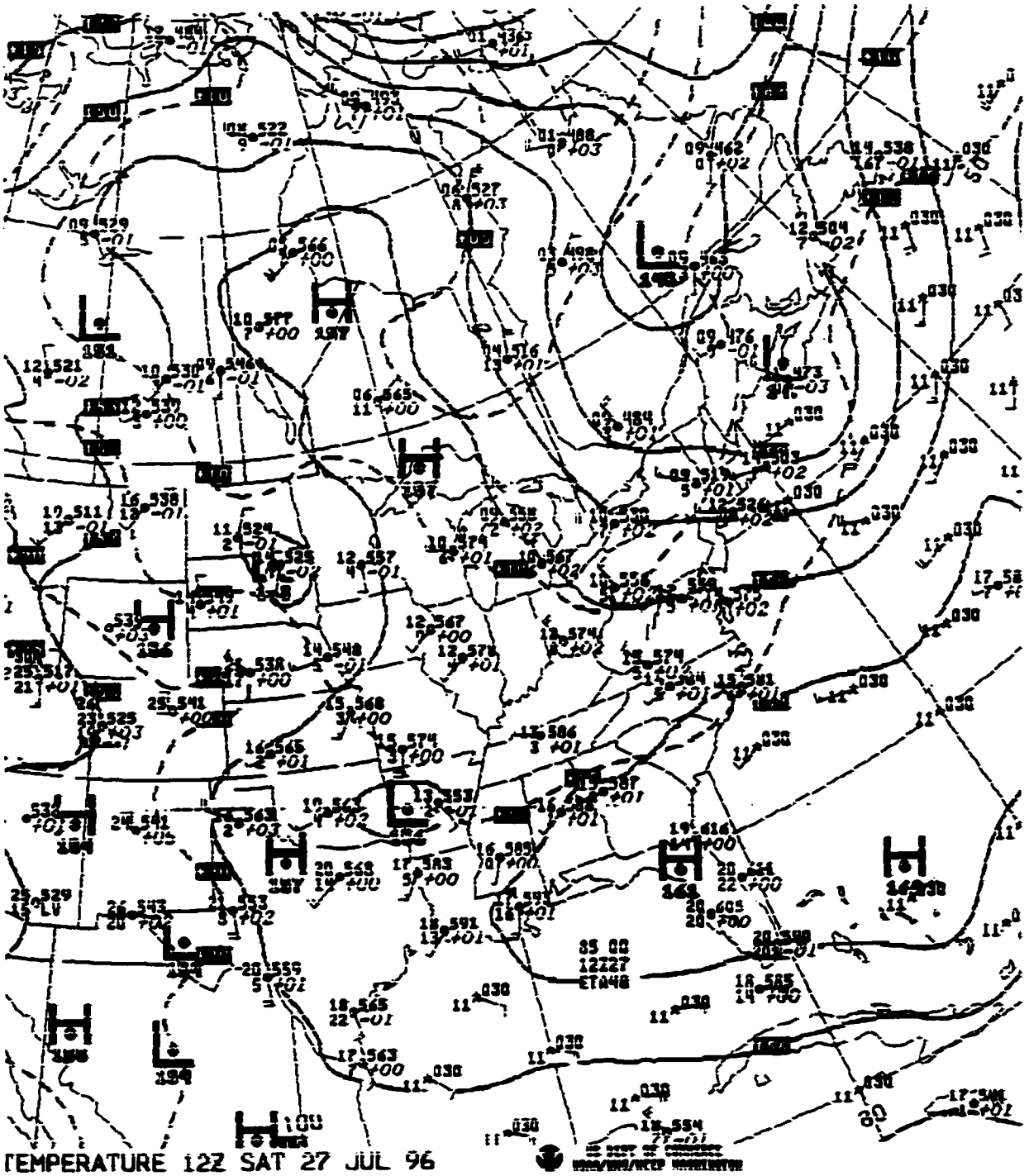


Figure 6

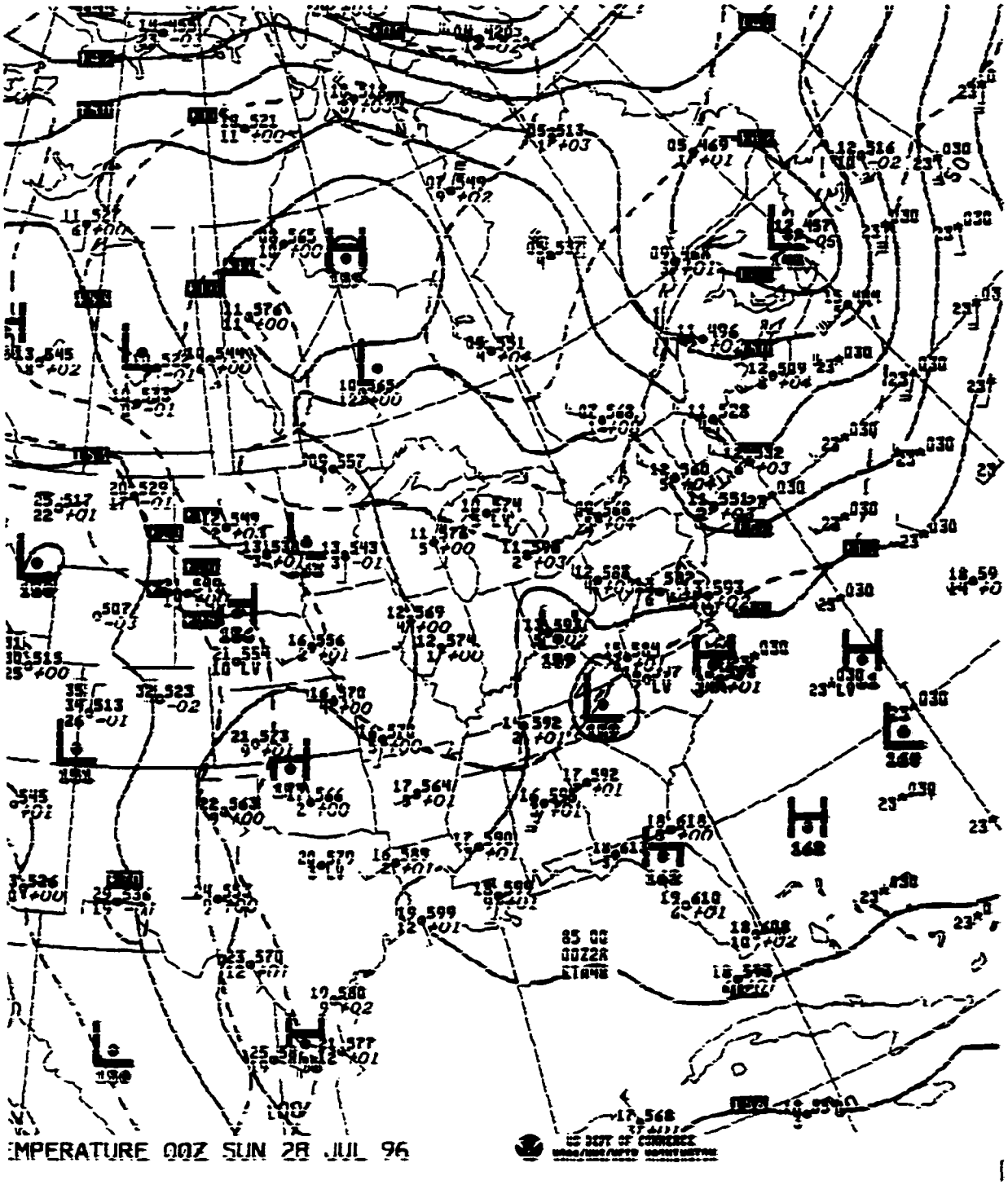


Figure 7

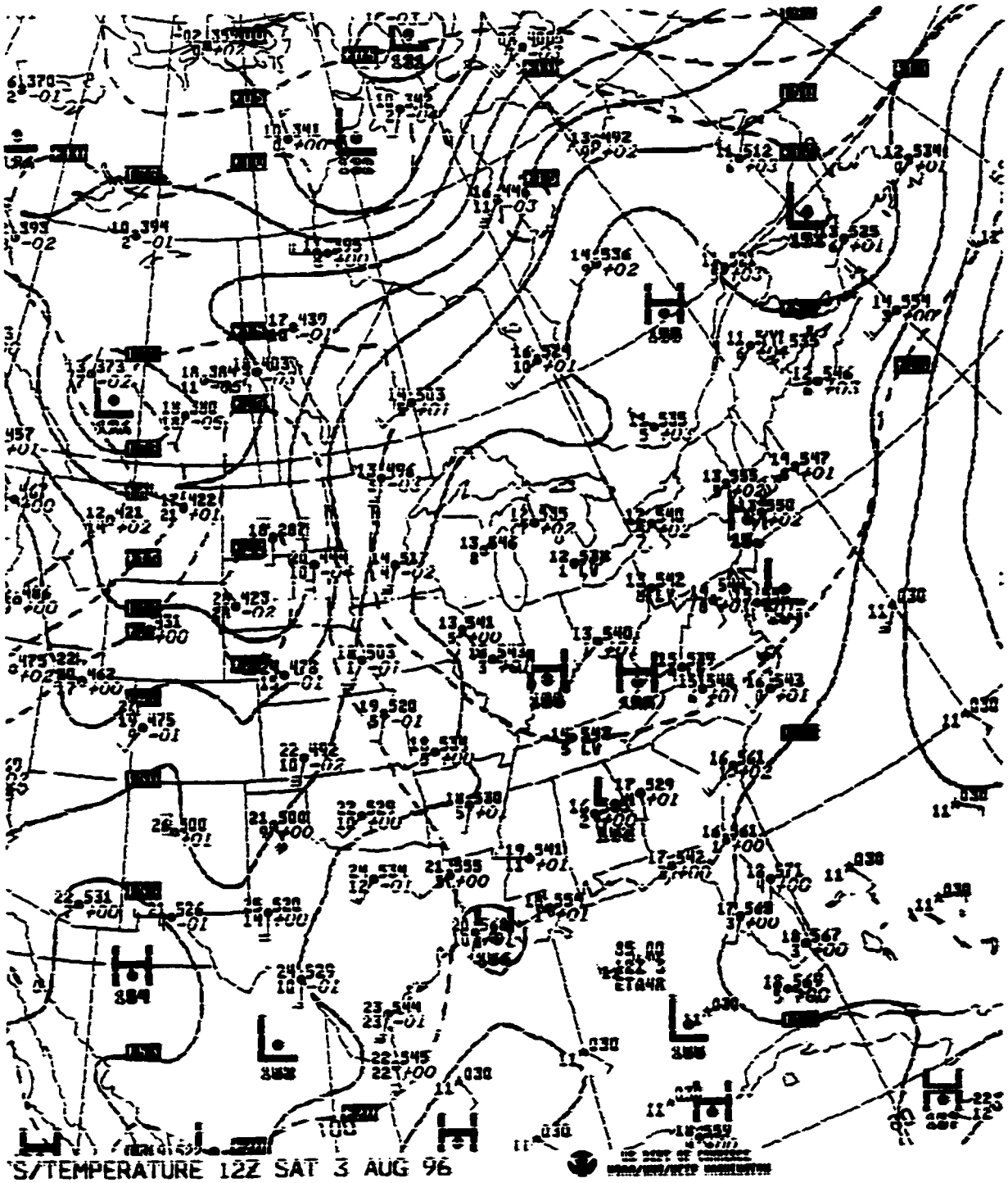


Figure 8

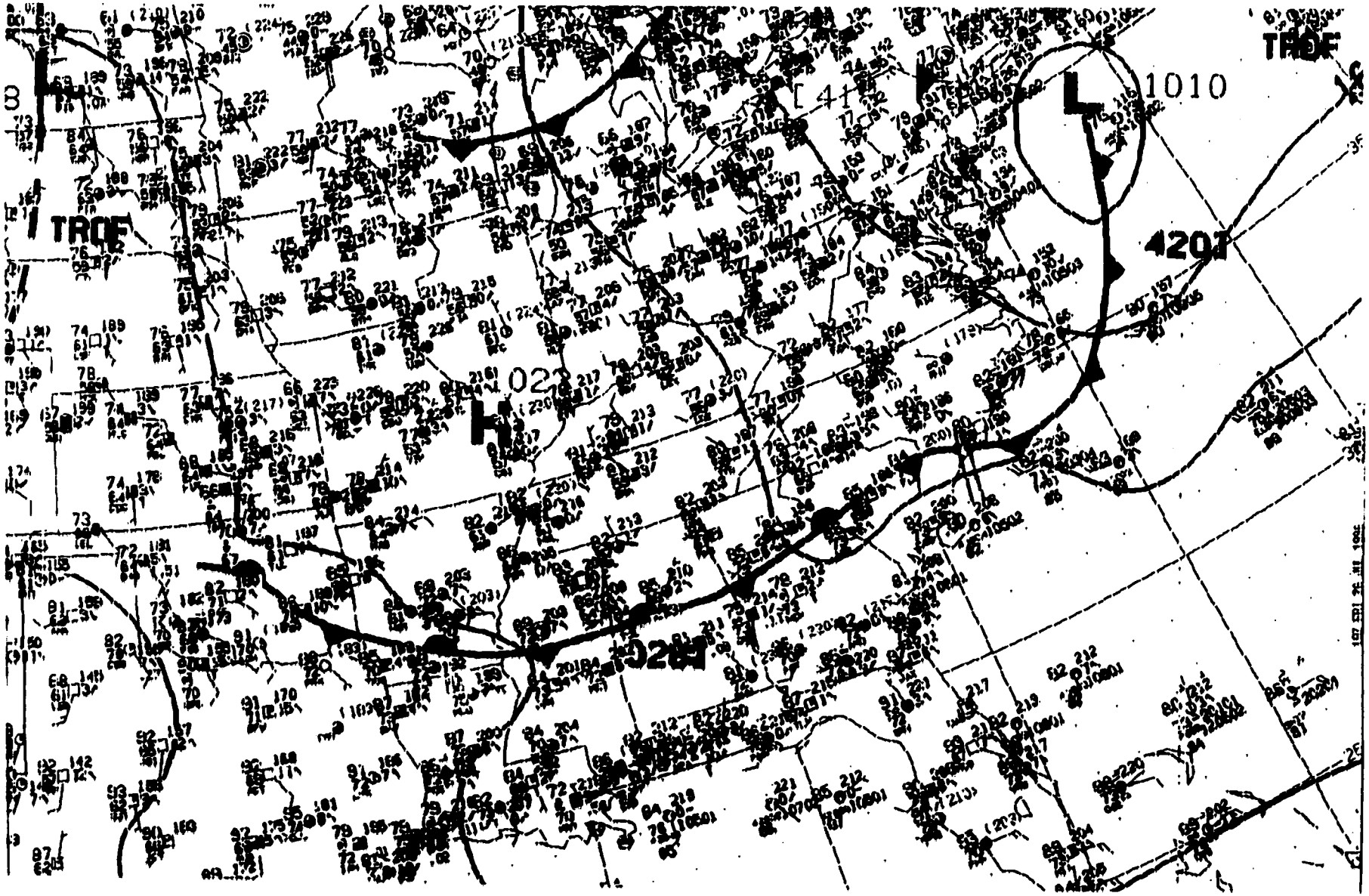


Figure 9

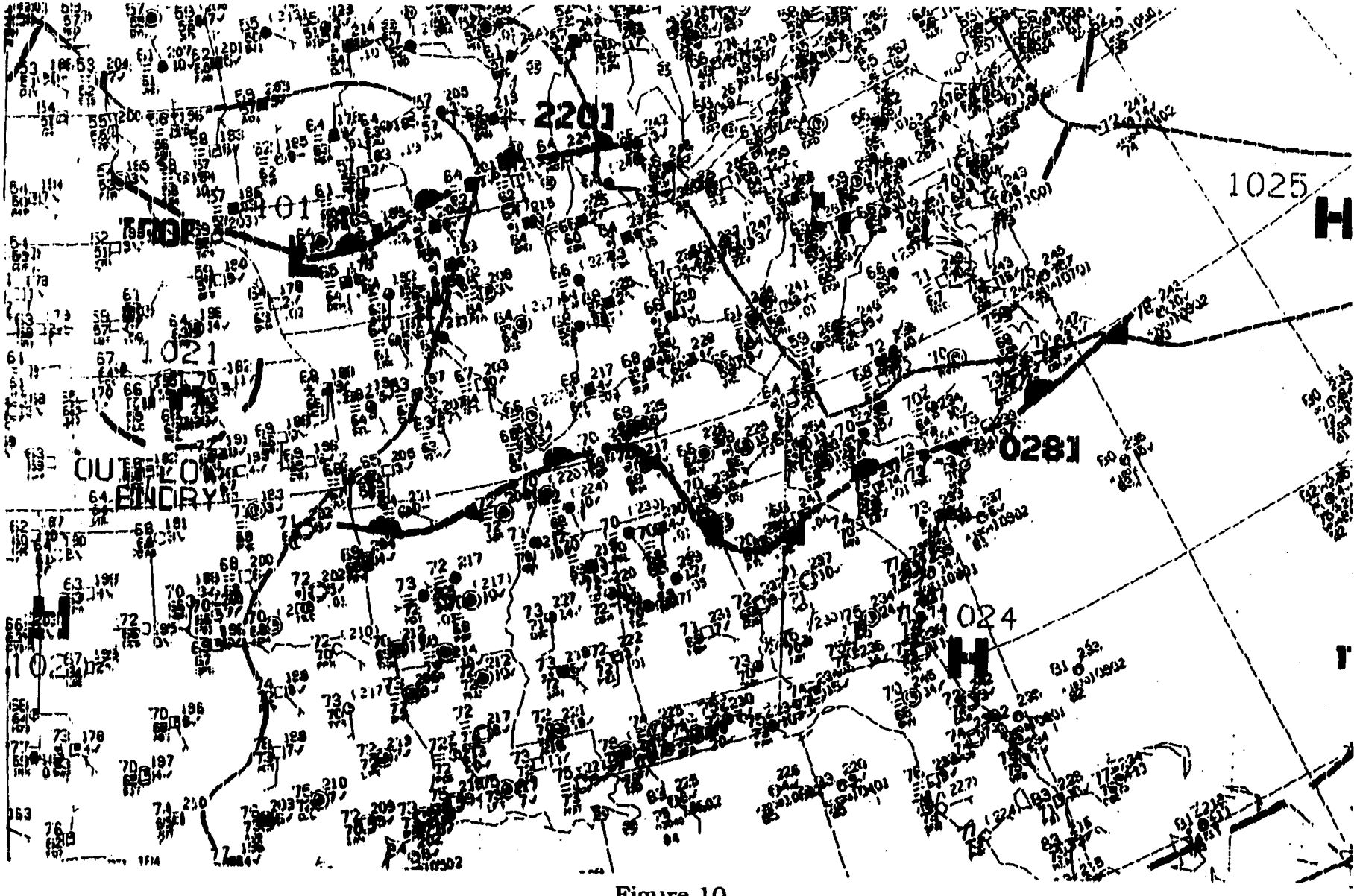


Figure 10

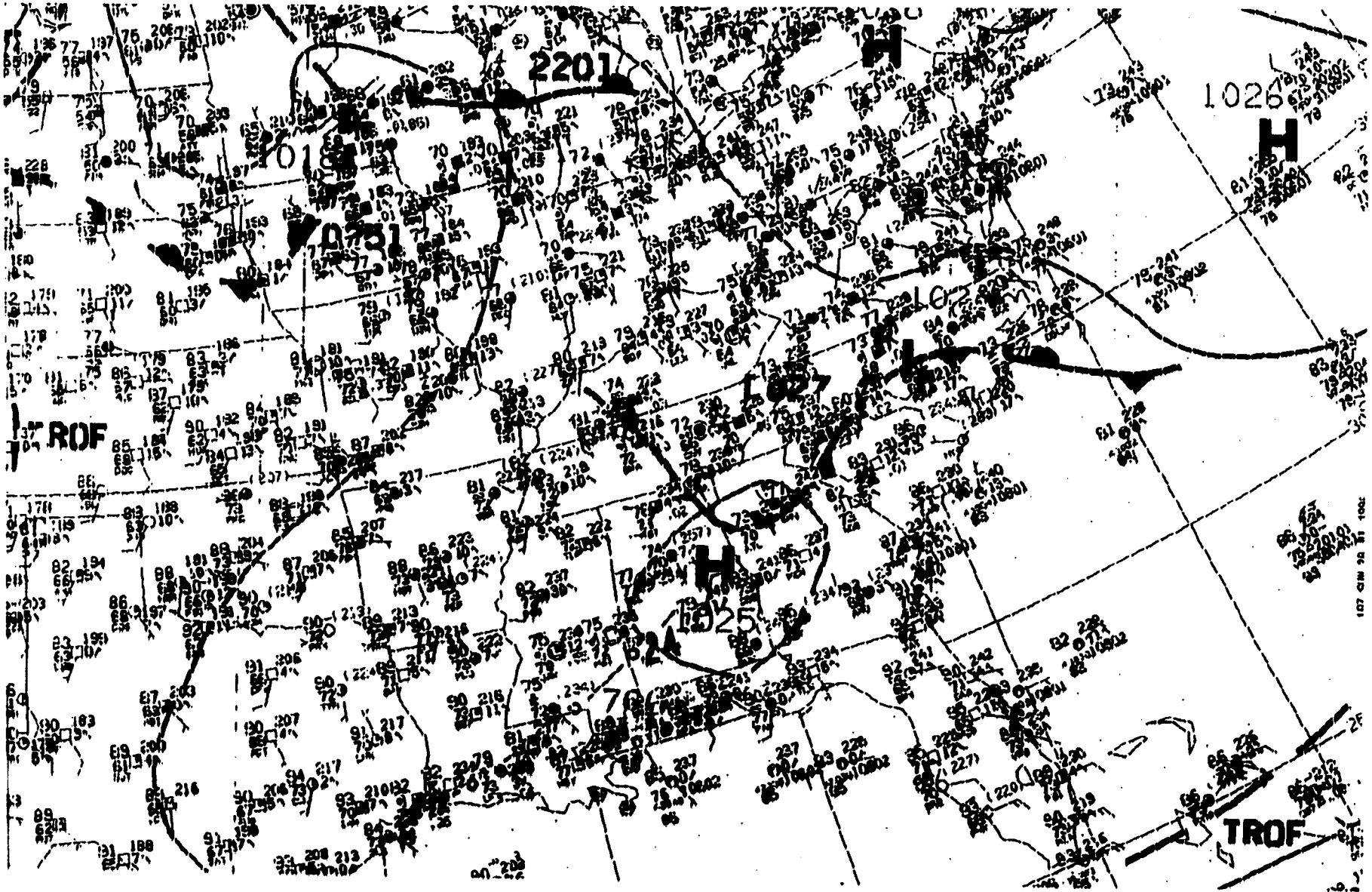


Figure 11

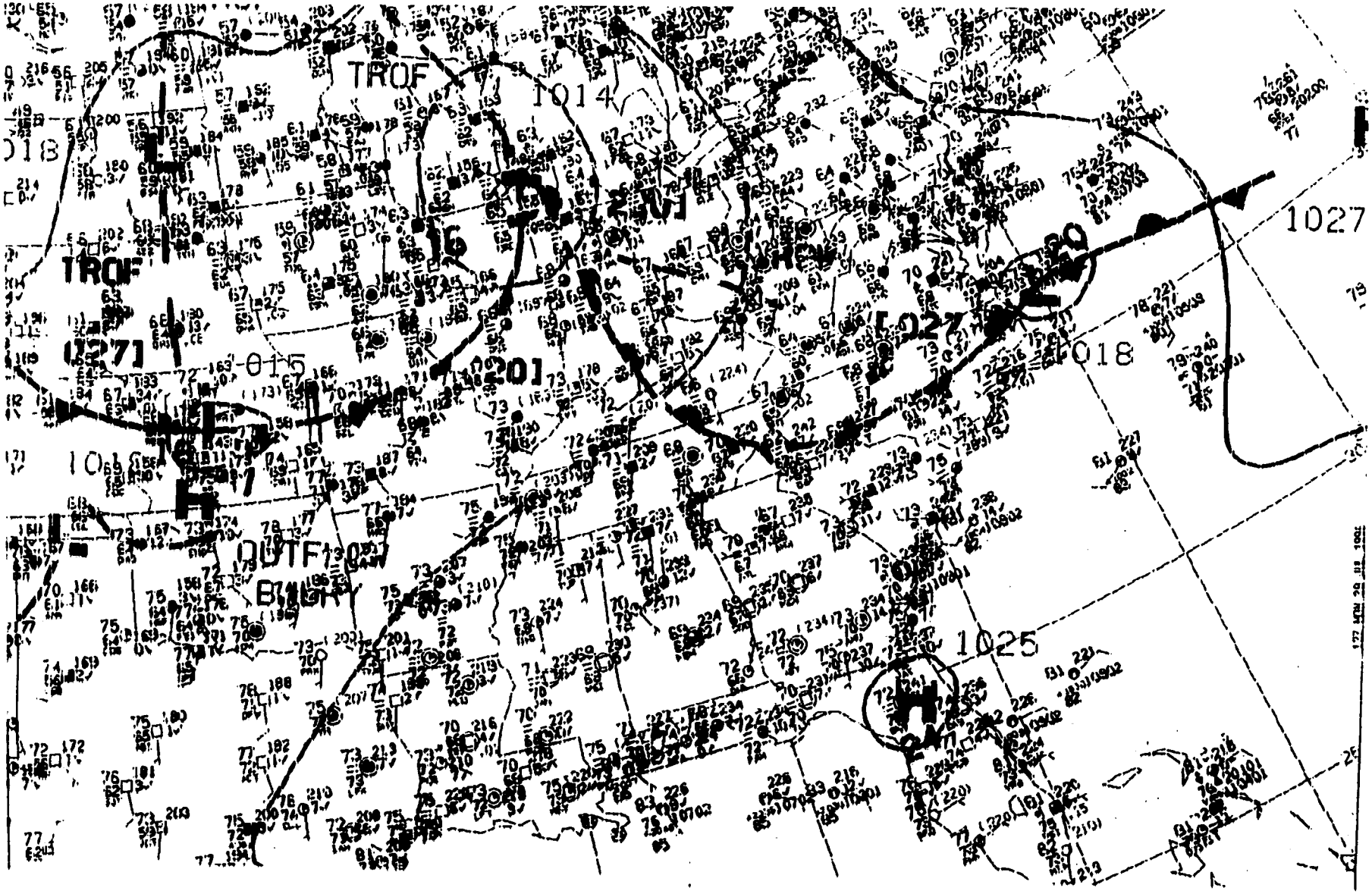


Figure 12

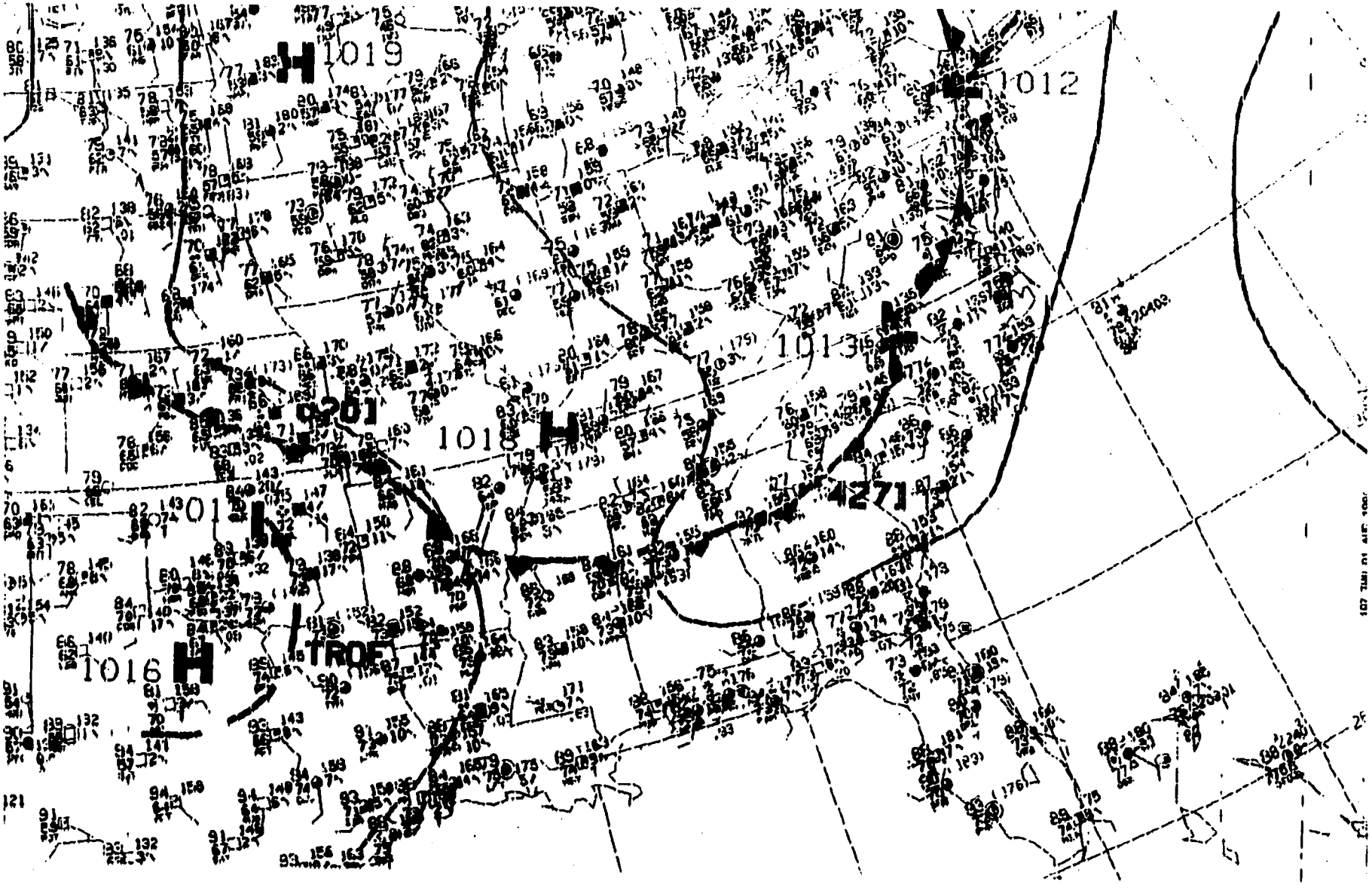


Figure 13

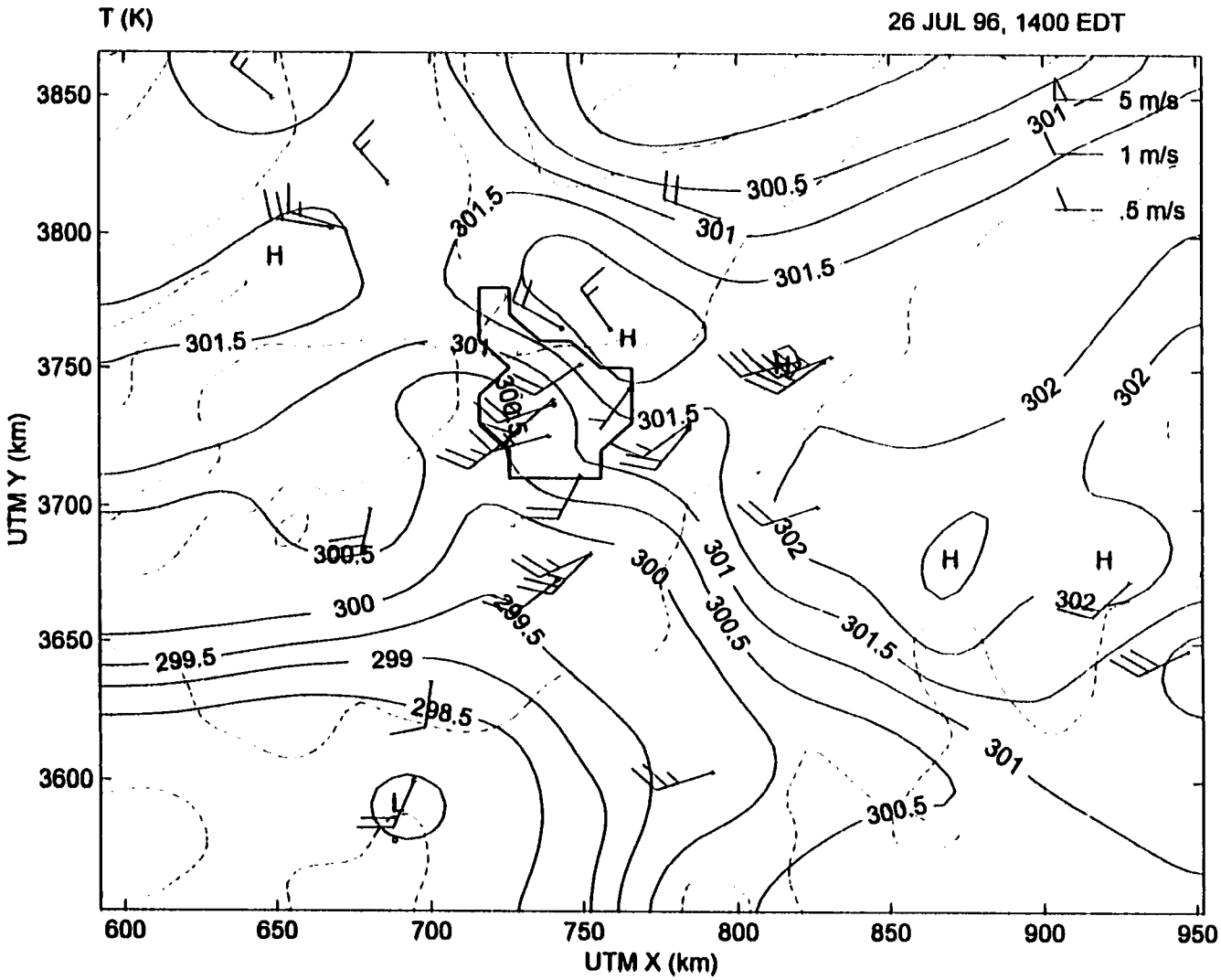
T (K)
26 JUL 96, 1400 EDT
5 m/s
1 m/s
.5 m/s
UTM Y (km)
UTM X (km)
3850
3800
3750
3700
3650
3600
600
650
700
750
800
850
900
950
H
L
301.5
301
300.5
300
299.5
299
298.5
302

Figure 14

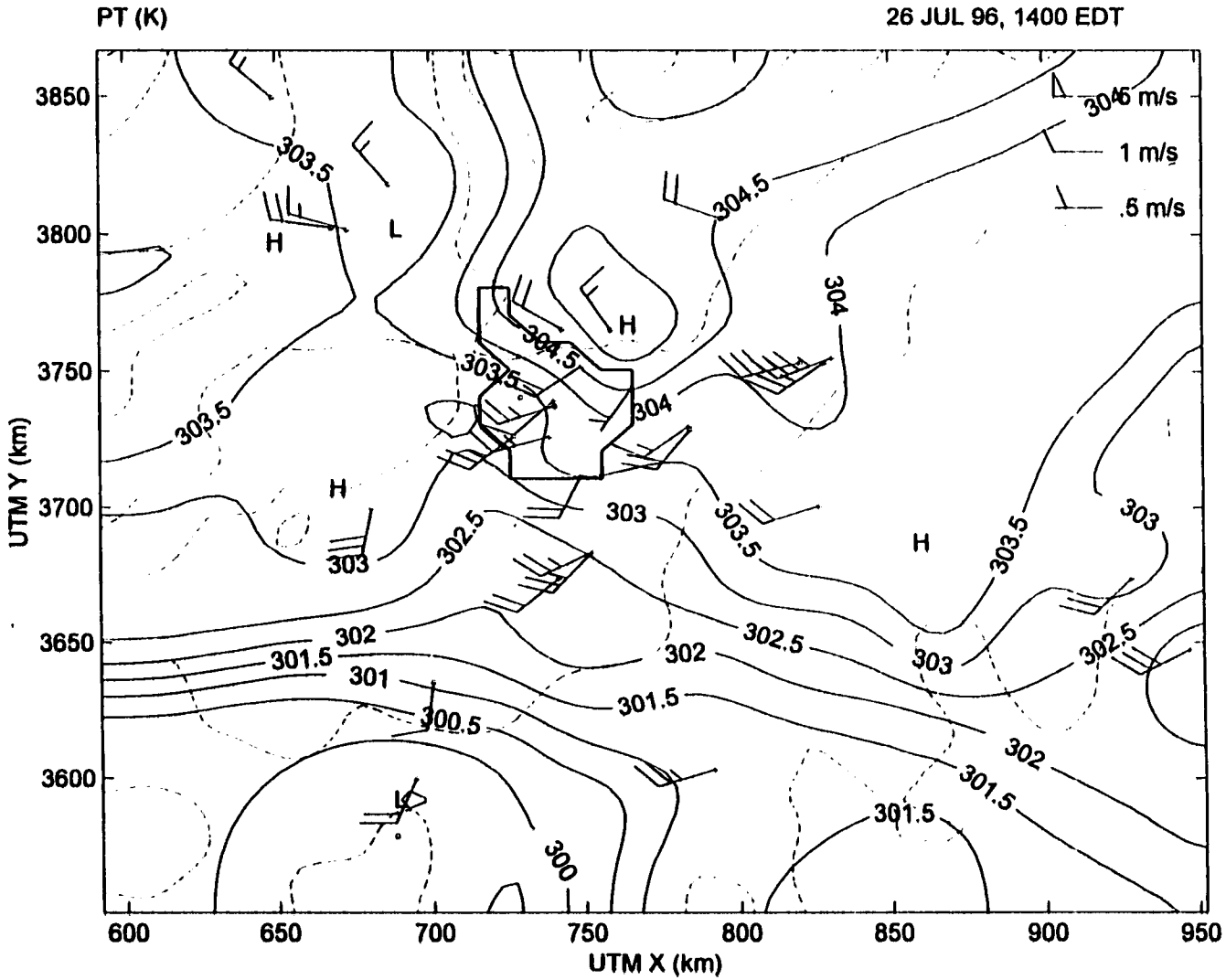
PT (K)
26 JUL 96, 1400 EDT
5 m/s
1 m/s
.5 m/s
UTM Y (km)
UTM X (km)
3850
3800
3750
3700
3650
3600
600
650
700
750
800
850
900
950
H
L
303.5
304.5
304
303
302.5
302
301.5
301
300.5
300

Figure 15

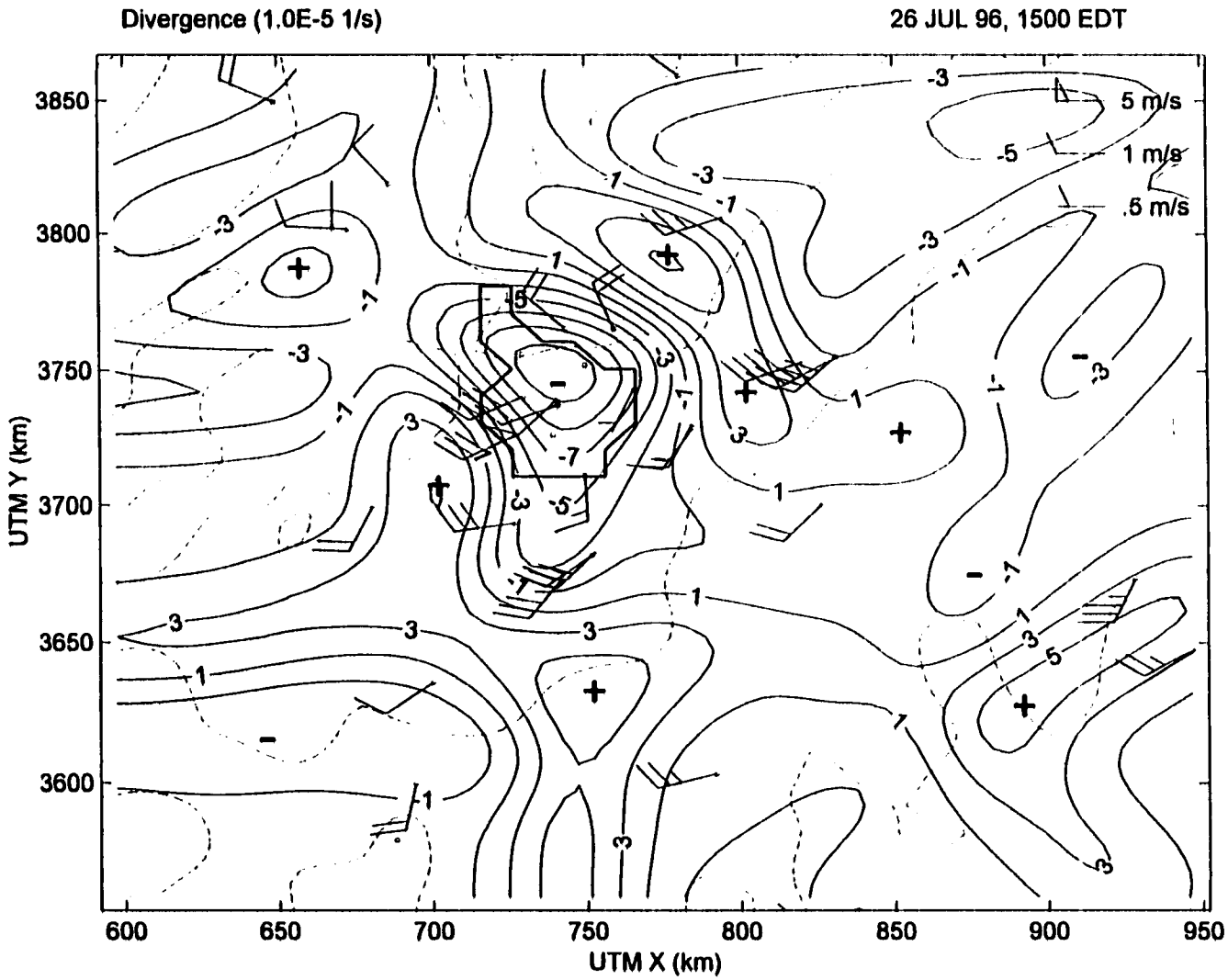
Divergence (1.0E-5 1/s)
26 JUL 96, 1500 EDT
5 m/s
1 m/s
.5 m/s
UTM Y (km)
UTM X (km)
3850
3800
3750
3700
3650
3600
600
650
700
750
800
850
900
950

Figure 16

Figure 17

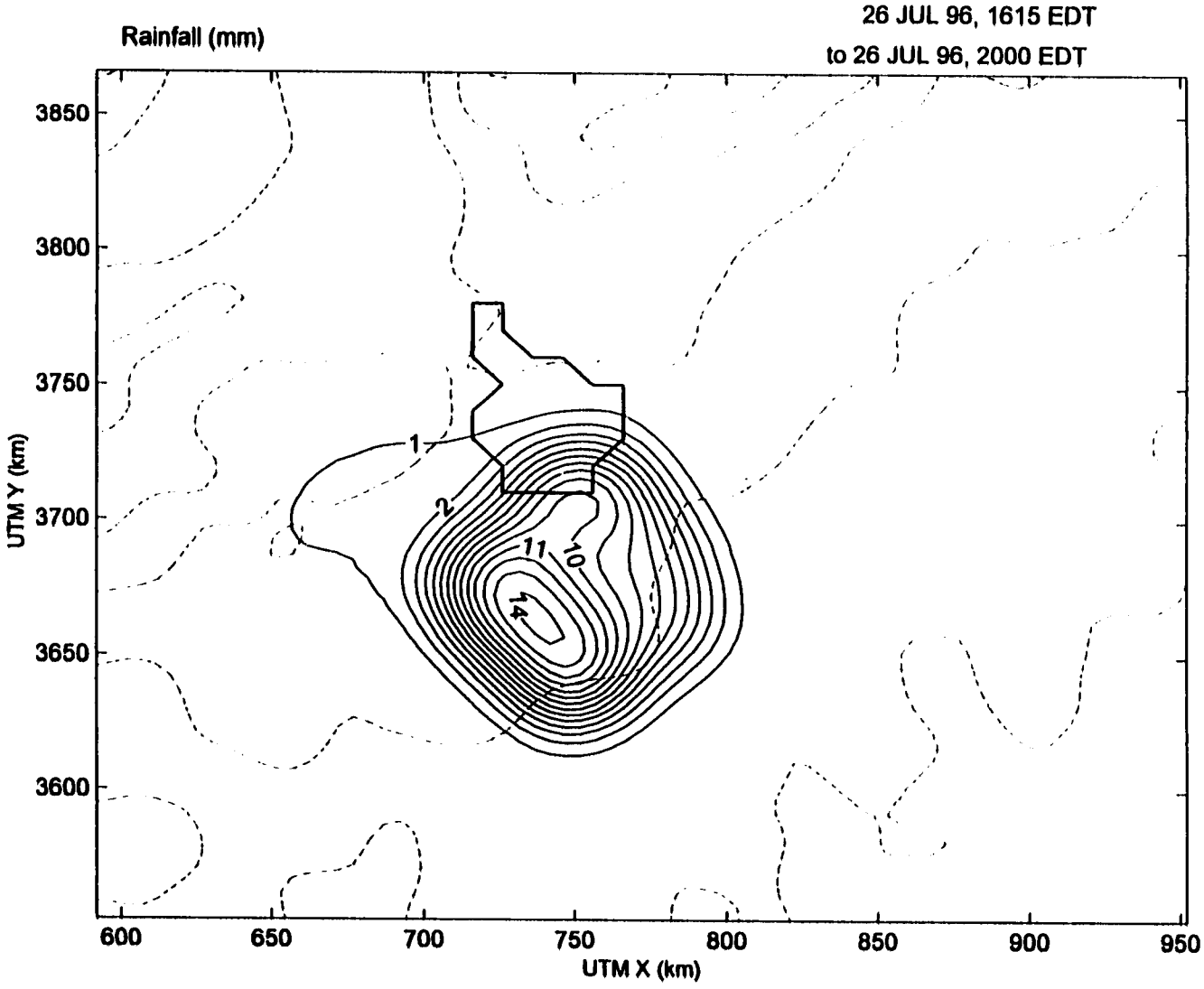
Rainfall (mm)
26 JUL 96, 1615 EDT
to 26 JUL 96, 2000 EDT
3850
3800
3750
3700
3650
3600
UTM Y (km)
600
650
700
750
800
850
900
950
UTM X (km)
1
2
11
10
14

Figure 18

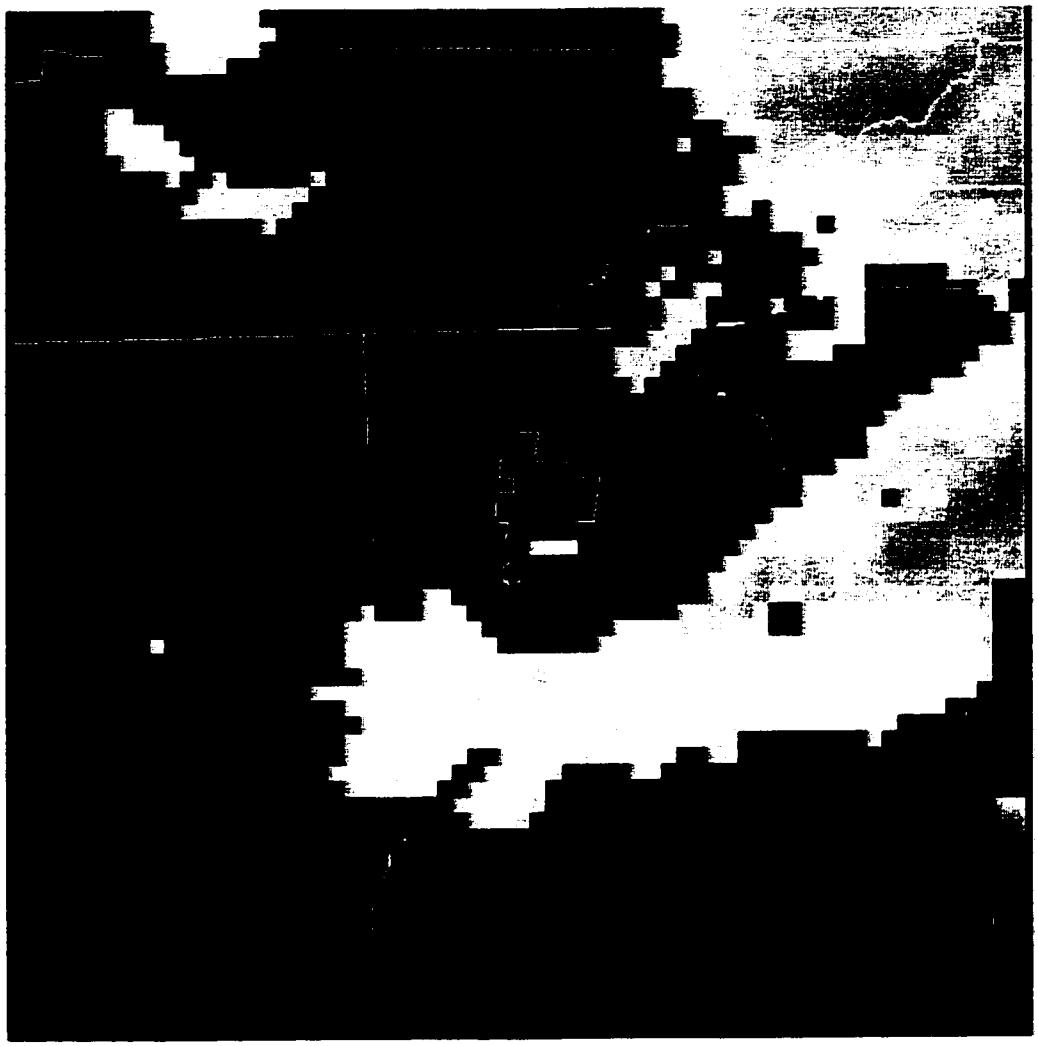

Figure 19

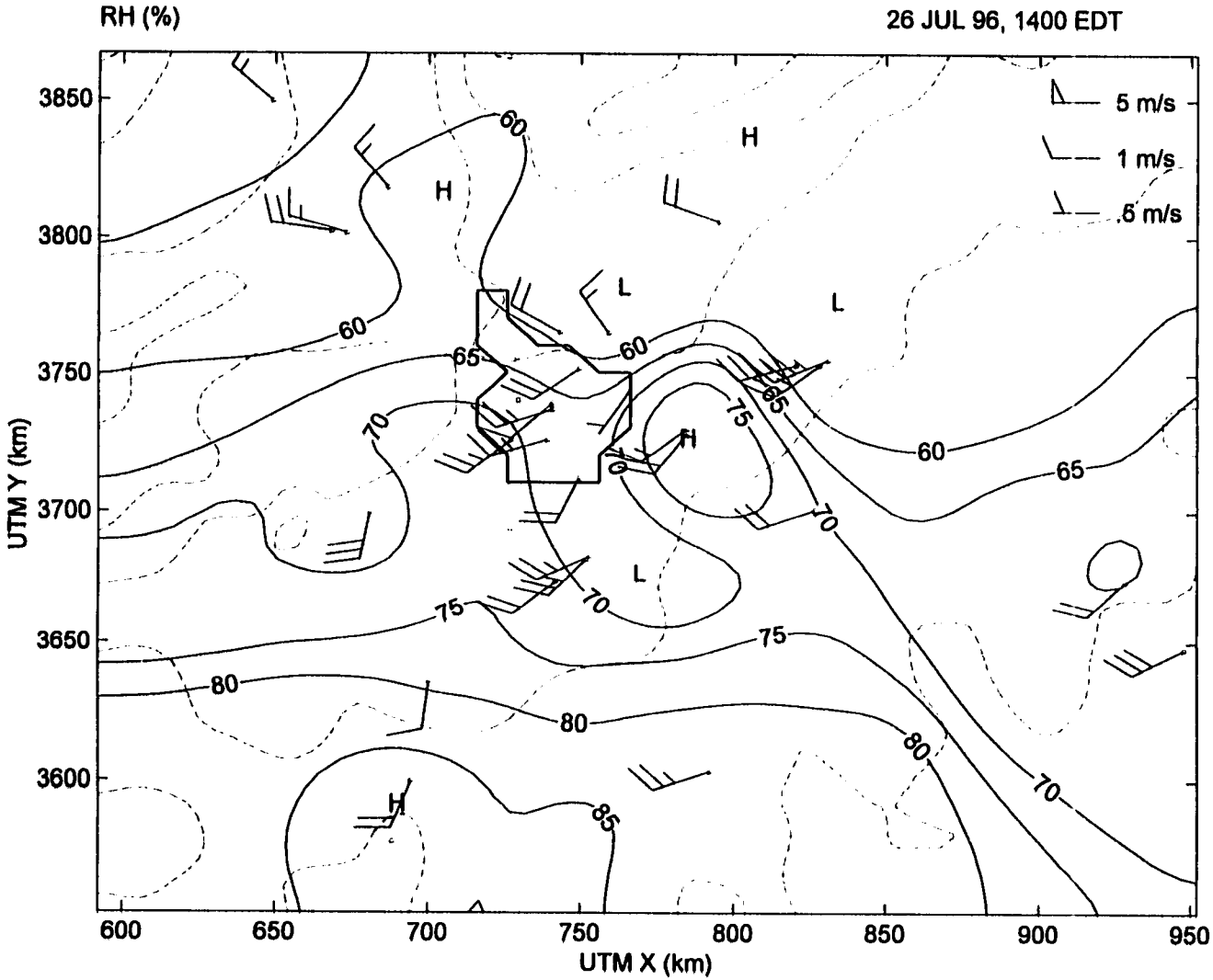
RH (%)
26 JUL 96, 1400 EDT
5 m/s
1 m/s
.5 m/s
UTM Y (km)
UTM X (km)
3850
3800
3750
3700
3650
3600
600
650
700
750
800
850
900
950
H
L
60
65
70
75
80
85

Figure 20

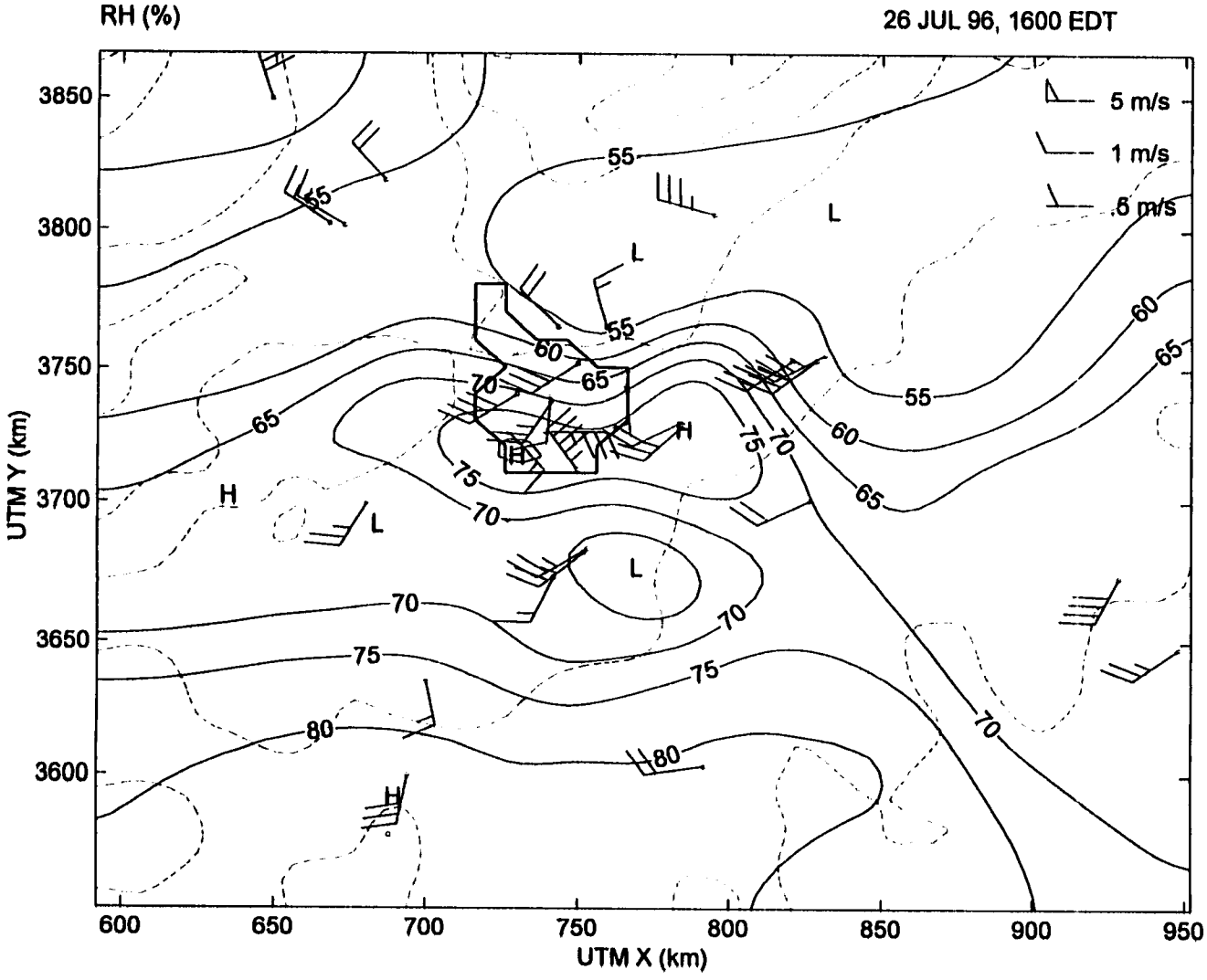
RH (%)
26 JUL 96, 1600 EDT
5 m/s
1 m/s
5 m/s
UTM Y (km)
UTM X (km)
3850
3800
3750
3700
3650
3600
600
650
700
750
800
850
900
950
55
60
65
70
75
80
H
L

Figure 21

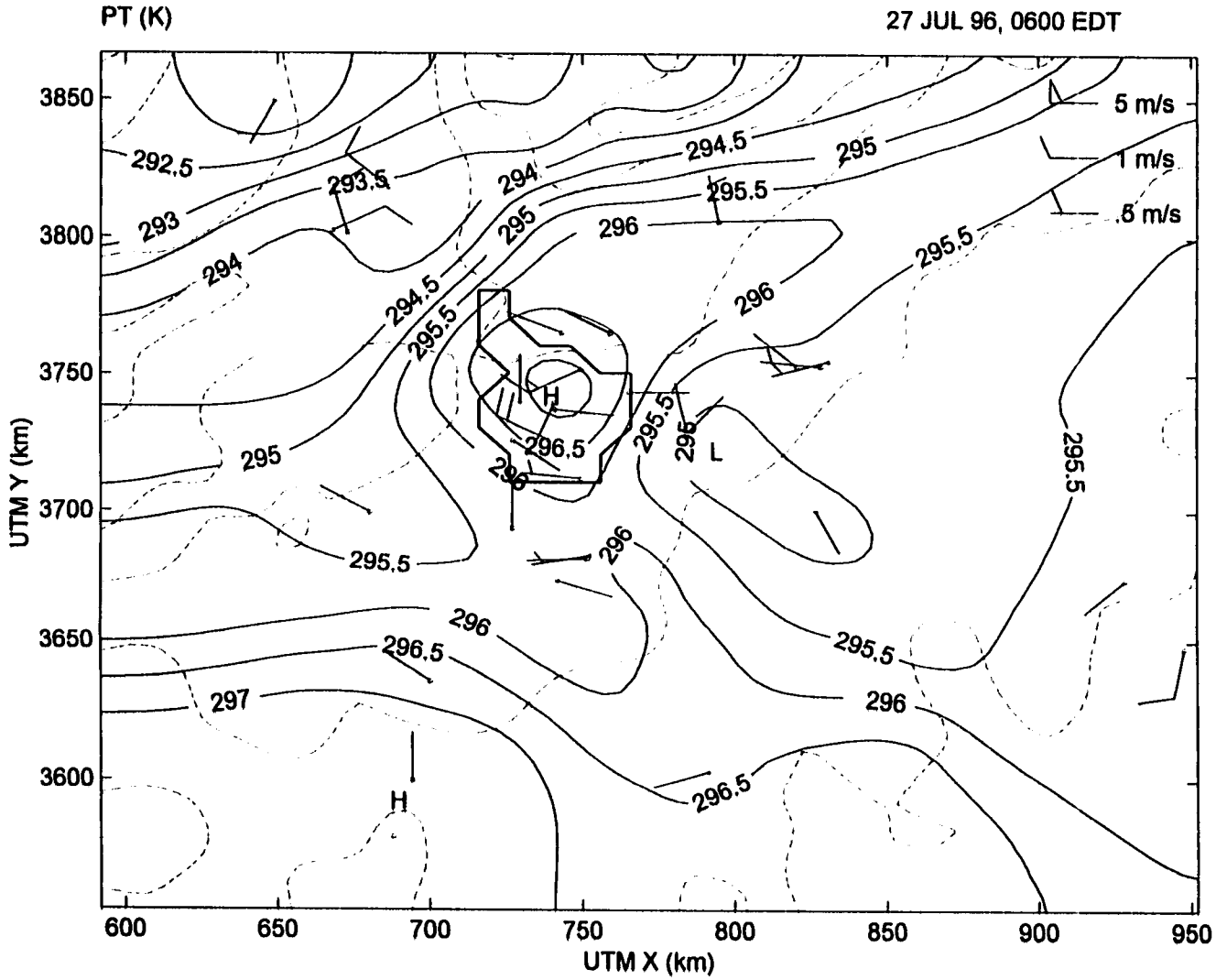
PT (K)
27 JUL 96, 0600 EDT
5 m/s
1 m/s
.5 m/s
UTM Y (km)
UTM X (km)
3850
3800
3750
3700
3650
3600
600
650
700
750
800
850
900
950
292.5
293
293.5
294
294.5
295
295.5
296
296.5
297
H
L

Figure 22

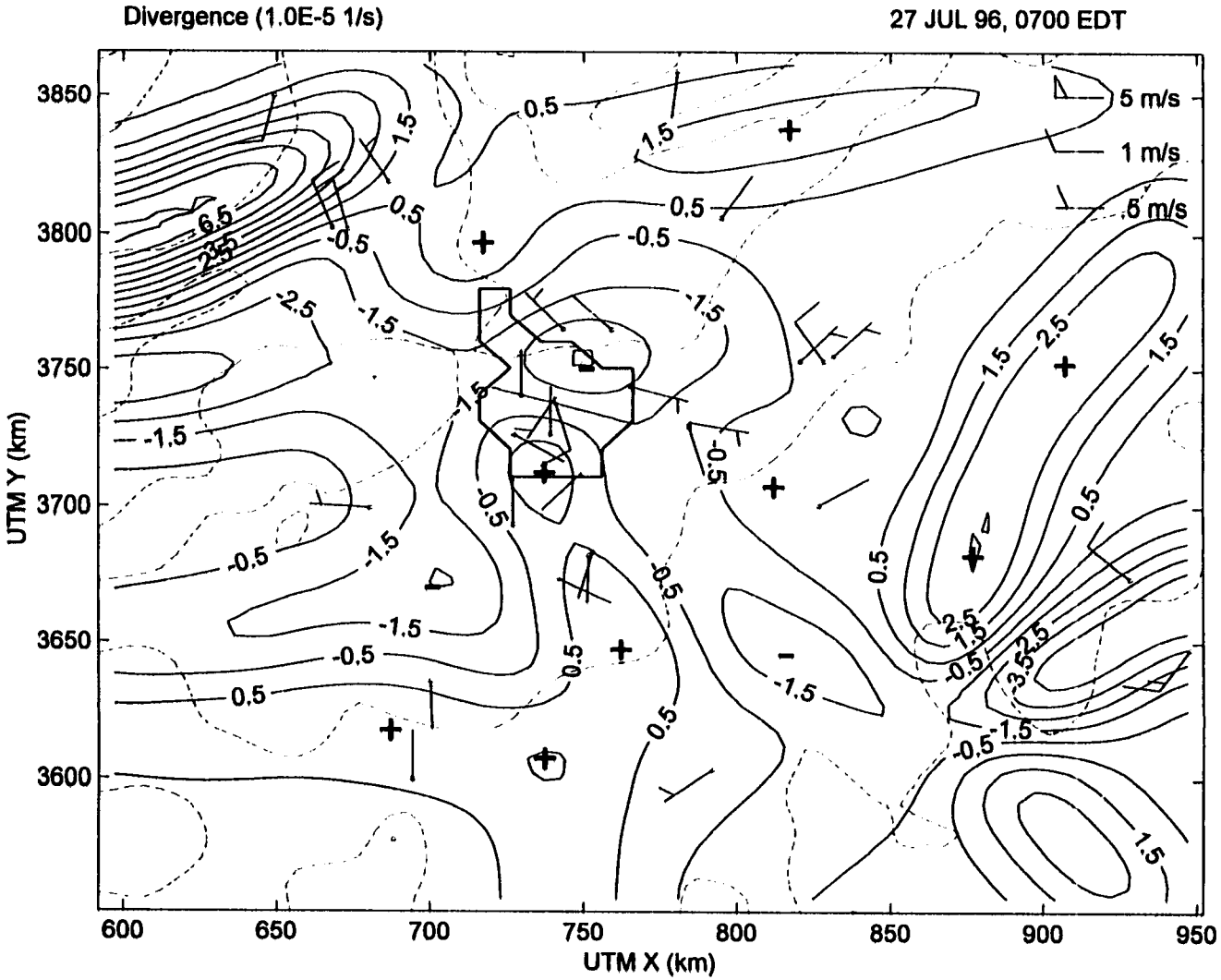
Divergence (1.0E-5 1/s)
27 JUL 96, 0700 EDT
5 m/s
1 m/s
5 m/s
UTM Y (km)
UTM X (km)
3850
3800
3750
3700
3650
3600
600
650
700
750
800
850
900
950

Figure 23

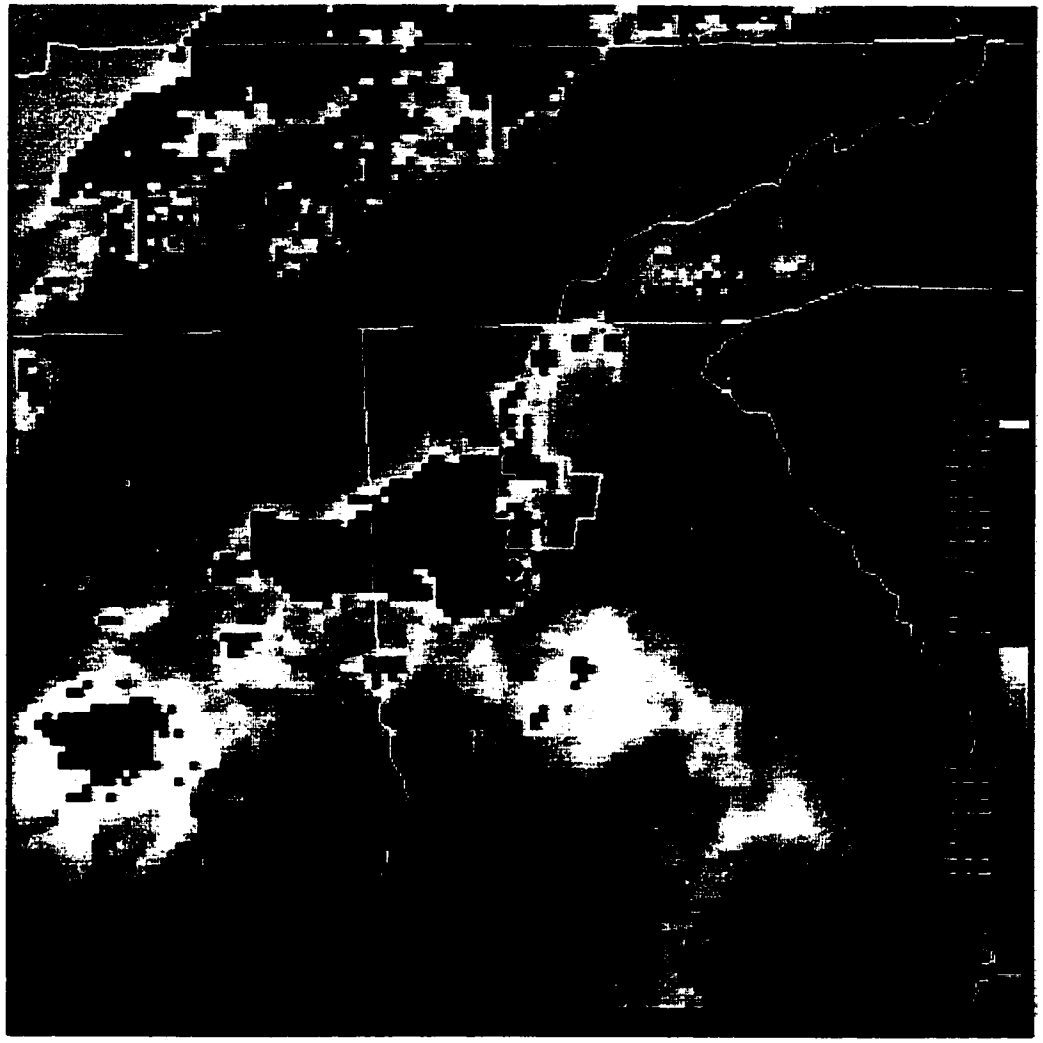

Figure 24

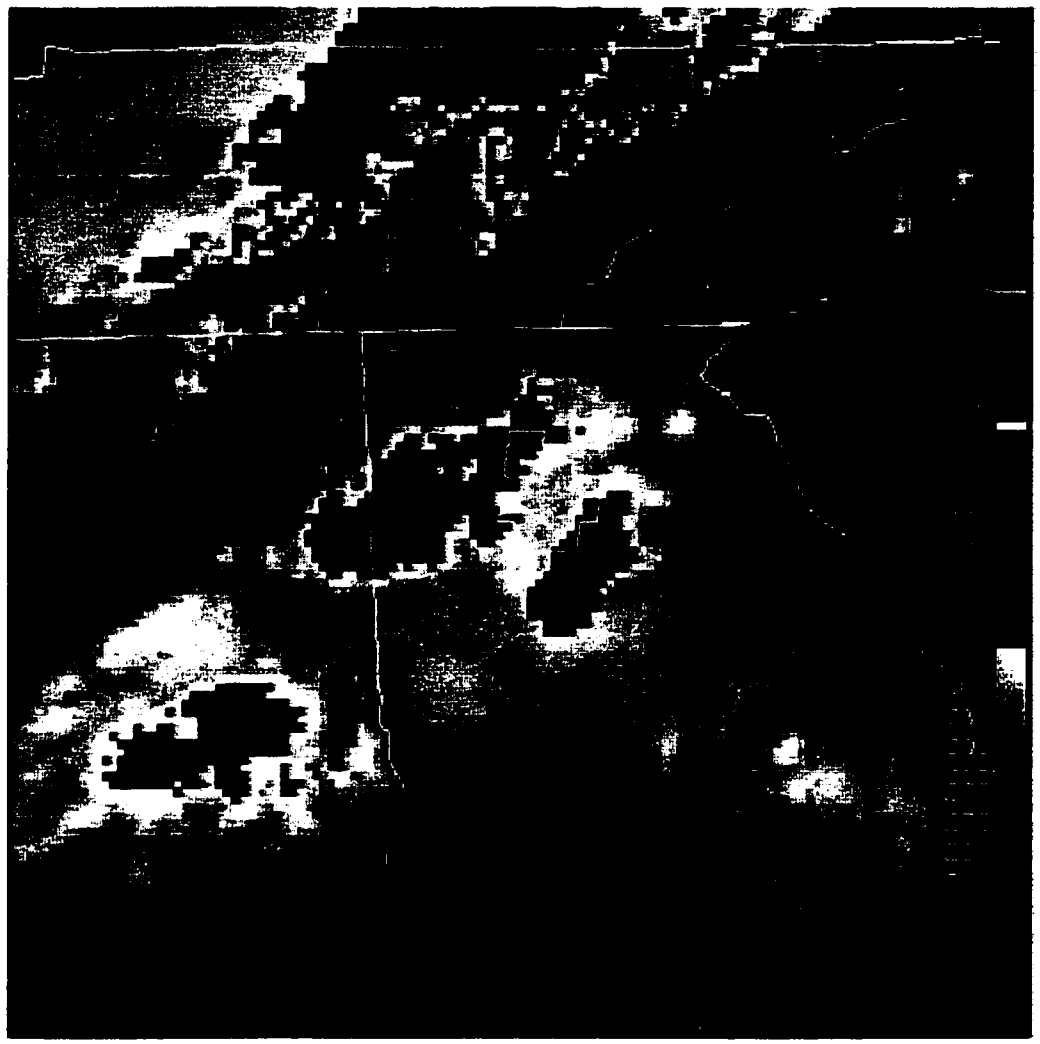

Figure 25

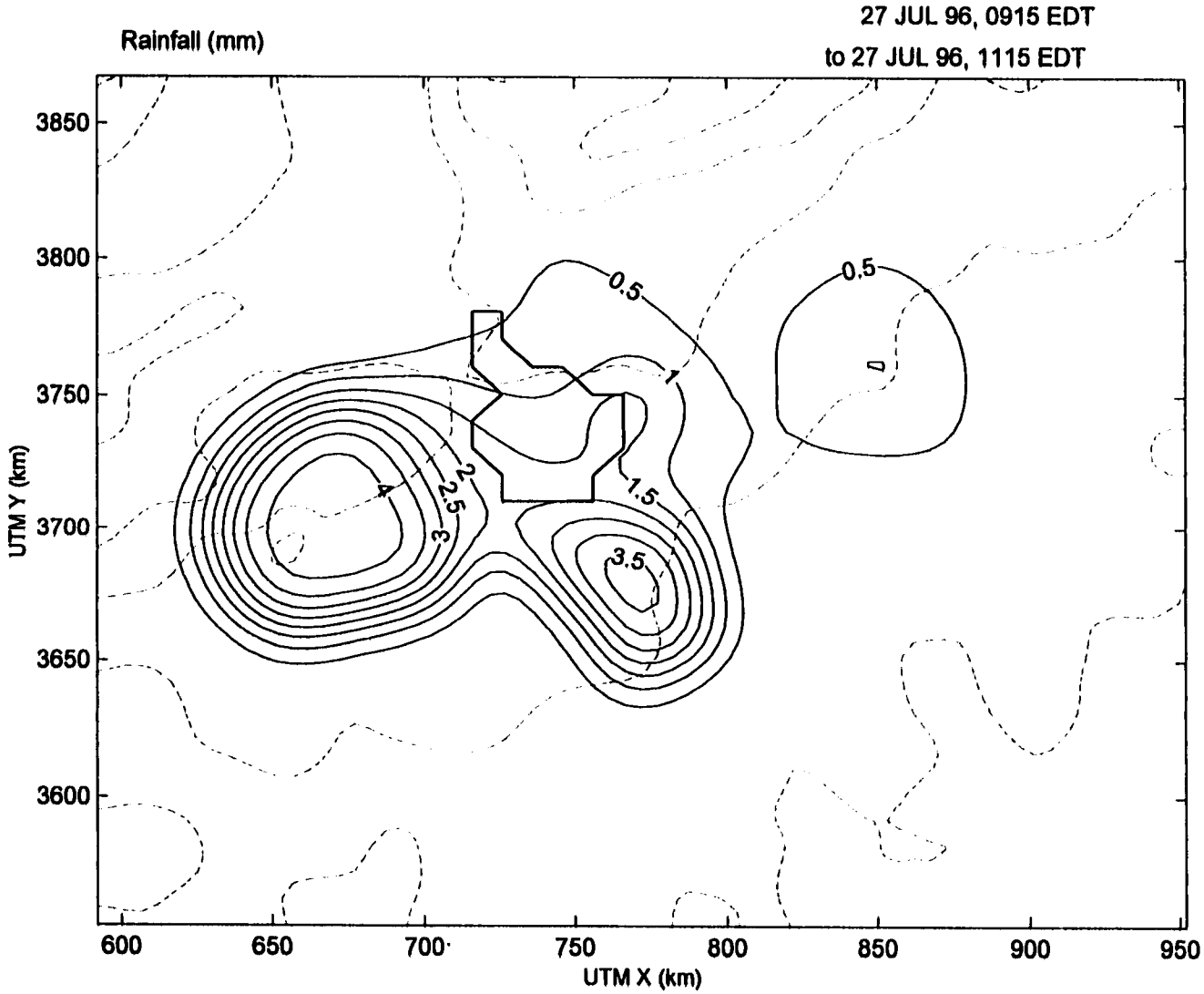
Rainfall (mm)
27 JUL 96, 0915 EDT
to 27 JUL 96, 1115 EDT
3850
3800
3750
3700
3650
3600
UTM Y (km)
600
650
700
750
800
850
900
950
UTM X (km)
0.5
1
0.5
0
1.5
2
2.5
3
3.5
4

Figure 26

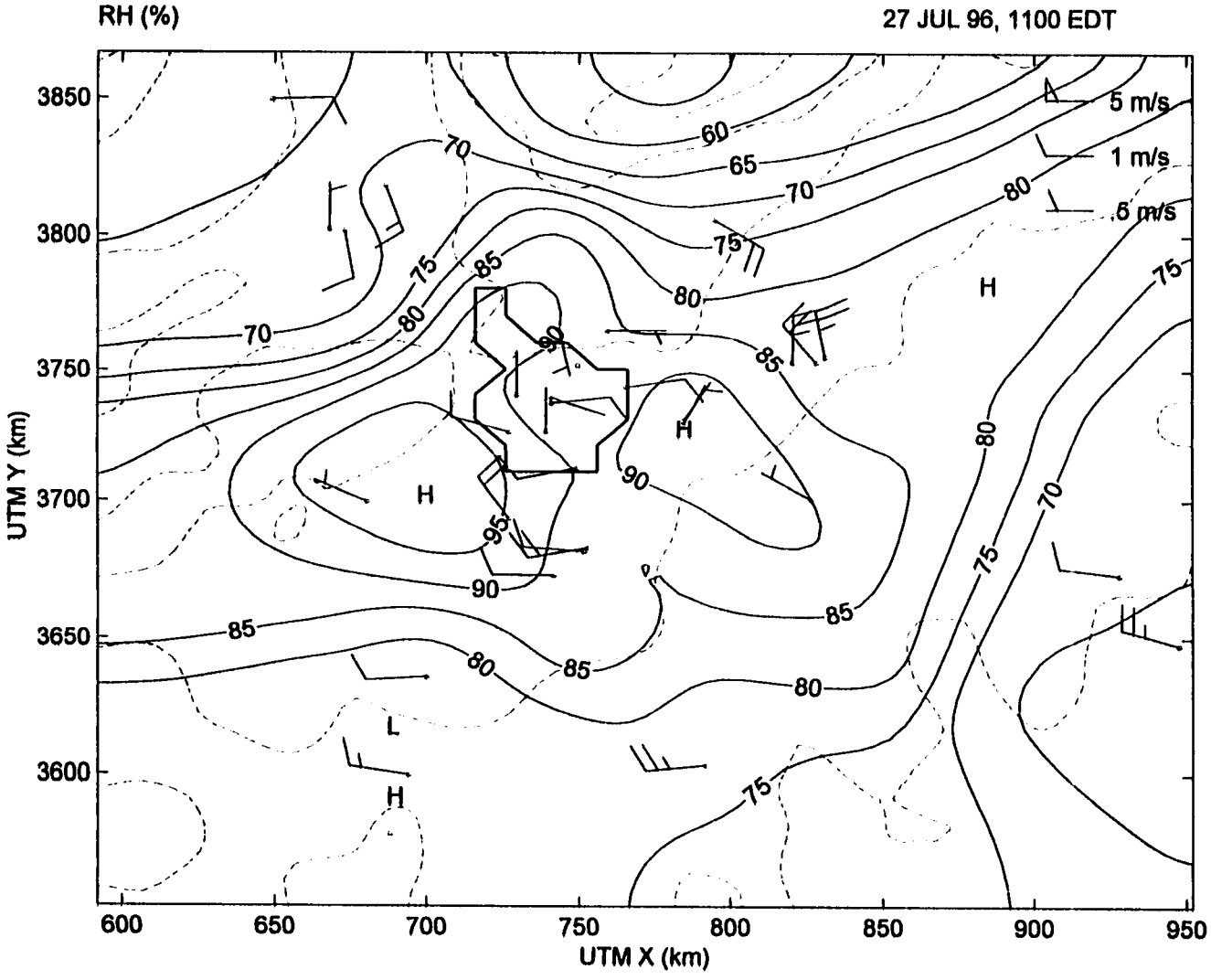
RH (%)
27 JUL 96, 1100 EDT
5 m/s
1 m/s
.5 m/s
UTM Y (km)
UTM X (km)
3850
3800
3750
3700
3650
3600
600
650
700
750
800
850
900
950
H
L

Figure 27

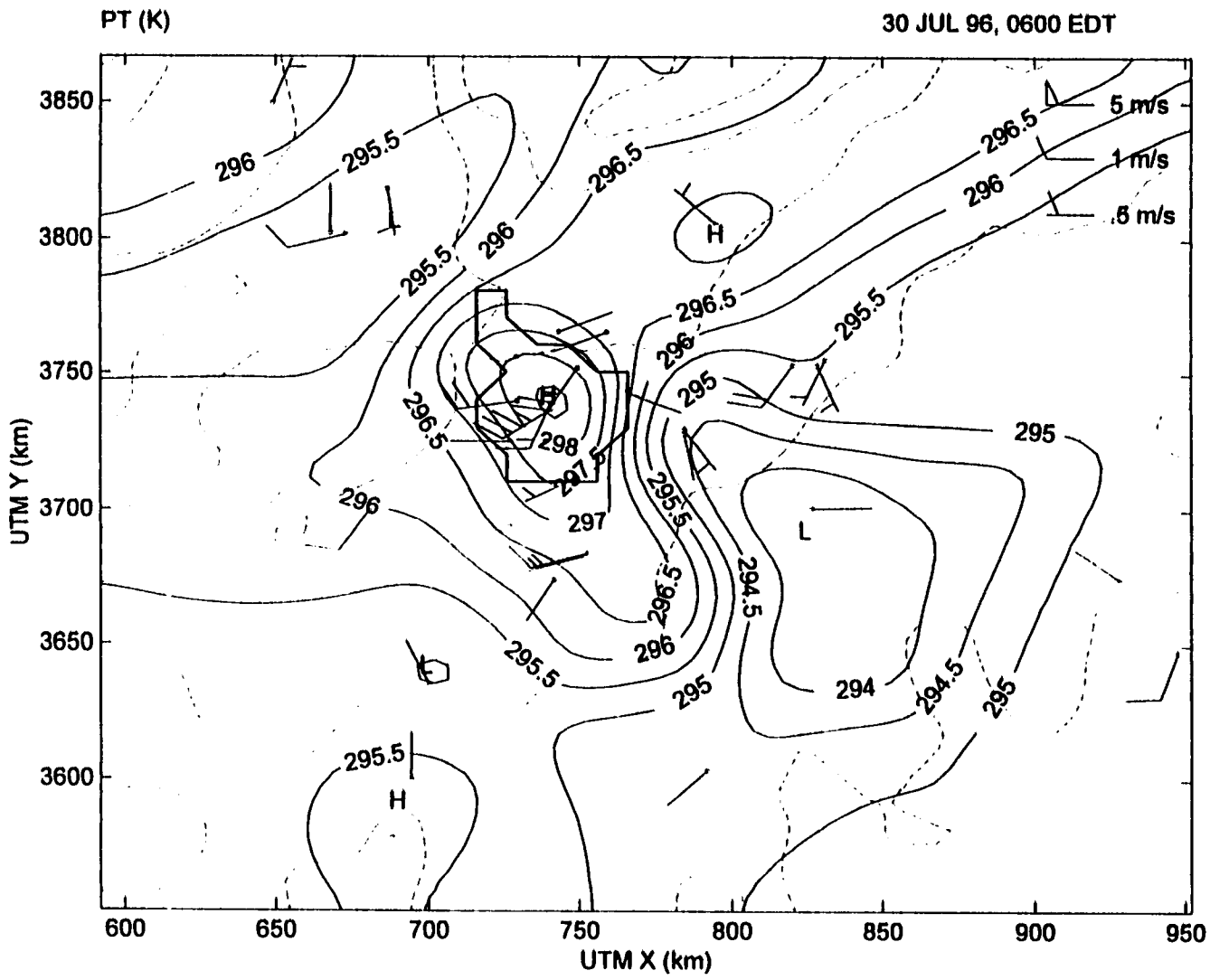
PT (K)
30 JUL 96, 0600 EDT
5 m/s
1 m/s
.5 m/s
UTM Y (km)
UTM X (km)
3850
3800
3750
3700
3650
3600
600
650
700
750
800
850
900
950
296
295.5
296.5
295
298
297.5
297
294.5
294
H
L

Figure 28

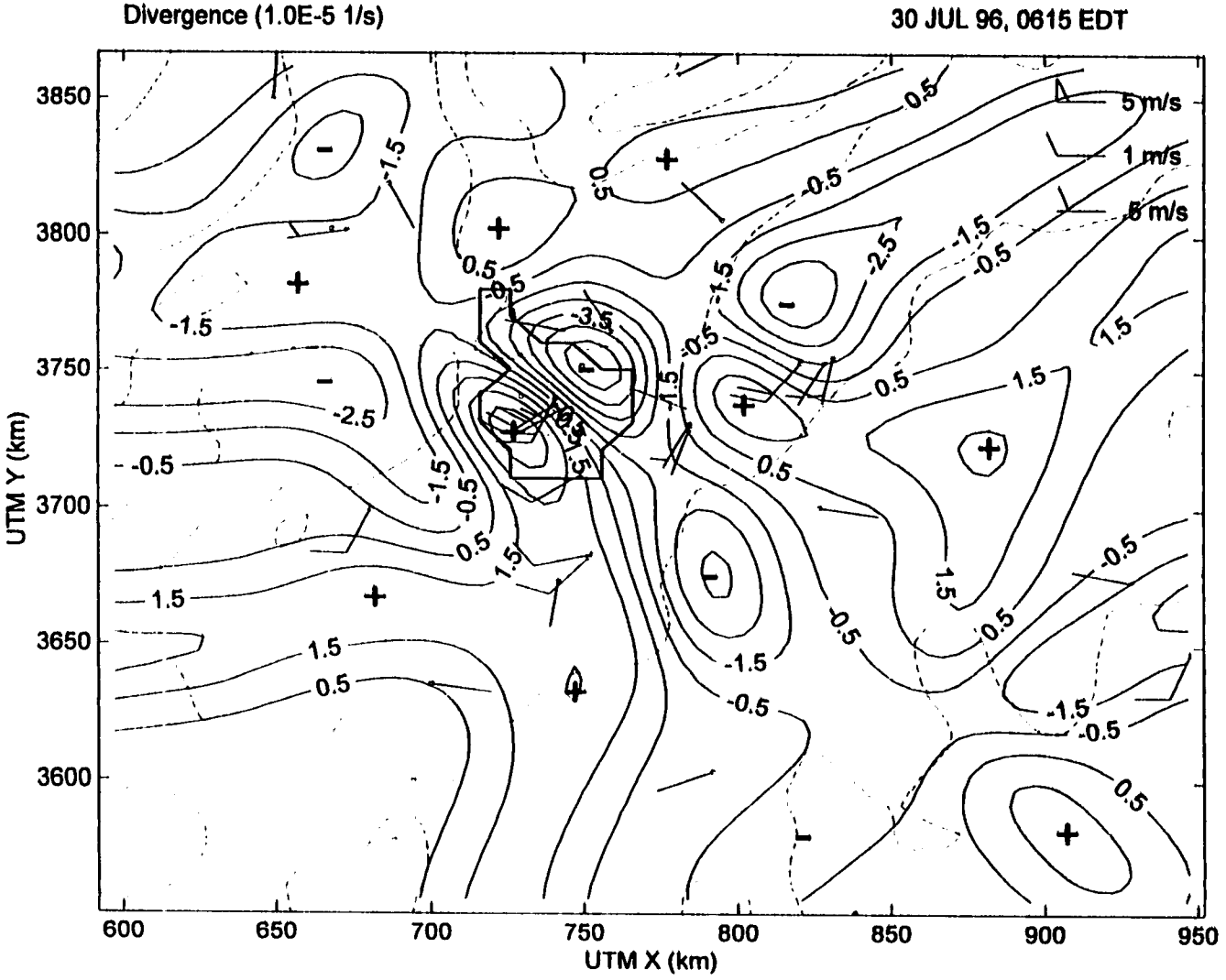
Divergence (1.0E-5 1/s)
30 JUL 96, 0615 EDT
5 m/s
1 m/s
5 m/s
UTM Y (km)
UTM X (km)
3850
3800
3750
3700
3650
3600
600
650
700
750
800
850
900
950

Figure 29

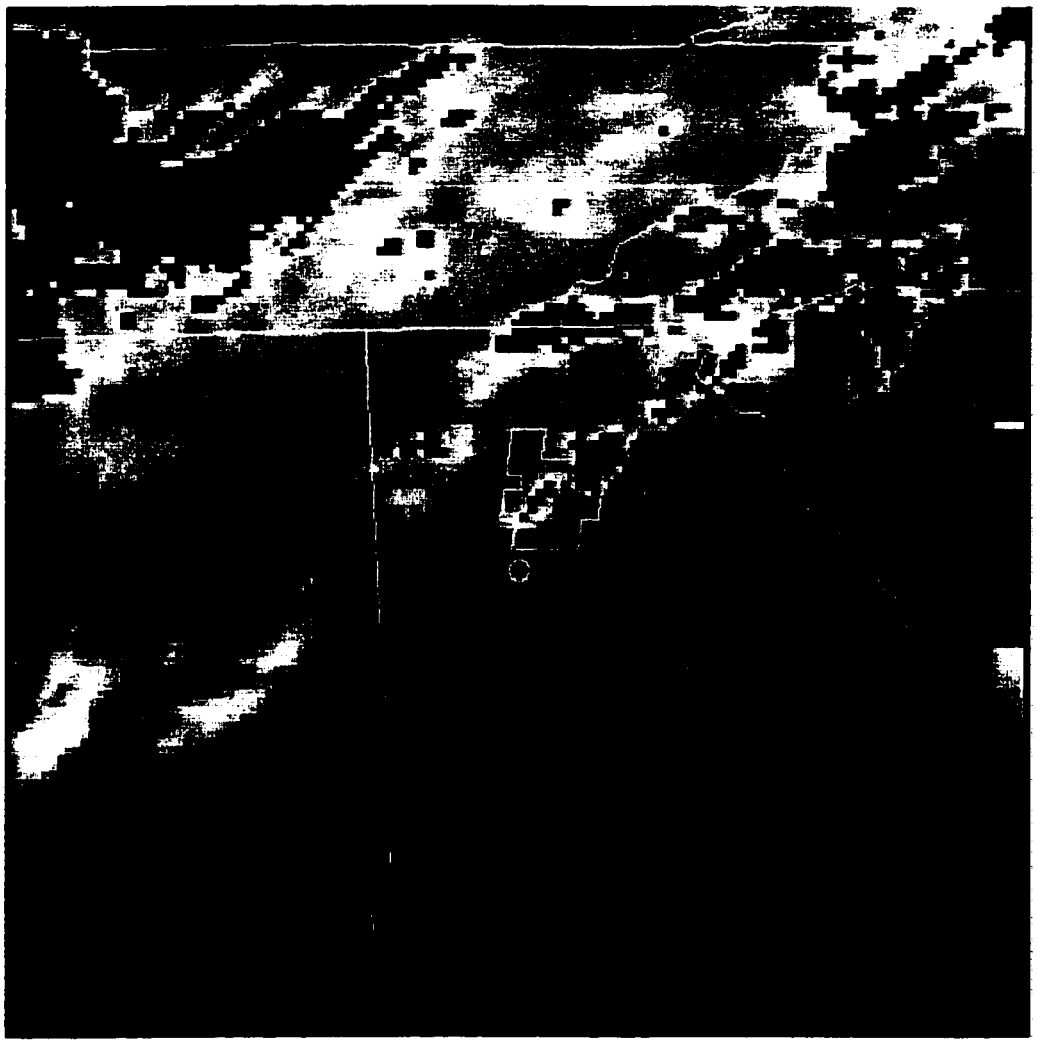

Figure 30

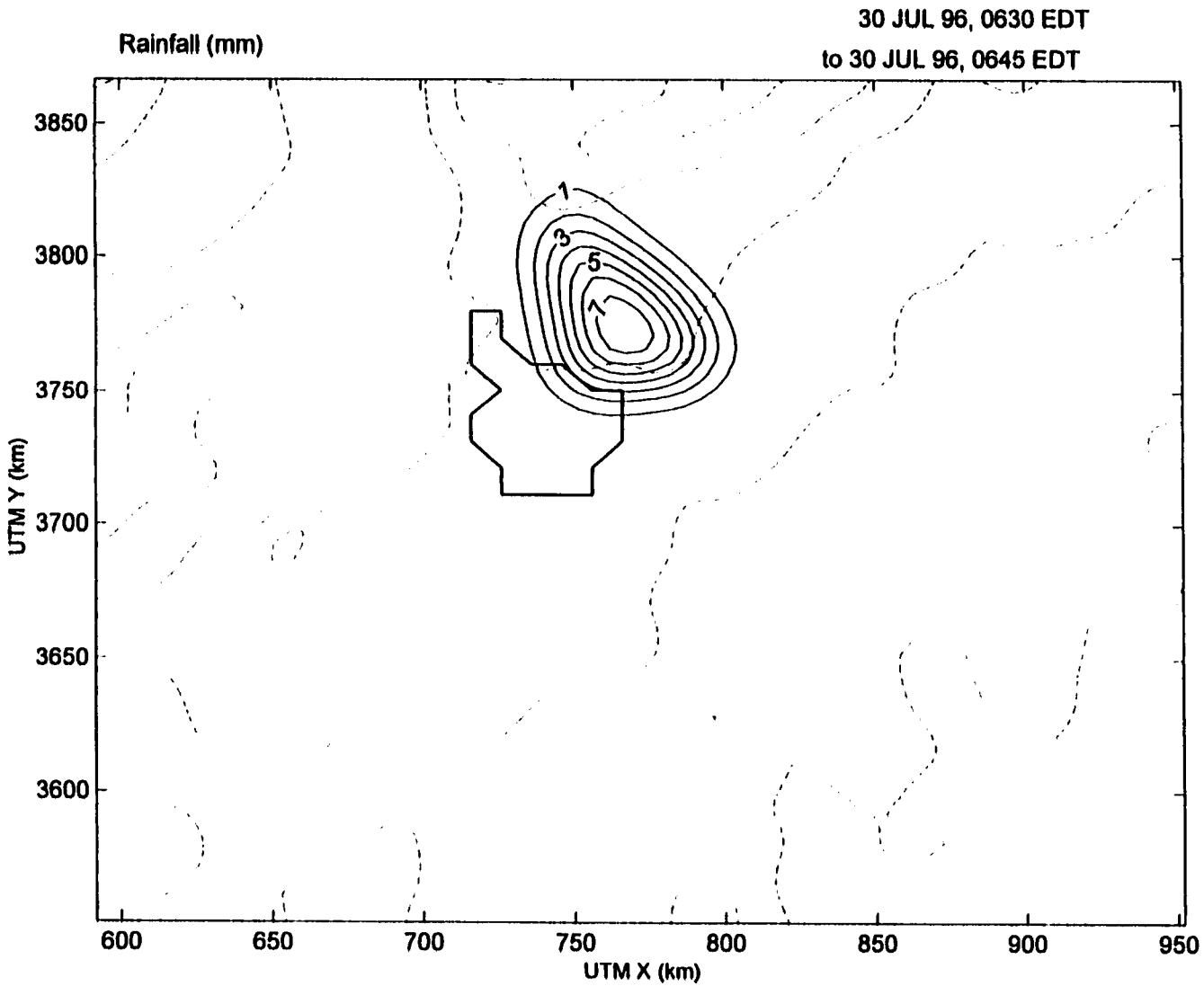
Rainfall (mm)
30 JUL 96, 0630 EDT
to 30 JUL 96, 0645 EDT
1
3
5
7
3850
3800
3750
3700
3650
3600
UTM Y (km)
600
650
700
750
800
850
900
950
UTM X (km)

Figure 31

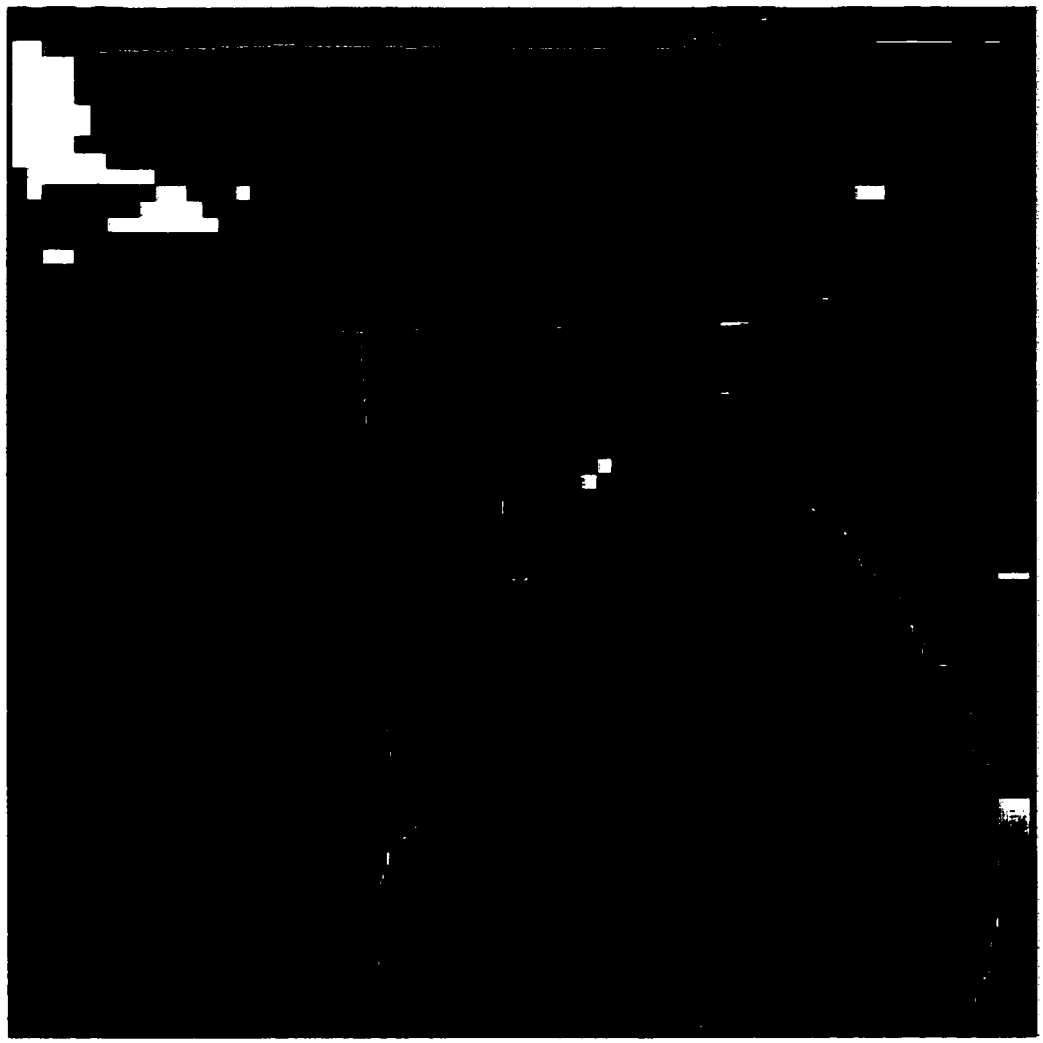

Figure 32

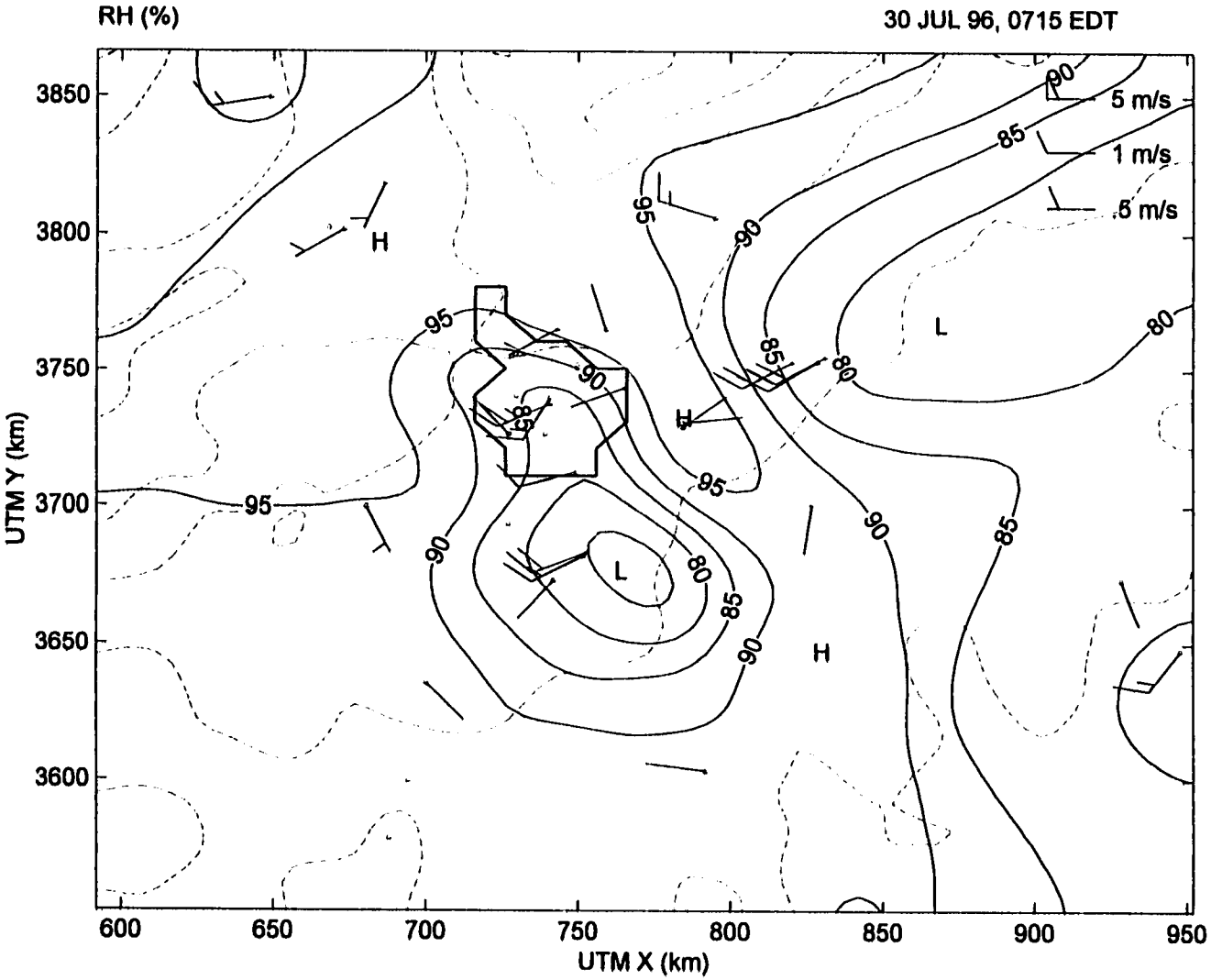
RH (%)
30 JUL 96, 0715 EDT
5 m/s
1 m/s
.5 m/s
UTM Y (km)
UTM X (km)
3850
3800
3750
3700
3650
3600
600
650
700
750
800
850
900
950
H
L
95
90
85
80

Figure 33

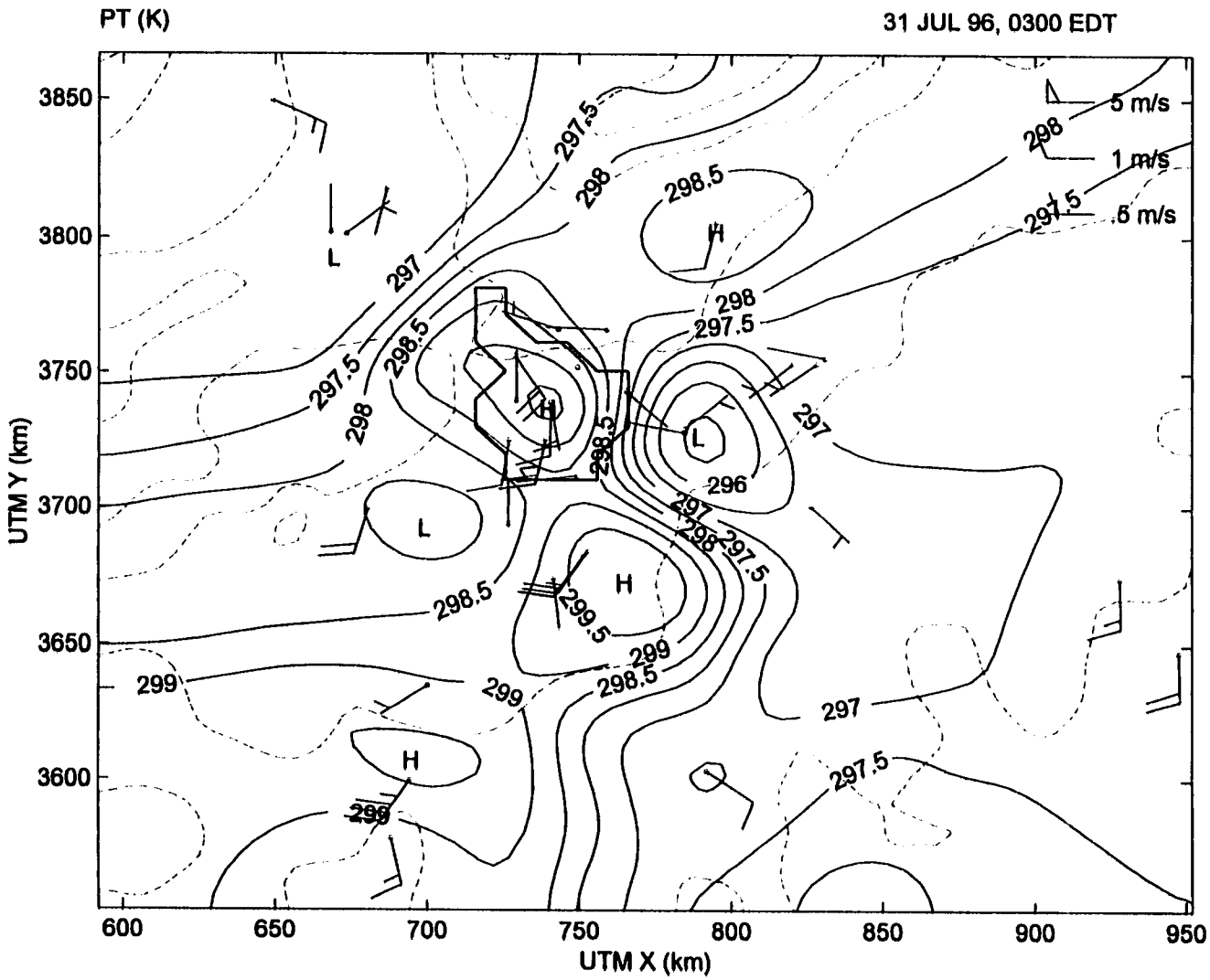
PT (K)
31 JUL 96, 0300 EDT
5 m/s
1 m/s
.5 m/s
UTM Y (km)
UTM X (km)
3850
3800
3750
3700
3650
3600
600
650
700
750
800
850
900
950
L
H
297
297.5
298
298.5
299
296

Figure 34

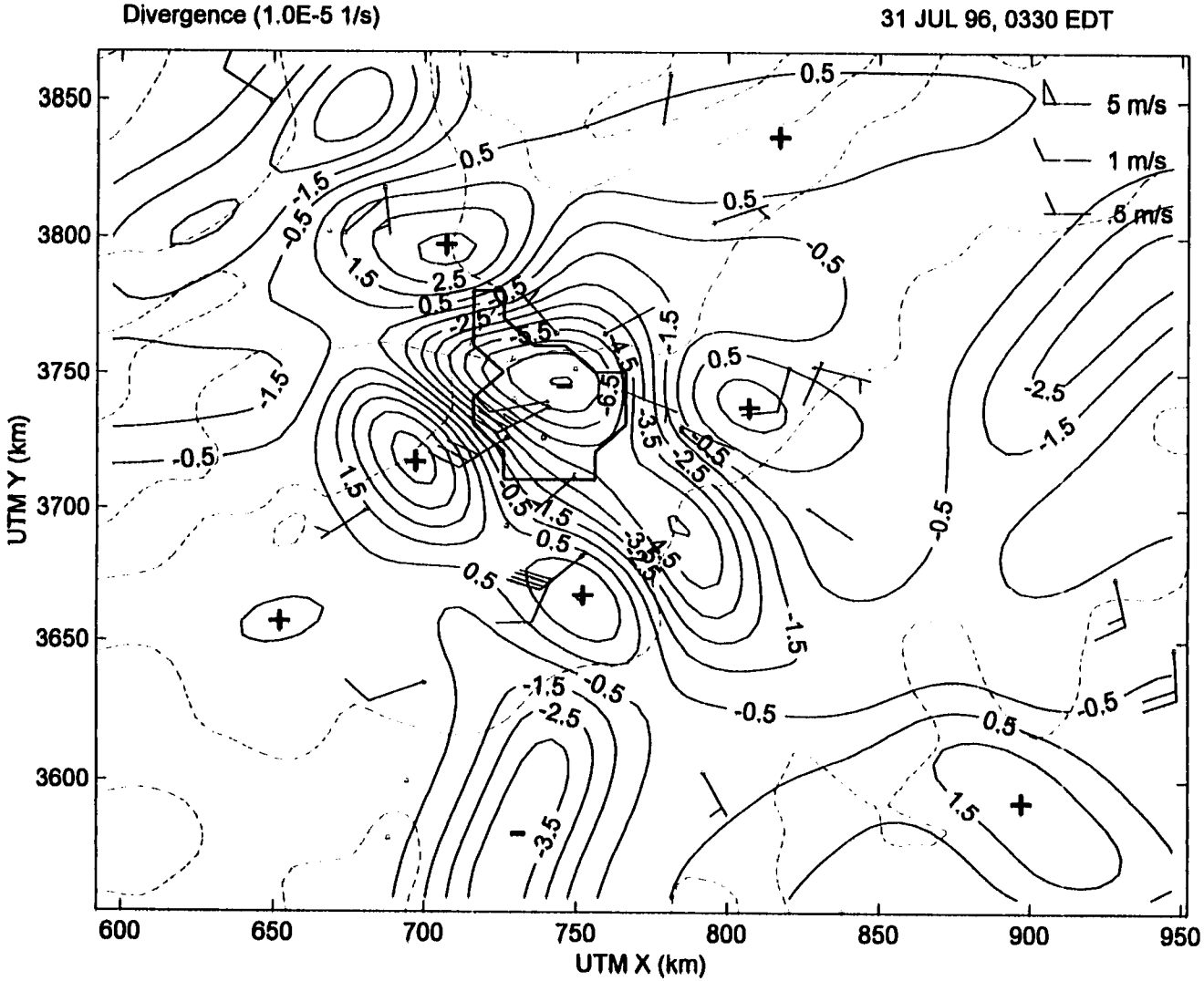
Divergence (1.0E-5 1/s)
31 JUL 96, 0330 EDT
5 m/s
1 m/s
.5 m/s
UTM Y (km)
UTM X (km)
3850
3800
3750
3700
3650
3600
600
650
700
750
800
850
900
950

Figure 35

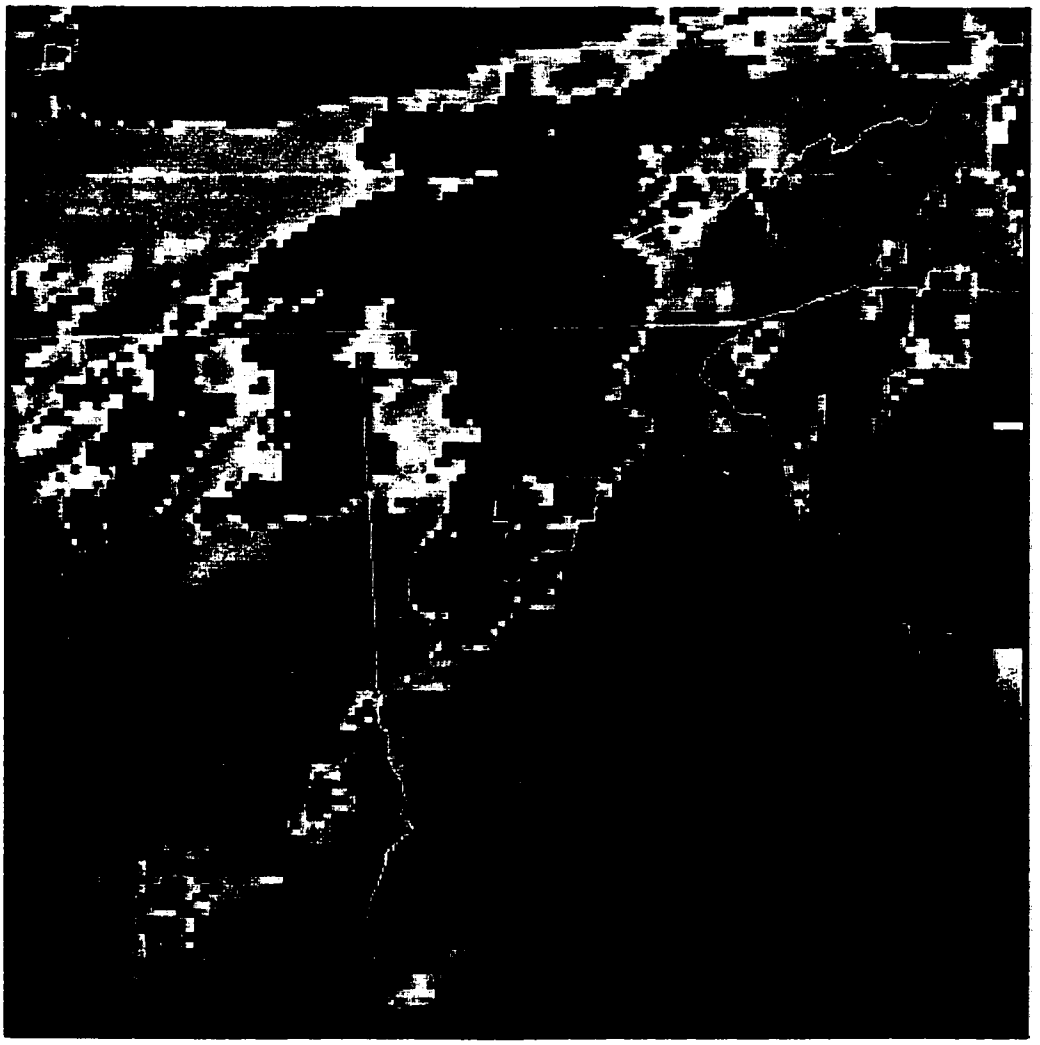

Figure 36

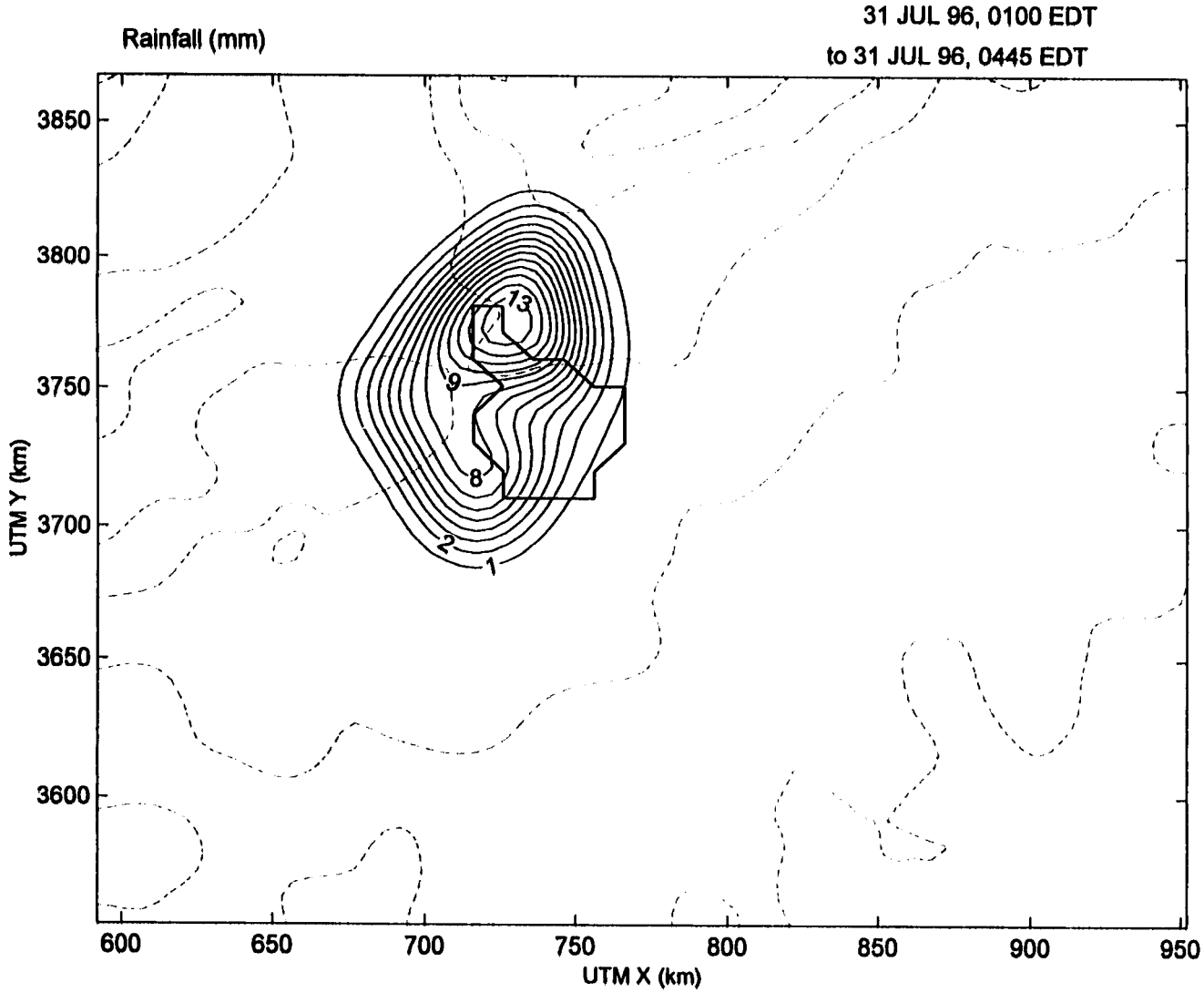
Rainfall (mm)
31 JUL 96, 0100 EDT
to 31 JUL 96, 0445 EDT
3850
3800
3750
3700
3650
3600
UTM Y (km)
600
650
700
750
800
850
900
950
UTM X (km)
13
9
8
2
1

Figure 37

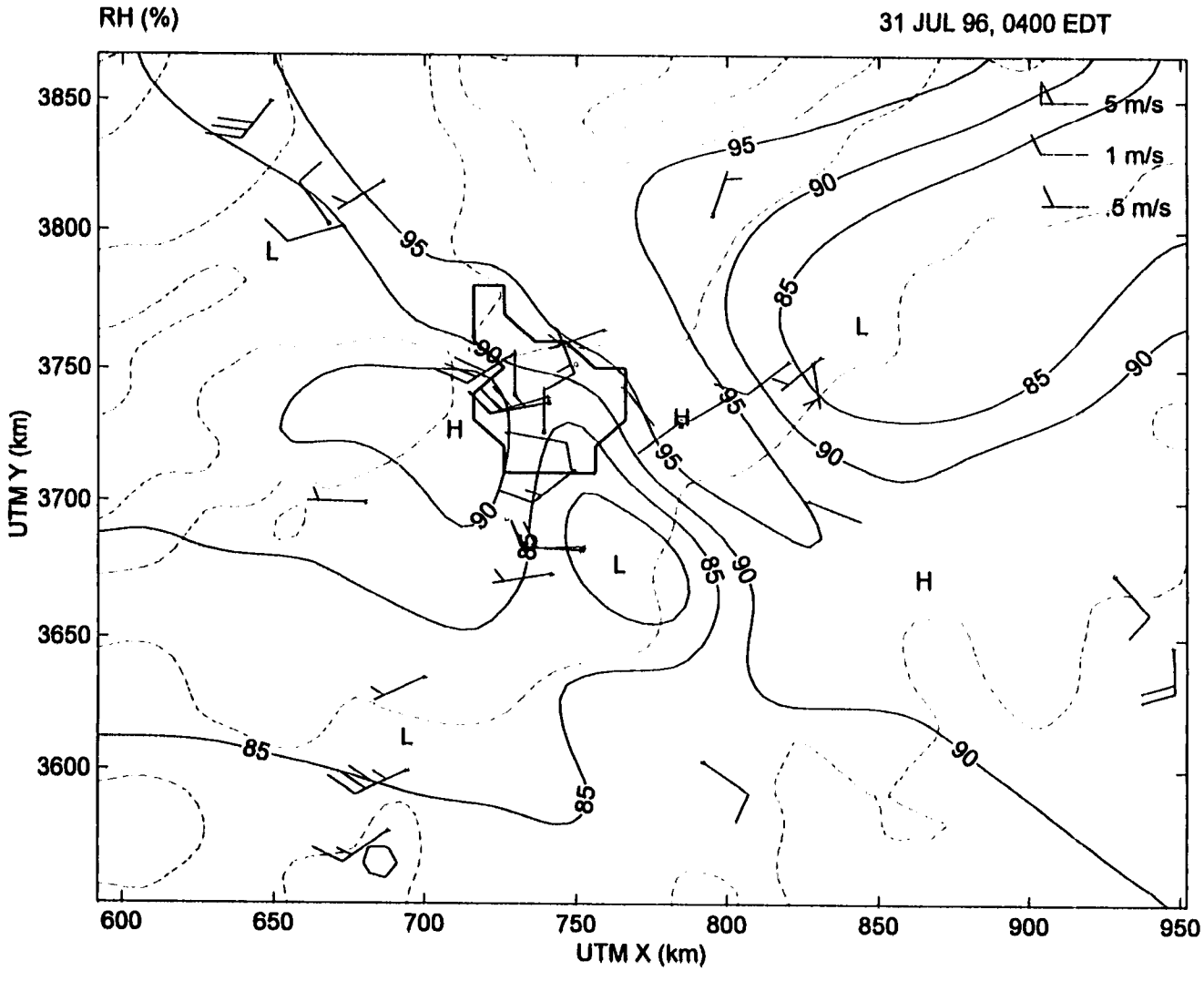
RH (%)
31 JUL 96, 0400 EDT
5 m/s
1 m/s
.5 m/s
UTM Y (km)
UTM X (km)
3850
3800
3750
3700
3650
3600
600
650
700
750
800
850
900
950
95
90
85
L
H

Figure 38

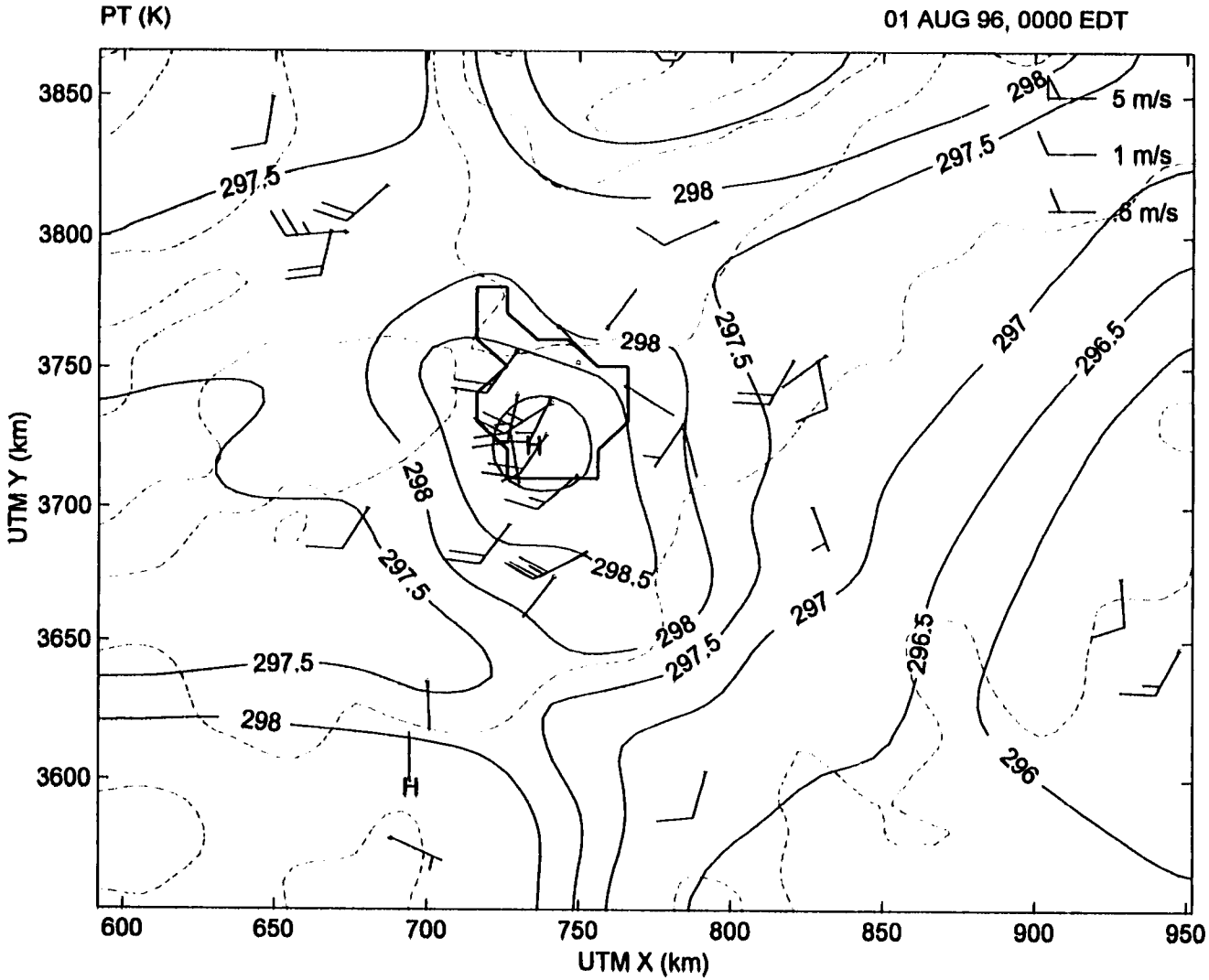
PT (K)
01 AUG 96, 0000 EDT
5 m/s
1 m/s
UTM Y (km)
UTM X (km)
3850
3800
3750
3700
3650
3600
600
650
700
750
800
850
900
950
297.5
298
298.5
297
296.5
296
H

Figure 39

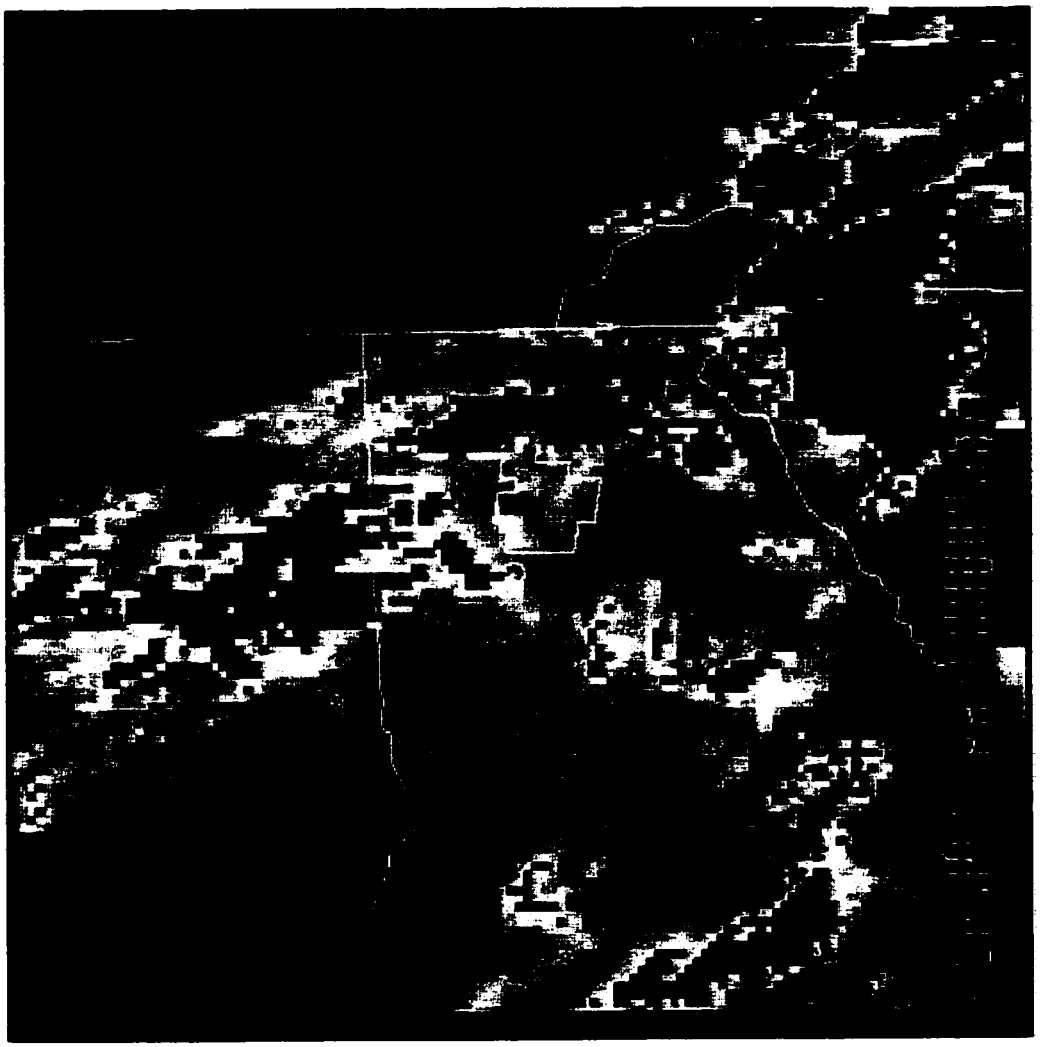

Figure 40 (a)

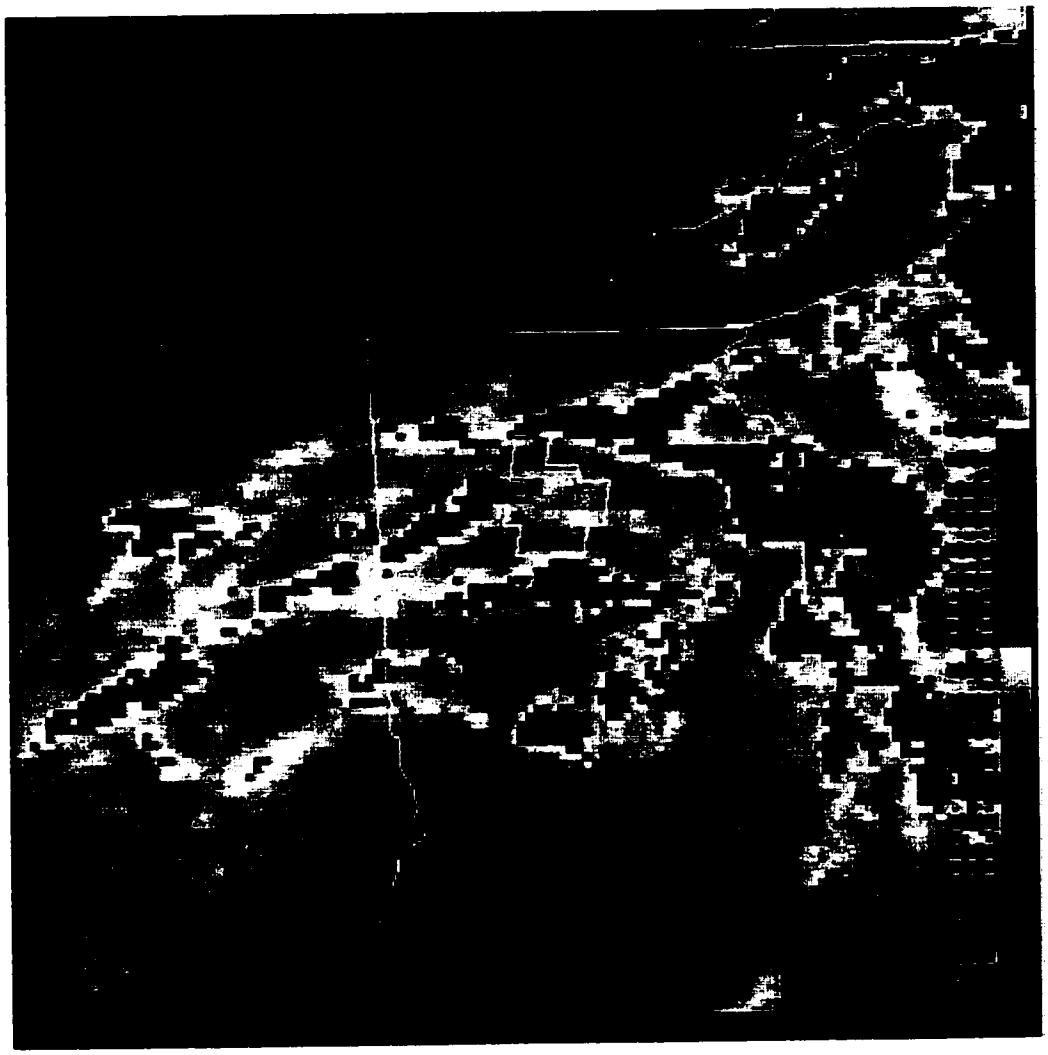

Figure 40 (b)

Figure 40 (c)

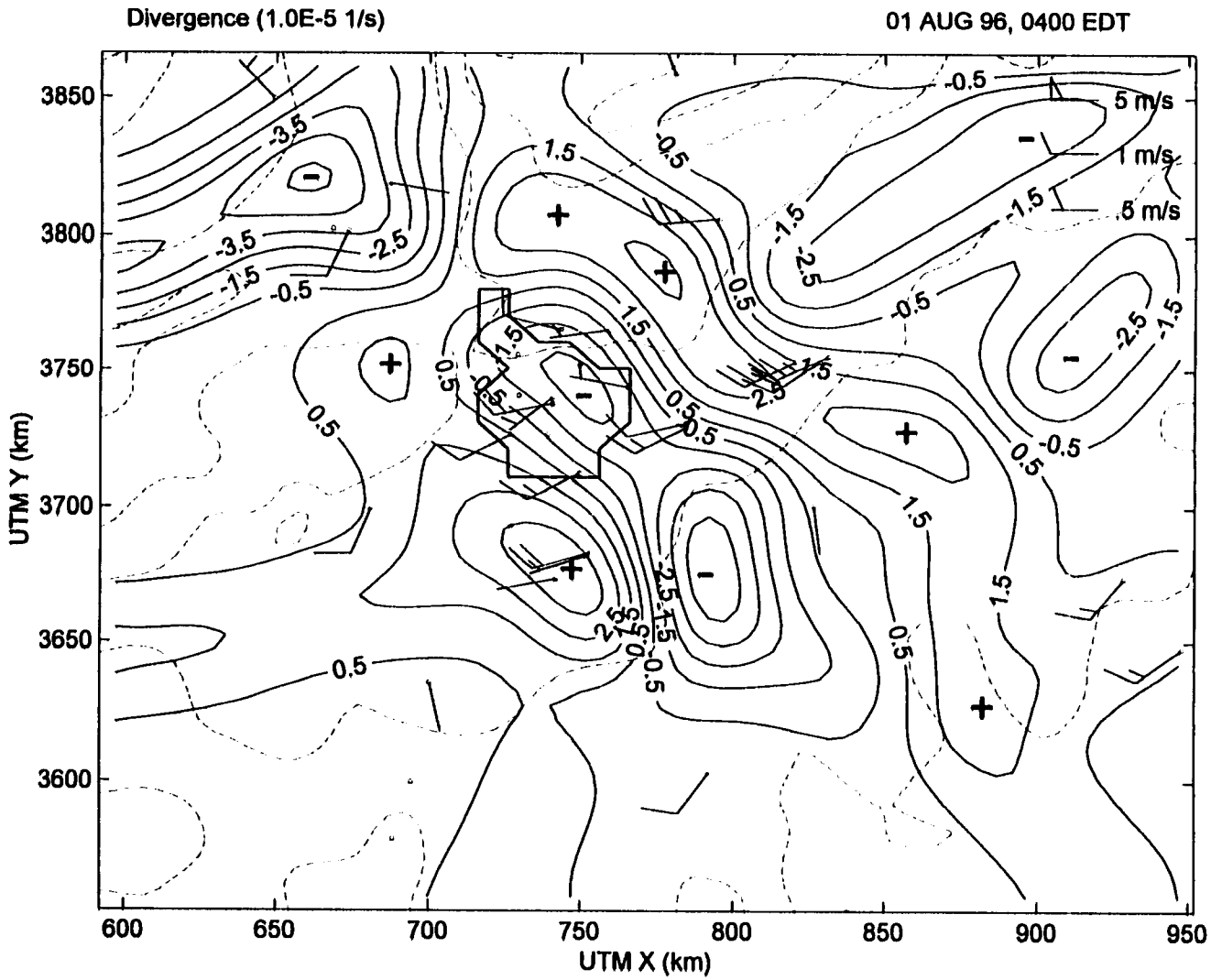
Divergence (1.0E-5 1/s)
01 AUG 96, 0400 EDT
5 m/s
1 m/s
.5 m/s
UTM Y (km)
UTM X (km)
3850
3800
3750
3700
3650
3600
600
650
700
750
800
850
900
950

Figure 41

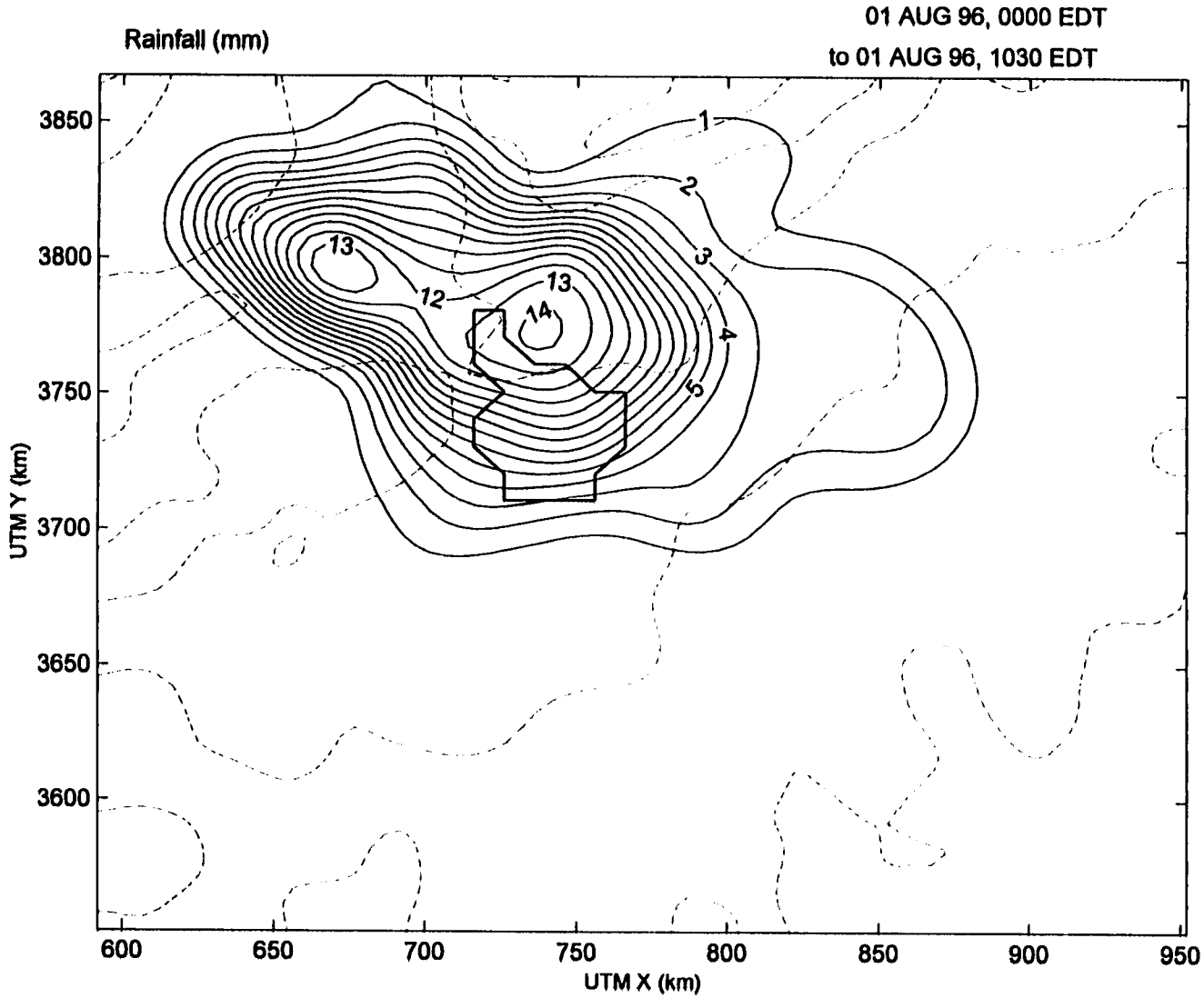
Rainfall (mm)
01 AUG 96, 0000 EDT
to 01 AUG 96, 1030 EDT
3850
3800
3750
3700
3650
3600
UTM Y (km)
600
650
700
750
800
850
900
950
UTM X (km)
1
2
3
4
5
12
13
13
14

Figure 42

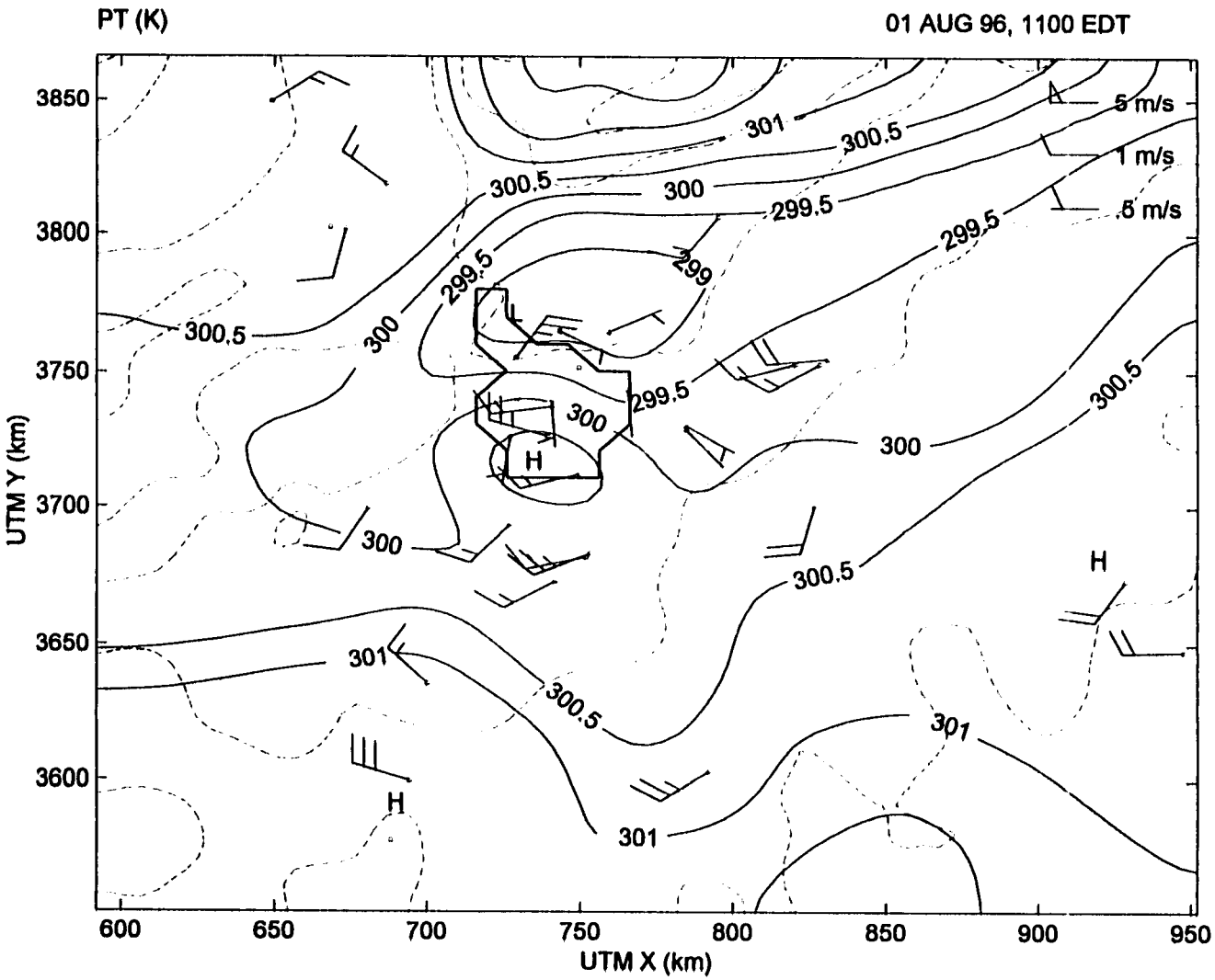
PT (K)
01 AUG 96, 1100 EDT
5 m/s
1 m/s
.5 m/s
301
300.5
300
299.5
299
H
UTM Y (km)
3850
3800
3750
3700
3650
3600
600
650
700
750
800
850
900
950
UTM X (km)

Figure 43

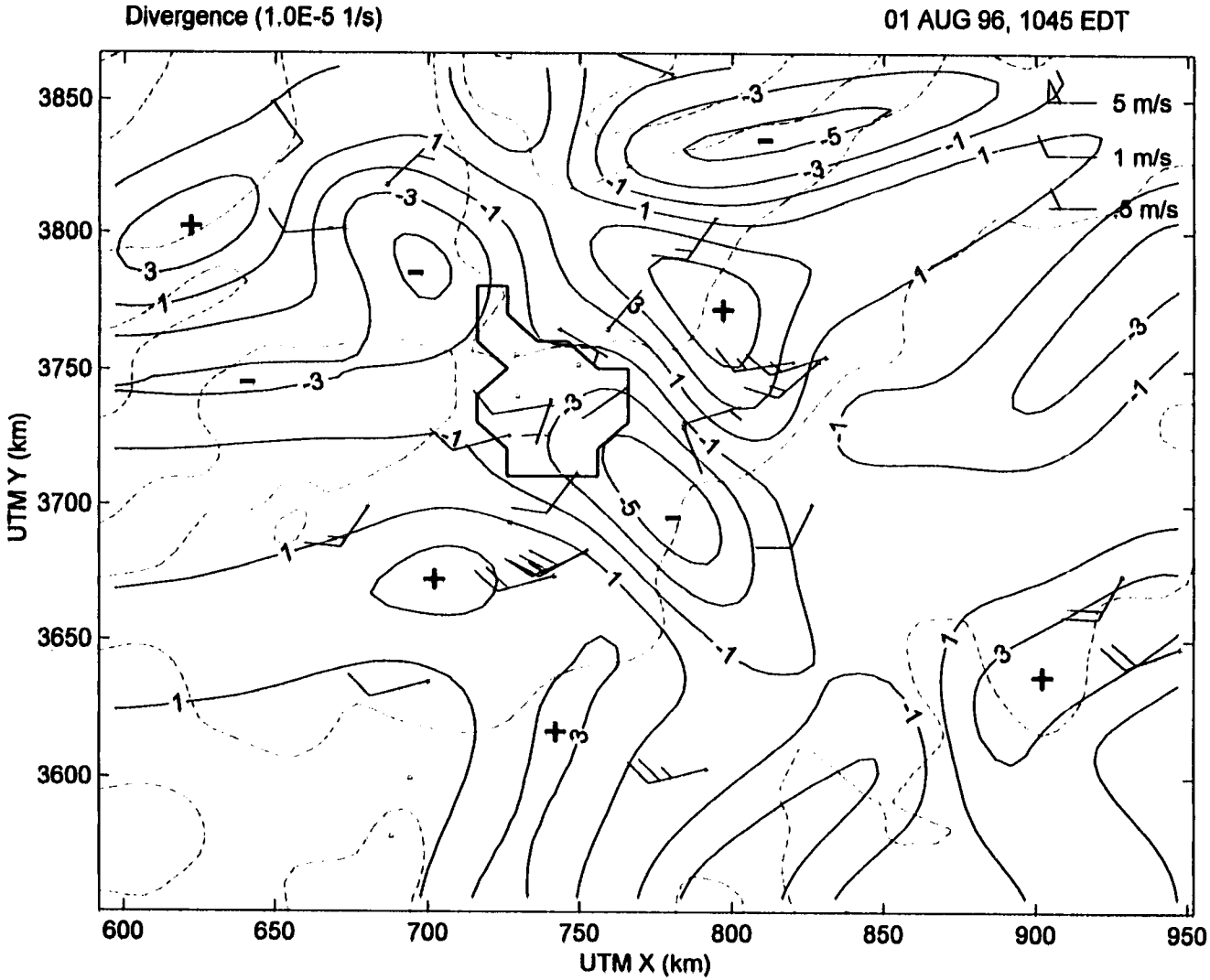
Divergence (1.0E-5 1/s)
01 AUG 96, 1045 EDT
5 m/s
1 m/s
UTM Y (km)
UTM X (km)
3850
3800
3750
3700
3650
3600
600
650
700
750
800
850
900
950

Figure 44

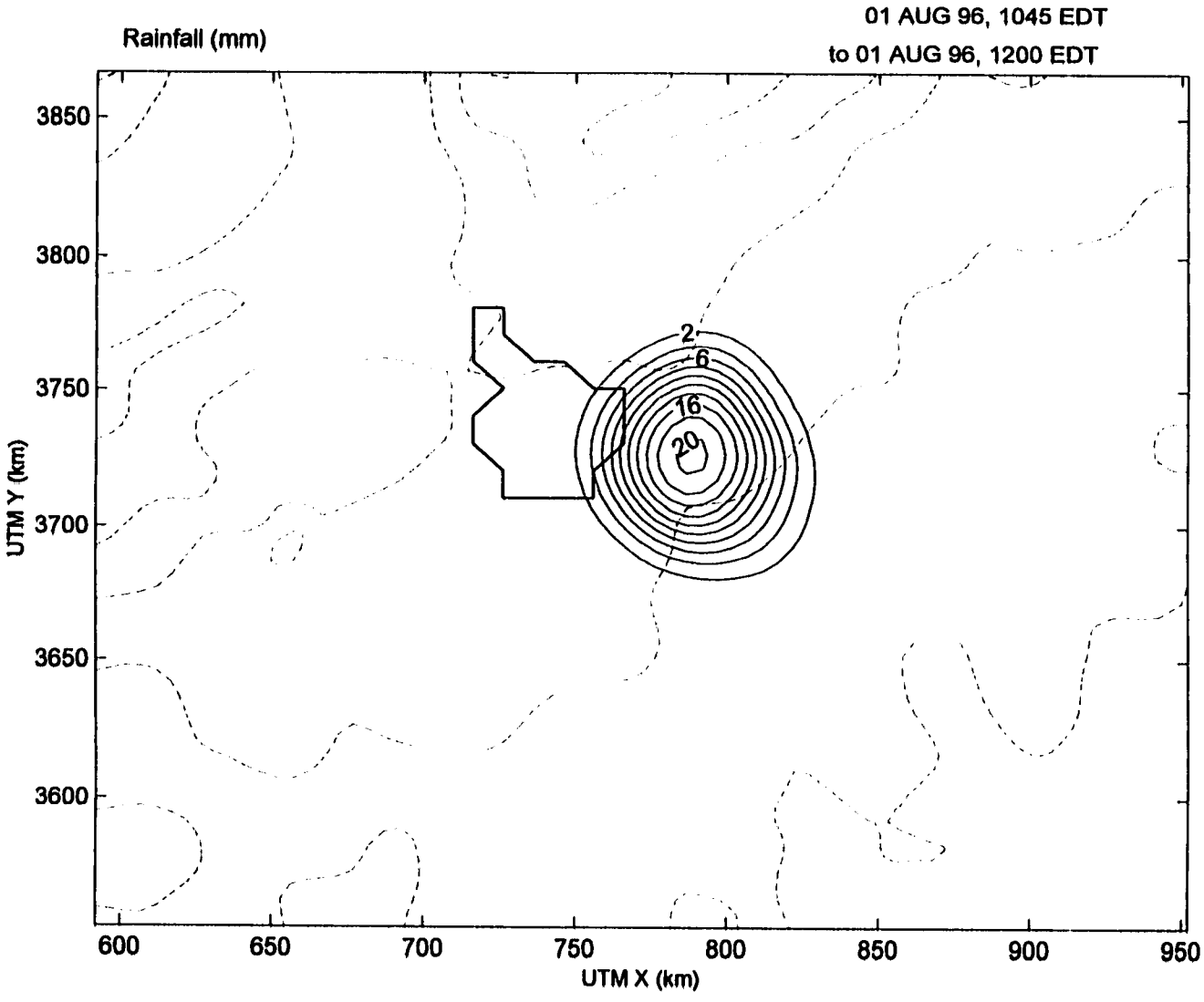
Rainfall (mm)
01 AUG 96, 1045 EDT
to 01 AUG 96, 1200 EDT
3850
3800
3750
3700
3650
3600
UTM Y (km)
2
6
16
20
600
650
700
750
800
850
900
950
UTM X (km)

Figure 45

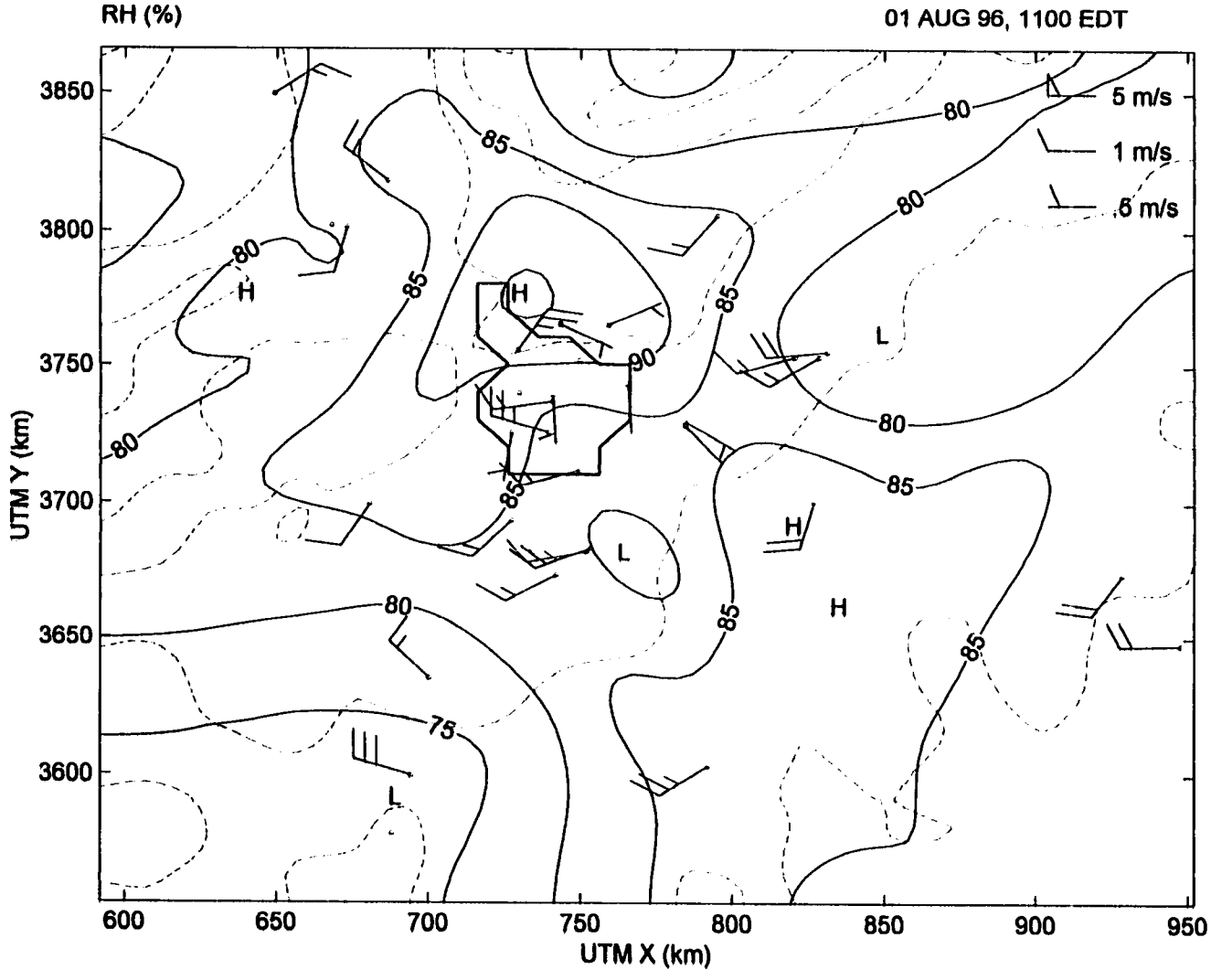
RH (%)
01 AUG 96, 1100 EDT
5 m/s
1 m/s
5 m/s
UTM Y (km)
UTM X (km)
3850
3800
3750
3700
3650
3600
600
650
700
750
800
850
900
950
80
85
90
75
H
L

Figure 46

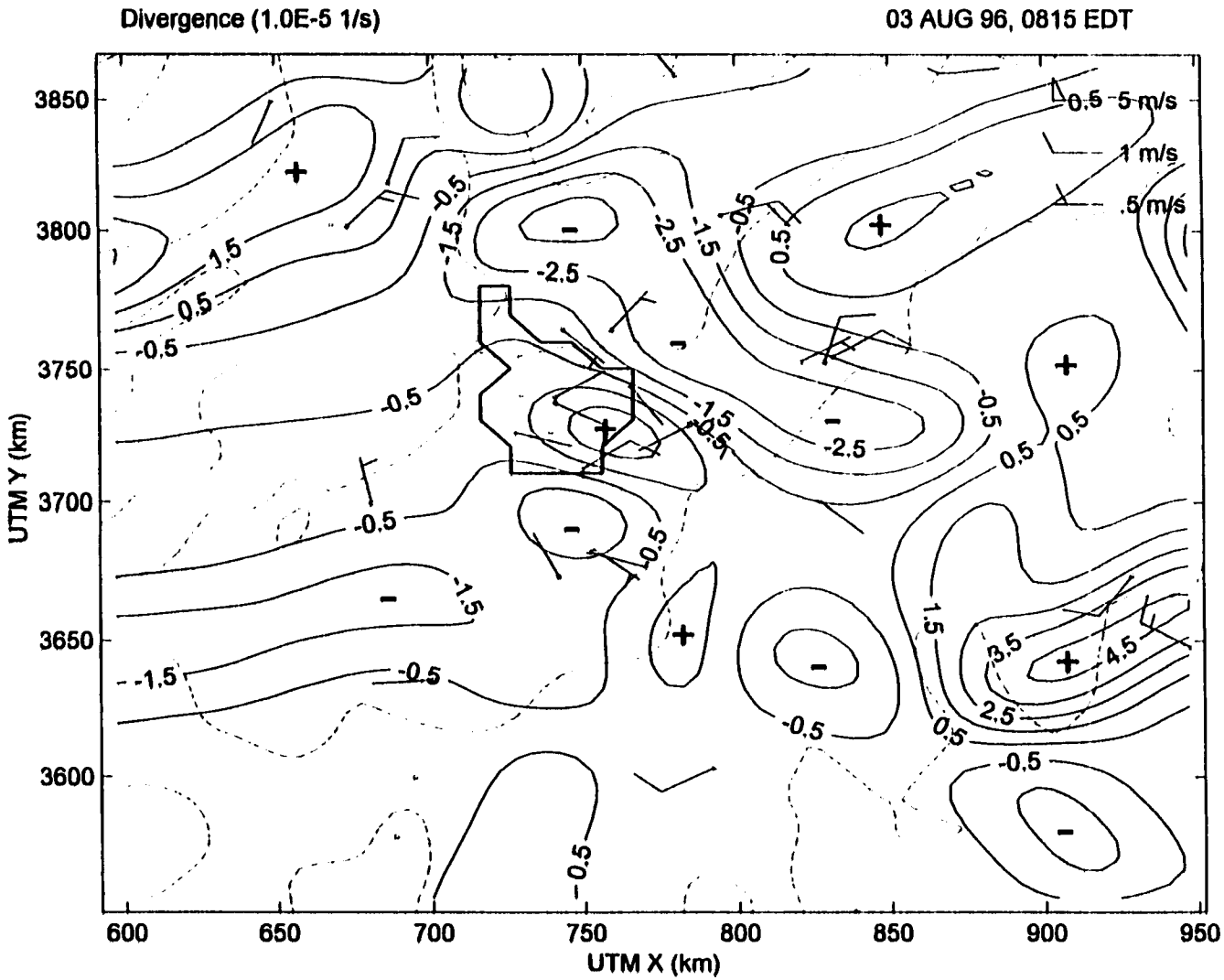
Divergence (1.0E-5 1/s)
03 AUG 96, 0815 EDT
5 m/s
1 m/s
.5 m/s
UTM Y (km)
UTM X (km)
3850
3800
3750
3700
3650
3600
600
650
700
750
800
850
900
950

Figure 48

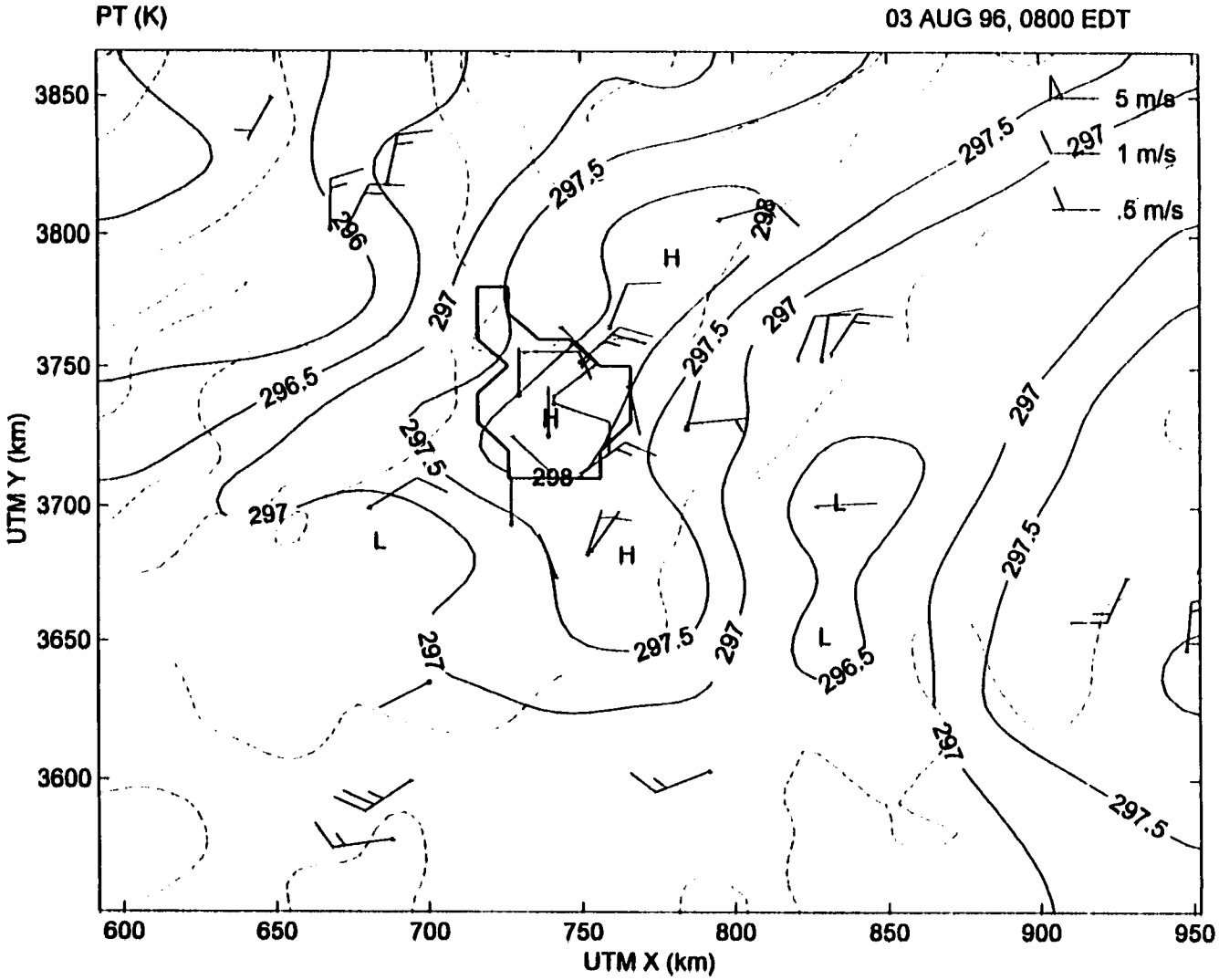
PT (K)
03 AUG 96, 0800 EDT
5 m/s
1 m/s
.5 m/s
UTM Y (km)
UTM X (km)
3850
3800
3750
3700
3650
3600
600
650
700
750
800
850
900
950
H
L
296.5
297
297.5
298

Figure 47

Figure 49

Figure 50

Figure 51

Figure 52

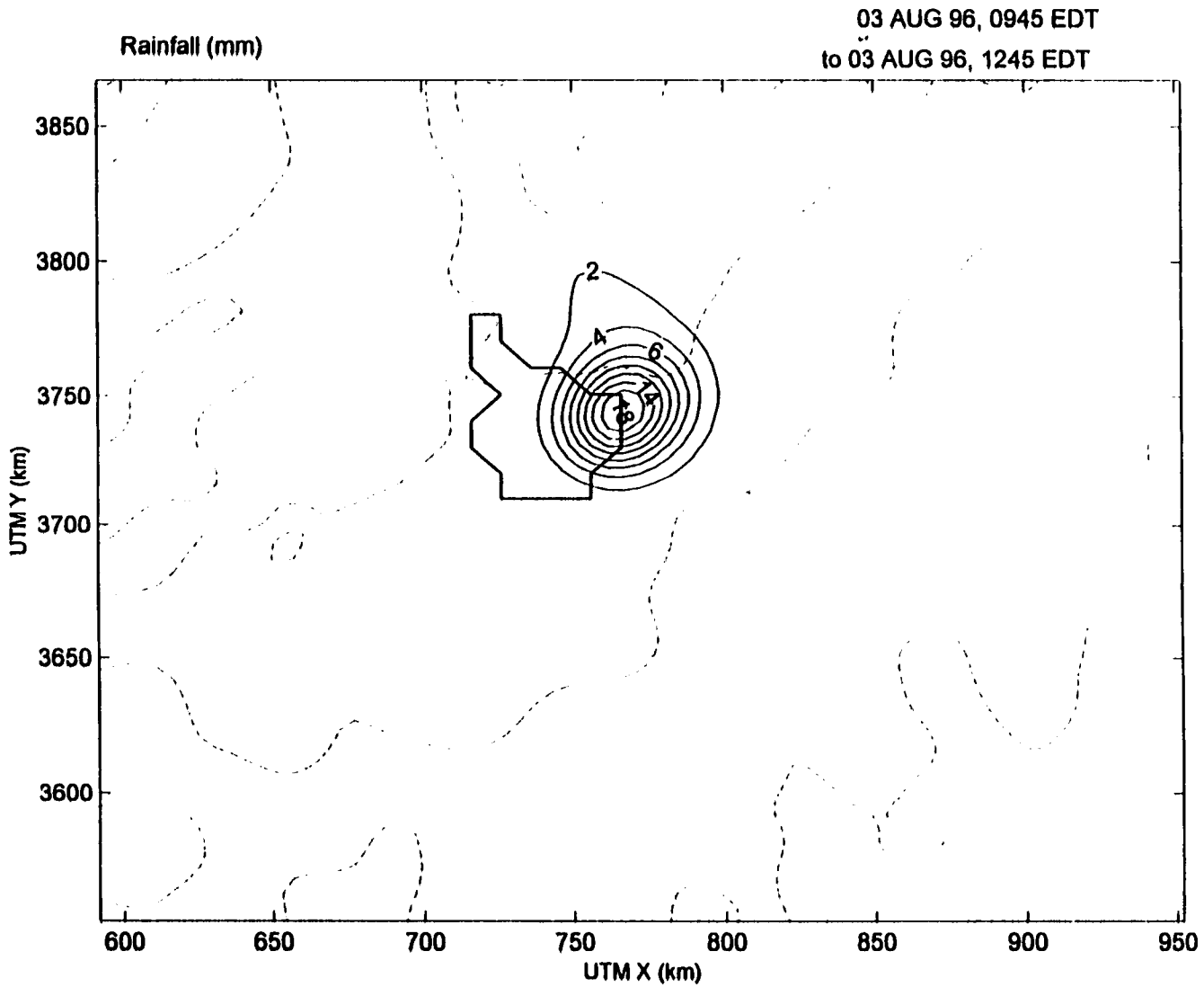
Rainfall (mm)
03 AUG 96, 0945 EDT
to 03 AUG 96, 1245 EDT
3850
3800
3750
3700
3650
3600
UTM Y (km)
600
650
700
750
800
850
900
950
UTM X (km)
2
4
6
8
10

Figure 53

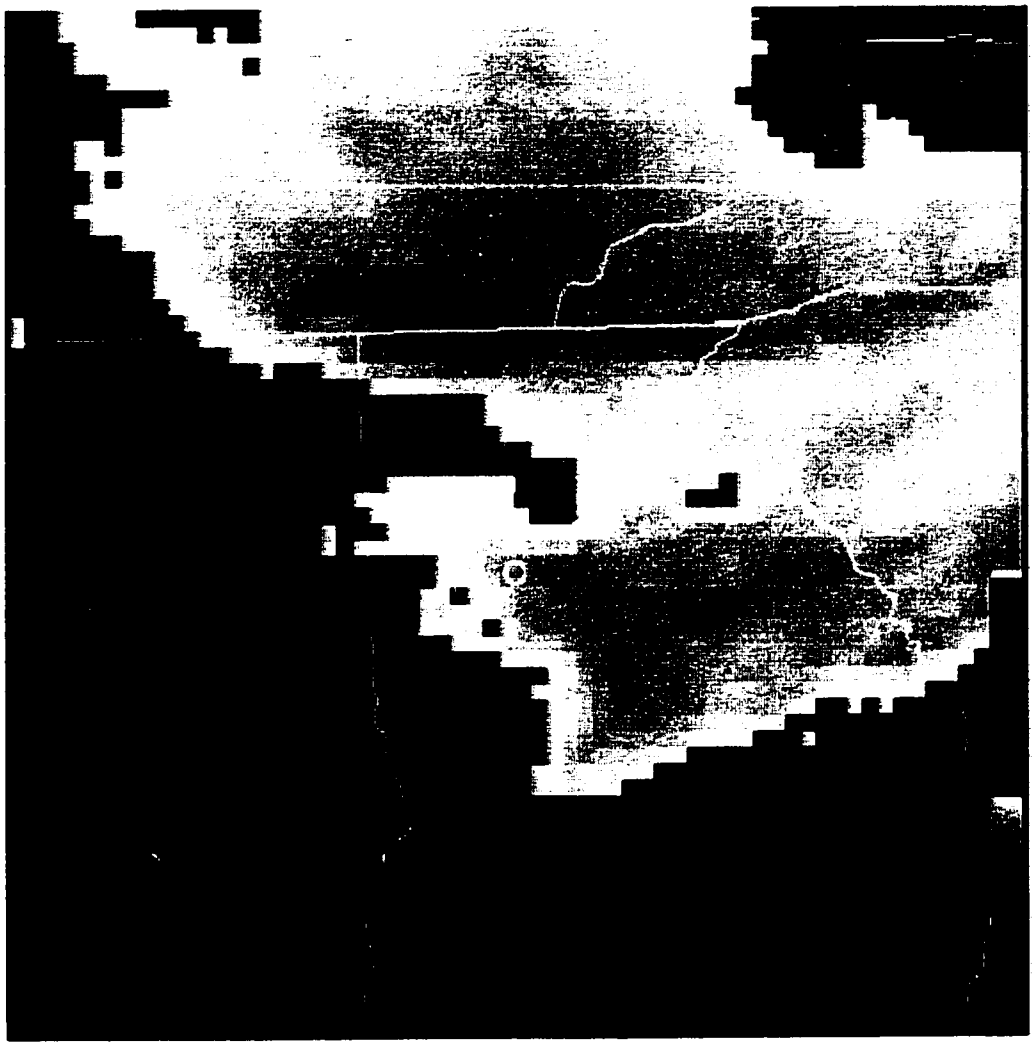

Figure 54

Figure 55

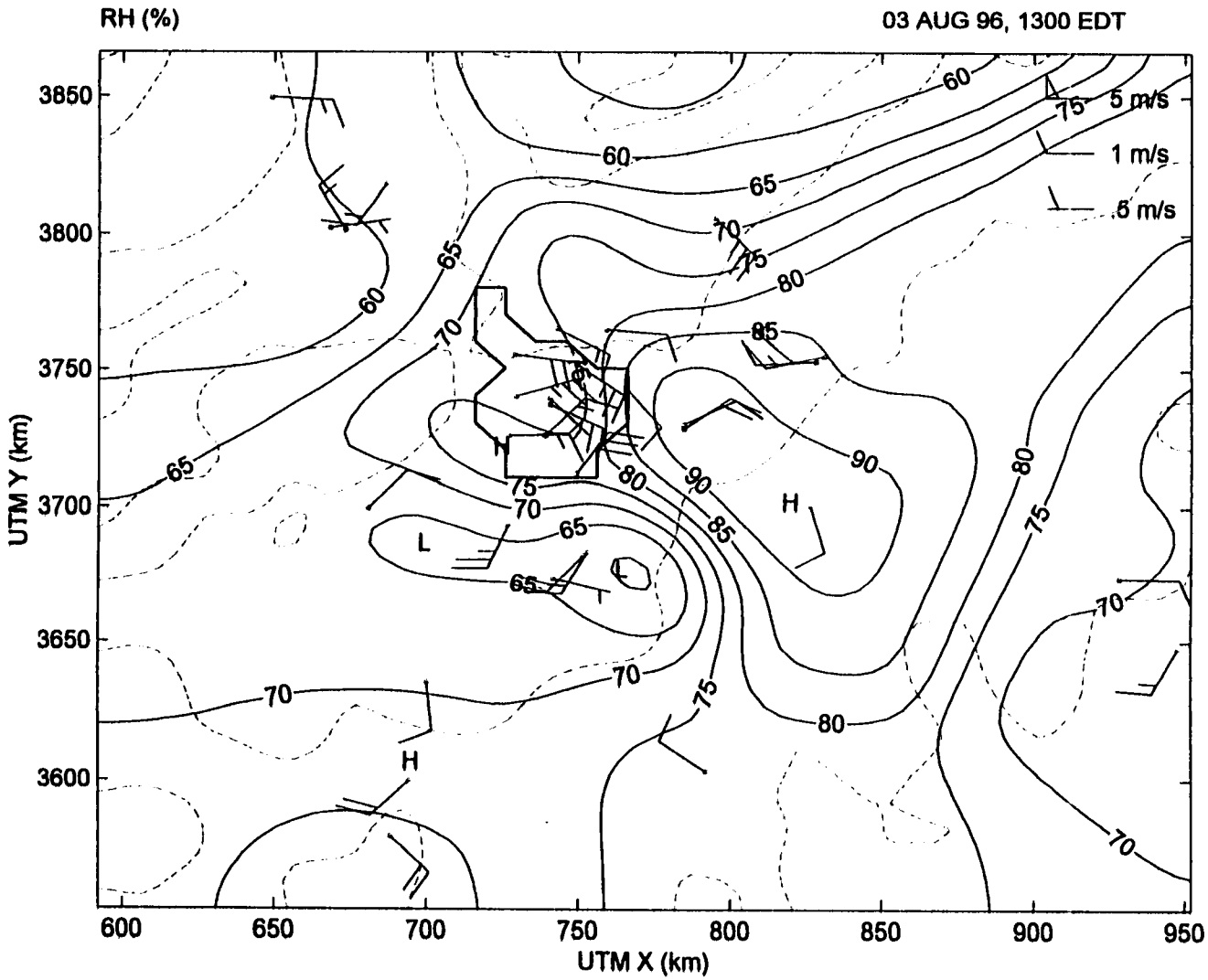
RH (%)
03 AUG 96, 1300 EDT
5 m/s
1 m/s
6 m/s
UTM Y (km)
UTM X (km)
3850
3800
3750
3700
3650
3600
600
650
700
750
800
850
900
950
H
L
H

Figure 56